Natural Resources Canada | Ressources naturelles Canada

GEOLOGICAL SURVEY OF CANADA
OPEN FILE 7999

# ARA05C Marine Research Expedition Canada-Korea-USA Beaufort Sea Geoscience Research Program: Summary of 2014 Activities

**Y.K. Jin and S.R. Dallimore (Editors)**

**2016**

Canada


**GEOLOGICAL SURVEY OF CANADA**
**OPEN FILE 7999**

# ARA05C Marine Research Expedition Canada-Korea-USA Beaufort Sea Geoscience Research Program: Summary of 2014 Activities

**Y.K. Jin[1] and S.R. Dallimore[2]**

[1] Korea Polar Research Institute, 26 Songdomirae-ro, Yeonsu-gu Incheon, 406-840, Korea
[2] Geological Survey of Canada, Natural Resources Canada, 9860 West Saanich Rd, Sidney, British Columbia, Canada

## 2016



doi:10.4095/297866

This publication is available for free download through GEOSCAN (http://geoscan.nrcan.gc.ca/).

**Recommended citation**
Jin, Y.K. and Dallimore, S.R. (ed.), 2016. ARA05C Marine Research Expedition, Canada-Korea-USA Beaufort Sea Geoscience Research Program: Summary of 2014 Activities; Geological Survey of Canada, Open File 7999, 107 p. doi:10.4095/297866

Publications in this series have not been edited; they are released as submitted by the author.

# ARA05C Cruise Report

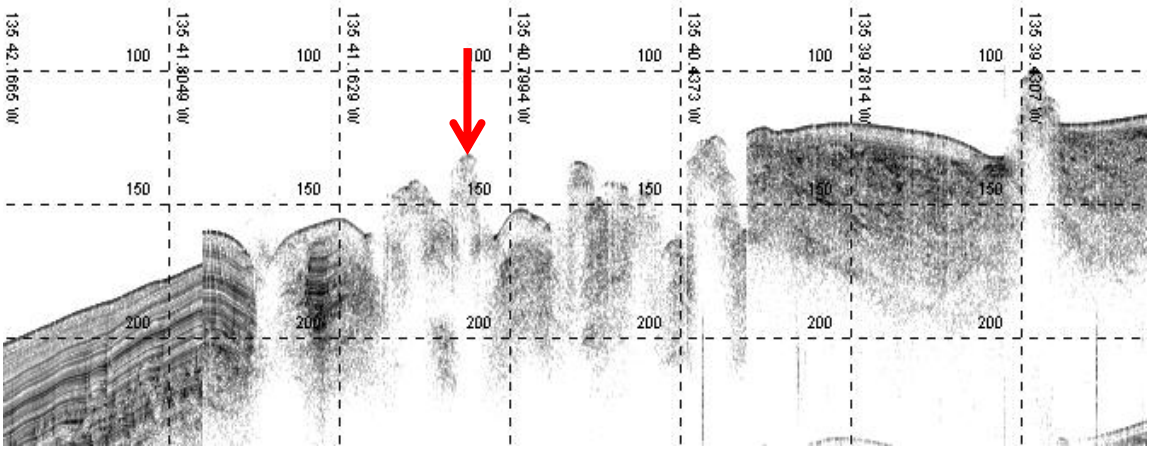


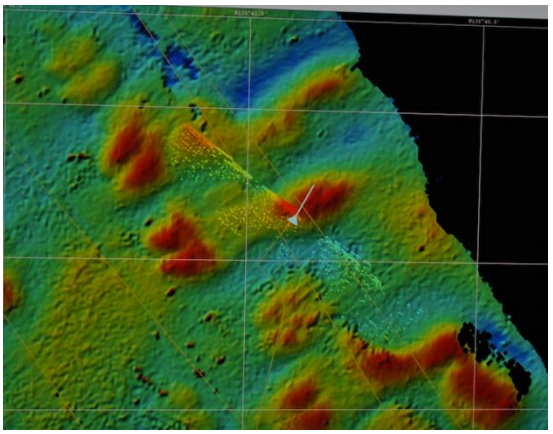


**Barrow, USA - Beaufort Sea, Canada - Nome, USA**
**28 August - 19 September, 2014**

KOPRI

CANADA GEOLOGICAL SURVEY - COMMISSION GEOLOGIQUE 1842

M B A R I

Fisheries and Oceans

**Author contact information by organization:**


| Authors | Affiliation and Address |
|---|---|
| Y.K. Jin<br>J.K. Hong<br>S.K. Kang<br>Y.-G. Kim<br>I.C. Kim<br>T.K. Kim<br>J.E. Kim<br>J.H. Yim<br>K.H. Jin<br>M.G. Lee<br>S. Kim<br>N.R. Seo<br>I.G. Lee<br>D.S. Shin<br>S.H. Kim<br>Y.H. Noh<br>J.Y. Lee<br>T.W. Ko<br>C.Y. Gang<br>H.J. Kim | Korea Polar Research Institute<br>26 Songdomirae-ro, Yeonsu-gu, Incheon 219900, KOREA |
| S.R. Dallimore<br>M. Riedel<br>M.M. Côté | Geological Survey of Canada, Natural Resources Canada<br>9860 West Saanich Rd, Sidney, BC, V8L 4B2, CANADA |
| R. Gwiazda | Monterey Bay Aquarium Research Institute<br>7700 Sandholdt Road, Moss Landing, CA 95039, USA |
| C.M. Kim | Seoul National University<br>Gwanak-ro, Gwanak-gu, Seoul 08826, KOREA |
| C.B. Jeong<br>D.H. Lee | Hanyang University<br>55 Hangyangdaehak-ro, Sangnok-gu, Ansan, Gyeonggi-do, 15588, KOREA |
| G. Wiemer | MARUM - Center for Marine Environmental Sciences<br>University of Bremen, Leobener Str., D-28359 Bremen, GERMANY |

***Steering Committee Members***

Young Keun Jin; Korea Polar Research Institute, KIOST

Scott Dallimore; Geological Survey of Canada-Pacific

Charles Paull; Monterey Bay Aquarium Research Institute

Timothy Collett; United States Geological Survey

Humfrey Melling; Fisheries and Oceans Canada

Michael Riedel; Geological Survey of Canada-Pacific

Jong Kuk Hong; Korea Polar Research Institute, KIOST

## TABLE OF CONTENTS

# ARA05C Cruise report

## CHAPTER 1 - Overview of research activities

### Y. K. Jin, S.R. Dallimore and R. Gwiazda

Expedition ARA05C was a highly multidisciplinary undertaking conducted in the southern Beaufort Sea on the research ice breaker RV Araon from August 30 to September 19, 2014. The program was carried out as a collaboration between the Korea Polar Research Institute (KOPRI), Geological Survey of Canada (GSC), Monterey Bay Aquarium Research Institute (MBARI), Department of Fisheries and Ocean (DFO) with participation by Bremen University (BARUM). Multiple research experiments were undertaken to study geological processes related to degrading permafrost, fluid flow and degassing, seismostratigraphy, and associated geohazards, of the Beaufort shelf and slope region (see Figs 1.1 and 1.2). In addition, physical and chemical oceanography measurements of the Arctic Ocean were undertaken with linked atmospheric studies from the vessel. The expedition focused on two main research areas in the Canadian Beaufort Sea: the central shelf and slope areas offshore of the Tuktoyaktuk Peninsula from August 30 to September 10, 2014, and areas offshore of the Mackenzie Trough from September 11 to September 15, 2014. Expedition ARA05C builds on research program ARA04C undertaken by the same collaborators in September 2013 in the same study area (Jin et al., 2015).

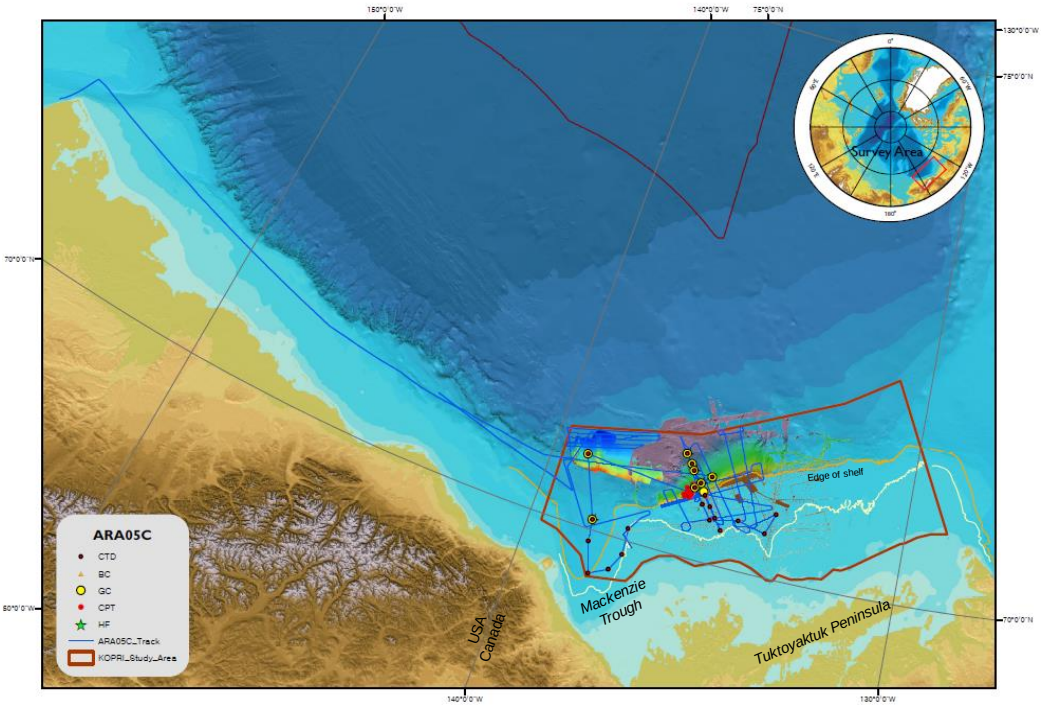


**Figure 1.1 - Overview map of the ship track and stations for Expedition ARA05C. The expedition undertook research in two main study areas in the Canadian Beaufort Sea: the central shelf and slope areas offshore of the Tuktoyaktuk Peninsula and areas north of the Mackenzie Trough.**

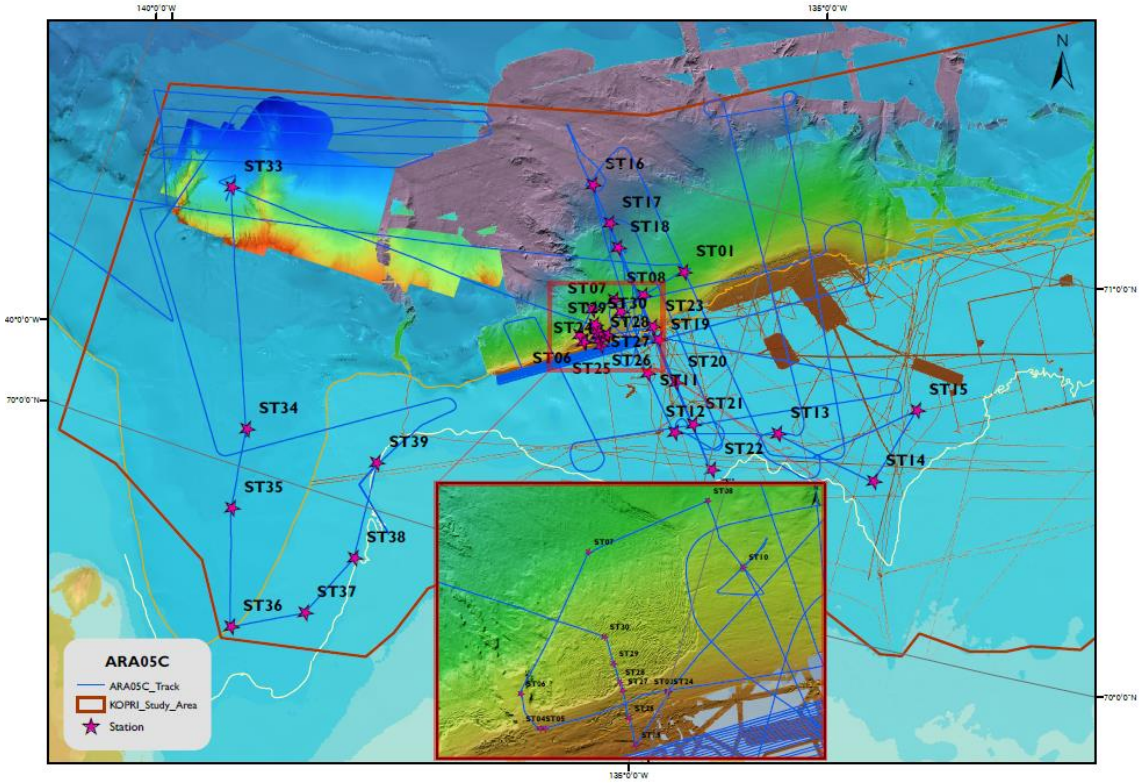


**Figure 1.2 - Details of the ship track and stations for Expedition ARA05C.**

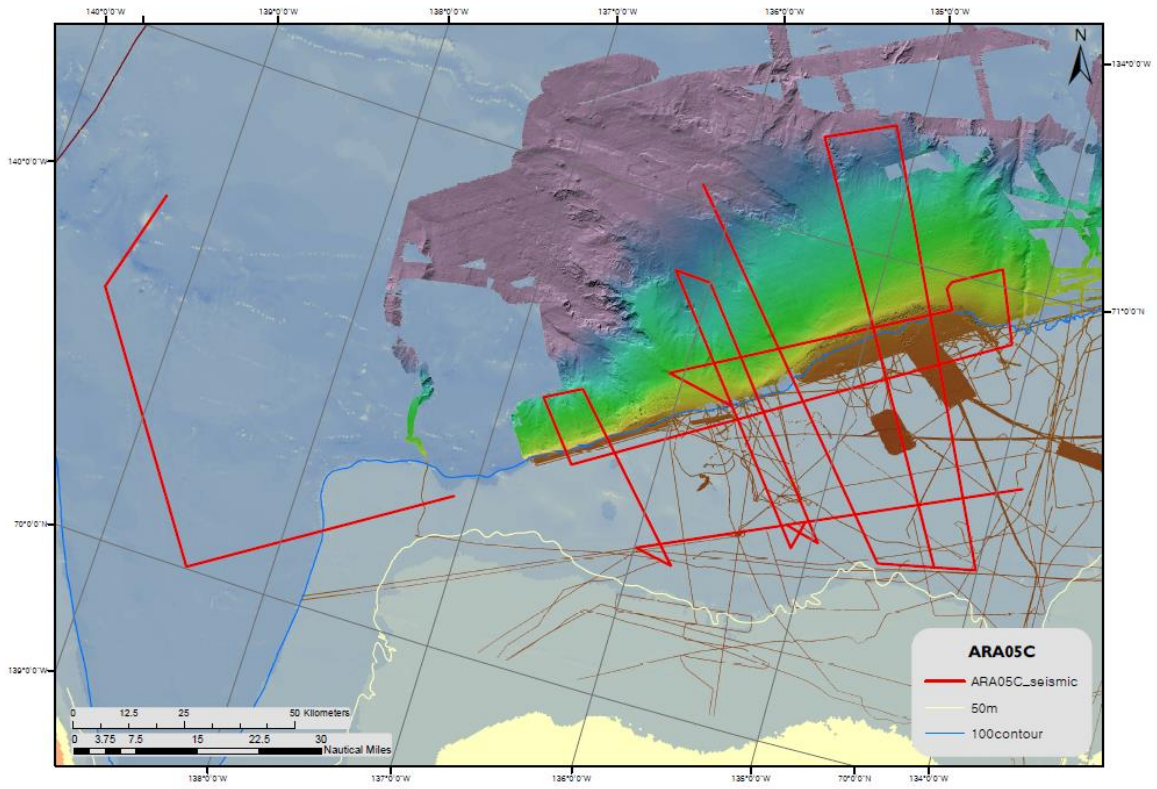


**Figure 1.3 - Map showing seismic survey lines acquired during Expedition ARA05C.**

Multichannel seismic data were collected to support drilling proposals, particularly International Ocean Discovery Program (IODP) pre-proposal #806 (Paull et al., 2012) and #753 (O'Regan, 2010), and to verify distribution and internal structures of the offshore permafrost occurrences (Fig. 1.3). The multichannel seismic data were acquired on the outer continental shelf and upper slope of the Canadian Beaufort Sea, totaling 20 lines with ~1,000 line-kilometers and ~20,000 shot gathers from September 1 to September 13, 2014 (see Chapter 3 for more details). The multichannel seismic data will be processed post-expedition at KOPRI and the GSC. The seismic and ocean bottom seismometer data (OBS) data obtained in 2013 and 2014 cruises will allow: 1) detailed velocity analyses to investigate the permafrost signature at the shelf edge and help mapping zones of high-velocity sediments indicative of the presence of pore ice along the four main lines crossing the OBS stations (see Chapter 4 for more details on the OBS study), 2) detailed deep structures of the mud volcanoes (fluid expulsion structures) in the slope area, and 3) detailed investigations of the seismostratigraphy of the upper several kilometers of sediments in this area.

Continuous sub-bottom profiler (SBP) and multibeam data were collected along all ship tracks for detailed imaging of bottom morphology and shallow subsurface sediments, as well as for verifying core-site location (see Chapter 5 and 6 for more details). During Expedition ARA05C, more than 3,000 line-kilometers of SBP data were collected, co-located with multibeam and backscatter data. These data are an essential part of the study of sub-seafloor permafrost distribution and provide insights into sediment dynamics at critical boundaries, especially the shelf edge. Here, the occurrence of isolated sea floor mounds result in a characteristic, rugged landscape with thousands of protrusions through the otherwise laminated sediments. Multibeam and backscatter data were collected along all ship tracks, adding to the database of existing information gathered through previous expeditions to the study region.

Heat flow measurements were undertaken at 5 stations and thermal conductivity measurements were also carried out on 5 gravity cores to study the geothermal conditions of shelf edge permafrost, of sea floor expulsion features in the upper slope, and background areas (see Chapter 7 for details). Temperatures observed at the sea floor expulsion feature at 740 m water depth are much higher than those observed at all other stations.

Geological sampling using gravity coring and box-coring was performed at strategic sites supporting ongoing international research linked to IODP pre-proposals #806 (Paull et al., 2012) and #753 (O'Regan et al., 2010), as well as at sites of regional interest to define key seismo-stratigraphic horizons critical to the understanding of geohazards in the region (see Chapter 8 for details). In total, 9 gravity cores and 22 box-cores were taken (Fig. 1.1). Most sediment analyses on the recovered cores will be performed post-expedition at various laboratories of KOPRI, MBARI, and other university-based collaborators in Korea. Onboard, sub-samples were taken from all gravity cores. On selected cores from the Canadian Beaufort study region, pore-waters were extracted using rhizone samplers after logging of physical properties. These samples will be analyzed post-expedition by research collaborators at MBARI.

A drop-cone penetration test (CPT) program was conducted from the RV Araon through collaboration with the University of Bremen. The components of the CPT are 1) an industrial 15 cm² piezocone cone and 2) an aluminium pressure-tight housing containing a microprocessor (Avisaro AG) logging unit, including a standard secure digital memory card (SD), power supply (battery package), tilt meter, accelerometer and data communication unit. Data collected from CPT drops can be used to interpret sediment properties including sediment strength and permeability. Sixteen sites were investigated with multiple drops at each site. The data reveals variable sediment strengths in the upper 2 m of section with useful correlation to the geology seen at the shelf edge transition and associated with sea floor mud volcanoes.

Water sampling and Conductivity-Temperature-Depth (CTD) profiling was undertaken at most core sites to study physical and chemical properties of the seawater (Fig. 1.1). These station-measurements were complemented by continuous water-property and atmospheric measurements when the RV Araon was underway. Most samples taken will be analyzed for DIC/TA, nutrients, DOC, and POC post-expedition at KOPRI. pH of seawater, underway data of $pCO_2$, $CH_4$, and $N_2O$, and a variety of calculations are required to produce an accurate data set. Methane was also measured with a methane sensor attached to the CTD tool and at the mud volcanos in 290 m, 420 m, and 740 m water depth. The methane plume was also acoustically imaged with the echo sounder systems on board the RV Araon. Further details on the water sampling and atmospheric measurements are given in Chapter 10 and 11.

### *Reference*

Paull CK, Dallimore SR, Collett TS, Jin YK, Mienert J, Mangelsdorf K, and Riedel, M. 2012. Drilling to investigate methane release and geologic processes associated with warming permafrost and gas hydrate deposits beneath the Beaufort Sea Shelf. IODP Pre-Proposal 806, available online at http://iodp.org

O'Regan M, de Vernal A, Hill P, Hillaire-Marcel C, Jokobsson M, Moran K, Rochon A, and St-Onge G. 2010. Late quaternary paleoceanography and glacial dynamics in the Beaufort Sea, IODP Pre-Proposal 753, available online at http://iodp.org

Jin YK, Riedel M, Hong JK, Nam SI, Jung JY, Ha SY, Lee JY, Kim GY, Yoo J, Kim HS, Kim G, Conway K, Standen G, Ulmi M, and Schreker M. 2015. Overview of field operations during a 2013 research expedition to the southern Beaufort Sea on the RV Araon, Geological Survey of Canada, Open File 7754, 181 p., doi:10.4095/295856

# CHAPTER 2 - Background

**Y.K. Jin, S.R. Dallimore, M. Riedel and M.M. Côté**

## *2.1) Context of research collaboration*

The Korean Polar Institute (KOPRI) is engaged in long-term collaborative studies in the Arctic Ocean with the Geological Survey of Canada/Natural Resources Canada (GSC), the Monterey Bay Aquarium Research Institute (MBARI) and Fisheries and Oceans Canada (DFO). The ongoing focus of research activities on the KOPRI ice breaker RV Araon is to investigate degrading permafrost and gas hydrates in the outer shelf and upper slope, paleoceanography, microbiology, monitoring of the upper-ocean waters and atmospheric science. These activities address issues related to active geologic processes and fluid/gas flux, offshore geohazards, ocean variability and the broad consequences of global climate change. Our goal is to identify and describe changes in the Arctic marine environment, and subsequently to understand why changes are occurring and whether they will continue into the future.

The core program for the KOPRI activities is enabled through bilateral memoranda of understanding between KOPRI and NRCan, and KOPRI and DFO. As such, the research program compliments ongoing research priorities and regional studies that have been conducted by NRCan and DFO over the past several decades primarily using Canadian Coast Guard ice breakers Sir Wilfred Laurier and Amundsen. The University of Bremen was also a participant in the 2014 program conducting cone penetration tests (CPT) as part of a research program led by A. Kopf to study CPT applications in marine environments.

## *2.2) Geologic Setting*

The shelf of the Canadian Beaufort Sea is underlain by thick terrestrial permafrost which has been inundated by relatively warm seawater as a consequence of post-glacial sea level rise. As described by Taylor et al. (2013) the permafrost body beneath the shelf extends far offshore pinching out at the shelf–slope break at approximately 100 m water depth. Gas hydrates, a solid form of natural gas wherein water molecules are arranged in a cage-like structure with methane (or occasionally other gases) are also found in this setting. Gas hydrates are unstable at atmospheric pressure and temperature, decomposing spontaneously into gas and water. Gas hydrates exist beneath the Beaufort Sea in two locales: conventionally in deep water (slope and basin) where pressure of more than 30 atmospheres provides stability, and as permafrost gas hydrate in shallow water over the continental shelf where low formation temperatures can maintain their stability at somewhat shallower depths. Geothermal modeling by Taylor et al. (2013) suggests that gas hydrates do not occur between the outer edge of subsea permafrost (~110 m water depth) and approximately 300 m water depth.

Warming and possible thawing of the permafrost and dissociation of permafrost gas hydrate as a consequence of the sea level rise may weaken subsurface sediments and lead to subsidence, reduction of sediment strength and release of free gas. Field studies, including those from CCGS Sir Wilfrid Laurier in 2003, 2010 and 2012, have documented the escape of methane from the seabed of the outer shelf and slope. Gas venting has been observed from some

conical mounds on the shelf which are referred to as pingo-like features (Paull et al., 2006) as well as from an area of large landslides at top of the continental slope near 100 m depth and from the upper slope associated with large conical features that appear similar to mud volcanoes described in other settings around the world. We propose that degrading permafrost and gas hydrates liberate gas and pore water that reduce the strength of subsurface sediments, leading to possible seabed instability.

### *2.3) Research Activities*

The RV Araon's 2014 science program sought to investigate the relationship between subsea permafrost, gas hydrates and seabed terrain features at various depths in the upper slope and outer shelf. A primary objective of the 2014 field work was to acquire baseline geophysical data (primarily seismic data) which could be used as a basis for siting of scientific research wells. In this regard the international ocean drilling community has acknowledged that comprehensive assessment of the consequences of warming of shelf permafrost and gas hydrates in the Arctic is a research topic of considerable interest in relation to global climate change studies and to evaluating geohazards in this setting. Our research will also assist interpretations of geologic processes in the Canadian Beaufort Sea and the understanding of the geologic history of this area.

The principal activities were:

- Multichannel seismic surveys to document the geology, permafrost and gas hydrate setting of the upper slope and outer shelf
- Collection of sediment core samples with gravity coring and box-coring equipment
- Deployment of drop probes for geothermal heat flux
- Deployment of drop cone penetration probes to measure shallow sediment strength
- Deployment of a grab and dredge for sampling surficial sediment
- Deployment of water sampling and profiling equipment (CDT) to measure the physical properties of the ocean
- Underway multibeam sonar for high resolution mapping of selected seabed features
- Underway surveys using ship-mounted 3.5-kHz CHIRP sonar for seismic visualization of shallow (10's of meters) sediments
- Underway measurements of water chemistry
- Underway measurements of atmospheric chemistry

## *2.4) Permits and Licensing*

The scientific research activities on the RV Araon were reviewed by a number of agencies who are responsible for administering marine research activities in the Canadian Beaufort Sea. The permits and licenses obtained for the 2014 research activities were based on submissions made for a similar program undertaken in 2013. Unfortunately, technical problems encountered during the 2013 program and restrictive ice conditions reduced the scientific accomplishments of this cruise. The 2014 program used similar equipment and methods to those used in 2013. The following key permits pertain to the 2014 program.

**Inuvialuit Environmental Impact Screening Committee (EISC)**
**Submission number 10/12-02:**

The Inuvialuit Environmental Impact Screening Committee reviews all research activities in the Inuvialuit Settlement Region. The 2014 program was approved as an amendment of the 2013 submission which was entitled Canada-Korea-USA Beaufort Sea Geoscience Research Program.

The Screening Panel, in advising its decision on 25 January 2013, recommended the following environmental terms and conditions which were incorporated into the field program:

1. *The developer is to adhere to program commitments made in their Project Description plus those subsequently committed to and noted on the EISC Public Record.*
2. *With reference to the Fisheries and Oceans Canada recommendation #1, in their letter dated December 19th, 2012, the developer shall have an MMO "on-duty" during active seismic shooting operations.*
3. *The Panel is concerned with bird mortality due to "fatal light attraction". Prior to commencement of its operations the developer is to contact Environment Canada for recommended measures to reduce the amount of strikes and make best efforts to mitigate this potential for bird mortality.*
4. *The developer must update their Waste Management Plan to be relevant to the project and its operation within the Canadian Beaufort Sea. The updated Waste Management Plan is to be submitted to Transport Canada prior to commencement of operations.*
5. *With reference to the concerns expressed by the Yukon Government, Environment Yukon, Parks Branch, in its comments submitted to the EISC Public Record, the developer shall, prior to commencement of its operations, consult with the Parks Branch on the potential use of Herschel Island, and its immediately surrounding waters, in order to come to an understanding on the conditions surrounding this use (permits, etc.).*

*Amendment April 24, 2014*

**Northwest Territories Scientific Research Licenses**
**Scientific Research License #15501**

The Government of the Northwest Territories coordinates all scientific investigations in the Northwest Territories through their Scientific Research License program. A scientific research license for the "Canada-Korea-USA Beaufort Sea Geoscience Research Program: 2014 Activities" was issued on issued 10 July, 2014. The main requirements of this license were to

publish the results and conduct, where appropriate, community consultations. This publication fulfils a commitment made in this regard**.**

### *Marine Scientific Research Permit*

The activity of foreign research vessels in Canadian waters is administered by the Department of Foreign Affairs, Trade and Development Canada (DFAIT). DFAIT approved the 2014 RV Araon research activities on 25 July, 2014. Their letter of authority is as follows:

**Note No. IDR 595**

The Department Foreign Affairs, Trade and Development Canada presents its compliments to the Embassy of the Republic of Korea and has the honour to refer to its application for the vessel RV ARAON to undertake marine scientific research in areas under the national jurisdiction of Canada from August 30 to September 15 2014.

The Department is pleased to confirm that the Government of Canada grants its consent to the Korean Polar Research Institute to undertake Marine Scientific Research in areas under the national jurisdiction of Canada, for the above-mentioned proposed cruise.

The Department notes that there will be no activity taking place inside Canada's territorial waters. Therefore, there are no reporting requirements to the Canada Border Services Agency (CBSA). While conducting its cruise, should the vessel require entry into Canada's territorial waters (inside the 12 nautical mile limit), reporting to the CBSA may be performed by telephone communication.

We further note that this application indicates no planned port calls in Canada. Any unscheduled port call will require Pre-Arrival Notice to be submitted to the National Targeting Centre at **CBSA-ASFC-PANS/AA@cbsa-asfc.gc.ca**.

Canada takes note that the ARAON is a government vessel on non-commercial service that will enjoy sovereign immunity in Canada's exclusive economic zone in the course of the scientific research. The Republic of Korea will be aware that pursuant to customary international law as reflected in article 236 of United Nations Convention on the Law of the Sea (UNCLOS), by the adoption of appropriate measures not impairing operations or operational capabilities, that this vessel should act in a manner consistent, so far as is reasonable and practicable, with UNCLOS. To comply with section 236 of UNCLOS, while operating within the exclusive economic zone of the Canadian Arctic, the ARAON should adopt all appropriate measures to comply with the marine environmental provisions of Canadian legislation and make contact with NORDREG prior to entering the Canadian EEZ so that the Canadian Coast Guard is aware of the vessel's entry and status.

In this regard, the Republic of Korea may find of use the following internet links to Canadian legislation intended to protect and preserve the marine environment and to promote safe and efficient navigation in Canadian Arctic waters:

1) Arctic Waters Pollution Prevention Act: http://laws.justice.gc.ca/eng/A-12/
2) Arctic Shipping Pollution Prevention Regulations http://laws.justice.gc.ca/eng/C.R.C.-c.353/
3) NORDREG vessel traffic reporting in the Arctic: http://www.ccg-gcc.gc.ca/eng/MCTS/Vtr_Arctic_Canada

It is recommended that the ARAON obtain a valid Canadian Arctic Pollution Prevention Certificate issued by the vessel's Classification Society. This is an indication of the vessel's compliance with the Arctic Shipping Pollution Prevention Regulations and will provide confirmation of the vessel's ice class.

For further information and guidance regarding vessel operation in Canadian Arctic waters, attached is a Transport Canada prepared document entitled Summary of Requirements for Ships Operating in Canadian Arctic Waters.

In addition to the above, the Canadian Coast Guard publication Ice Navigation in Canadian waters http://www.ccg-gcc.gc.ca/Ice_home/Ice_Publications/Ice-Navigation-in-Canadian-Waters provides guidance for vessels operating in Canadian Arctic waters.

As the ARAON will be entering the NORDREG zone, the vessel will be required to comply with the Northern Canada Vessel Traffic Zone Regulations. An information package regarding these regulations may be requested by email from IqaNordreg@innav.gc.ca.

Information on subsurface surveying and sampling, details of the operations, including locations, times and equipment used, may be required for NAVAREA warnings and Notices to Shipping promulgation. This information may be forwarded to the NAVAREA coordinator at navarea17.18@innav.gc.ca and/or MCTS Iqaluit at IqaNordreg@innav.gc.ca.

We are pleased that the research results, all the data, samples, and assessments thereof, derived from this research mission will be freely and generously shared. We also request copies of the preliminary and final research mission reports.

The Department of Foreign Affairs, Trade and Development avails itself of this opportunity to renew to the Embassy of the Republic of Korea the assurances of its highest consideration.

OTTAWA, July 25, 2014

# CHAPTER 3 - Multichannel seismic survey

**J.K. Hong, Y.K. Jin, S.K. Kang, M.G. Lee, S. Kim, N. Seo, H.J. Kim and C.M. Kim**

## *3.1. Introduction*

The multichannel seismic (MCS) survey was conducted in the outer continental shelf and slope of the Beaufort Sea, Arctic Ocean from 2$^{nd}$ to 13$^{th}$ September 2014 during the RV Araon expedition ARA05C. The main objective for the survey is to investigate sedimentary stratigraphy, locations of permafrost, and internal seismic velocity structures. Previous work in the area included acquisition of airgun seismic data, but no high quality MCS data of modern vintage exist over the shelf edge. During ARA04C cruise in 2013, KOPRI and GSC attempted to acquire MCS data in this area, but we only collected poor-quality data due to serious airgun problem. We obtained seismic data on 23 lines and the total survey length is about 998 line-km with 19,962 shots. In spite of harsh weather and unfriendly sea ice conditions, we completed 63% of the planned seismic lines. The newly acquired data will be integrated with existing older data (re-digitized analog records from industry surveys). The survey area consists of two major sub-areas, the "Main Seismic Area" and the "Western Seismic Area". The seismic data acquired in the Main Seismic Area will be utilized to support IODP pre-proposal #806 which is focused on geohazards associated with degrading permafrost and gas hydrates in the critical boundary zone of the shallow shelf and slope region. The seismic data acquired in the Western Seismic Area can also be utilized to support IODP pre-proposal #753 which is designed to understand Arctic Ocean paleoceanography and its relationship to abrupt climate change by recovering unprecedented high-resolution sediment records. Results from quick data processing show detailed sub-bottom stratigraphy and deep structures such as faults and folds.

Seismic data acquisition followed the guidelines for operation as defined in our Project Description approved by the Inuvialuit Environmental Screening Committee (EISC). A safety zone of 1 km radius around the vessel was defined, based on modeling of sound propagation through water with a maximum airgun array volume of 1,200 in$^3$. Prior to airgun operations, the marine mammal observers (MMOs) were on watch for at least one hour to observe that no mammals were within the safety zone. If no mammals were sighted within one hour, a ramp-up procedure for firing the airgun array was used. The ramp-up procedure followed a standard operation by firing the smallest airgun first and then adding an additional airgun every 5 minutes, until the maximum firing capacity was reached. Such ramp-up procedure took on average 40 minutes during this expedition. In total, seven attempts to acquire airgun data were made, with seven successful ramp-up procedures completed without any marine mammal sightings.

## *3.2. Methods*

### 3.2.1. Multichannel seismic system on the RV Araon

The multichannel seismic system on the RV Araon consists of an airgun array, a streamer, two compressors, and survey control systems (Fig. 3.1). The airgun array has eight airguns (Sercel G-Gun II) and a float that maintains the source depth at 6 m below the surface of the water (Figs 3.2, 3.3 and 3.4). Airguns release compressed air into the water resulting in an acoustic wave that is used as the source wave for the multichannel seismic survey. The airguns have the following volumes: two 250 $in^3$, two 200 $in^3$, two 90 $in^3$ and two 60 $in^3$. The total volume of the source is 1,200 $in^3$ (~19.7 L). A 1.5-km solid-type streamer (Sercel Sentinel) consists of ten sections which record reflected waves and other signals such as direct wave, refracted wave and background noise using hydrophones in the streamer. The group interval and channel number of the streamer are 12.5 meter and 120 channels, respectively. Total length of the streamer is 1.76 km including the tail buoy, two fluid sections and the lead-in cable. Seven cable levelers (birds) were attached on the streamer at every 150 m or 300 m to stabilize the streamer depth in the water (Fig. 3.5).

The seismic compressor generates compressed air and provides high-pressured air into the airguns. The RV Araon has one compressor for normal operations and a second compressor for back-up. The working pressure is maintained as a 150 bar (~2030 psi) during seismic data surveying. A seismic control system installed in the main dry lab consists of a navigation control system, an airgun controller, a bird controller, a recording system, a quality control system and a navigation editing system (Fig. 3.6).

The navigation system (EIVA NaviPac) controls position along the seismic lines and the event type, shooting interval, event start/stop with the gun controller and recording system. The airgun controller (RTS-Real Time Systems Bigshot) receives the event signal from the NaviPac and sends trigger signals to airguns. The Bigshot system displays the shooting-timing, quality and wave shape of all airguns. The bird controller defines streamer depth and displays the location, heading and status of the individual birds. The recording system, (Sercel Baby Seal) records all seismic data and copies the data to the final storage system. The quality control system (Sercel e-SQC pro) displays the real time data such as shot gather and near trace gather. The navigation editing system (EIVA NaviEdit) transforms the NaviPac survey files to standard navigation files such as UKOOA P1/90.

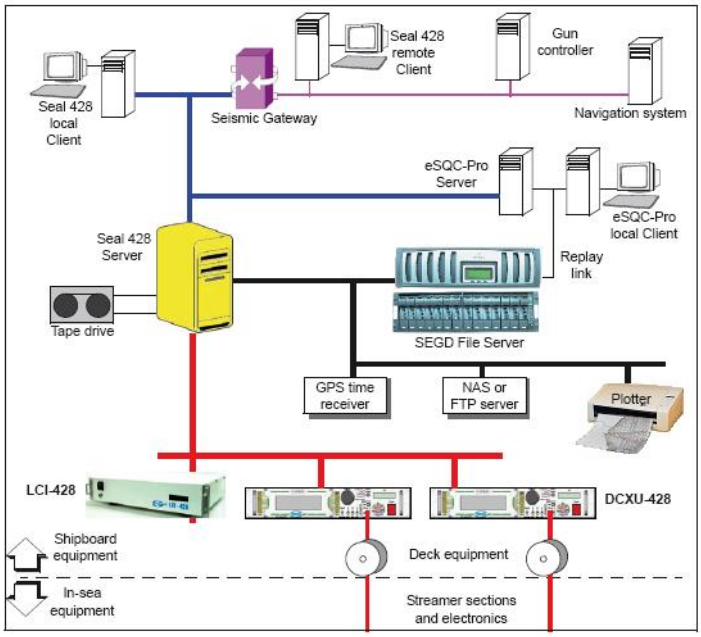


**Figure 3.1 - Schematic diagram of the multichannel seismic system on the RV Araon.**

**Figure 3.2 - Airguns attached to the airgun array.**

**Figure 3.3 - Deployment of the airgun array.**

**Figure 3.4 - Airgun array is launched on the sea. A float (red color tube) maintains the source depth at 6 m in the water.**

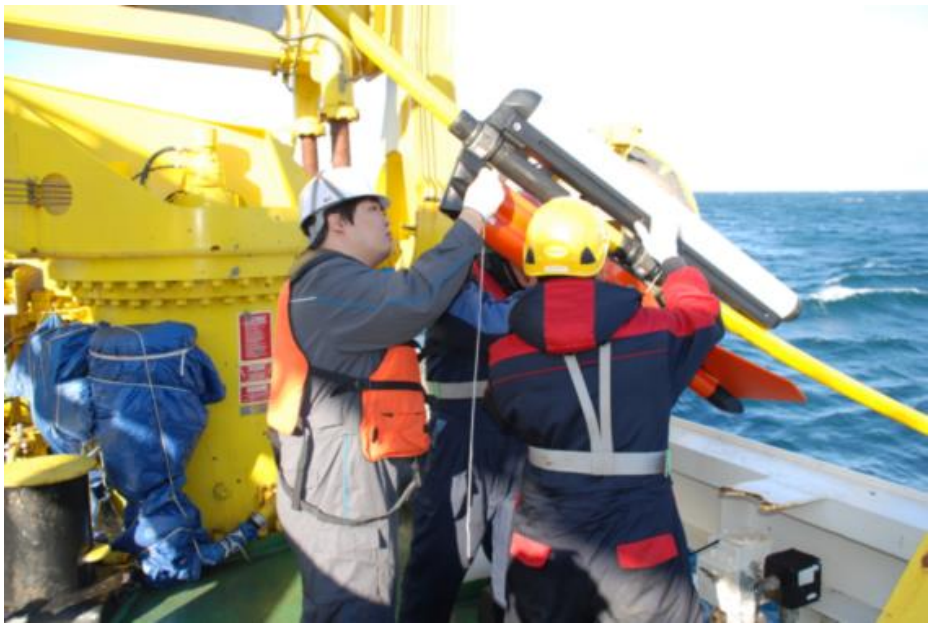

**Figure 3.5 - Launching the streamer. The cable leveler (bird) is attached and tested on the streamer.**

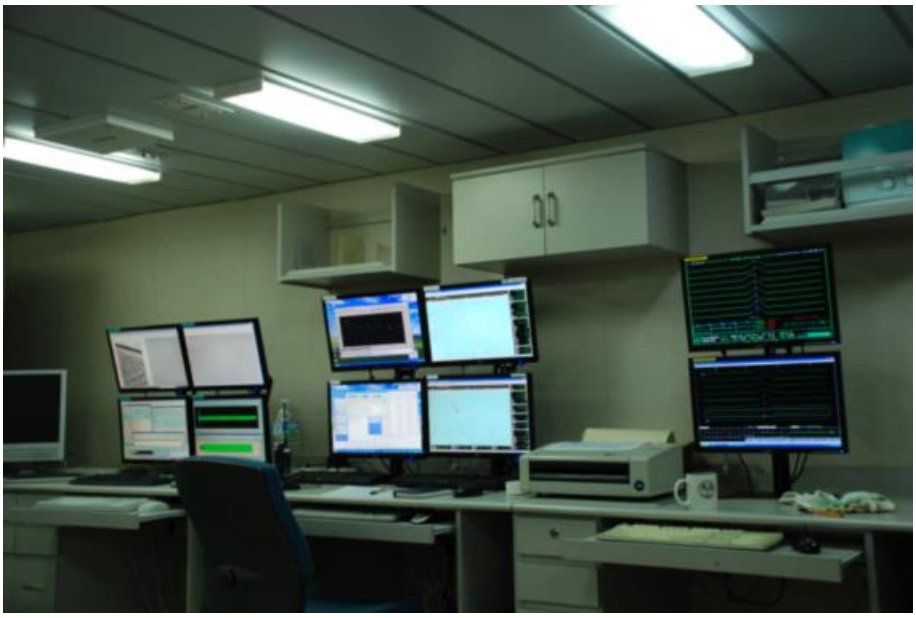

**Figure 3.6 - The seismic survey control system in the Main Dry Lab. Navigation, airgun controller, bird controller, recording system and quality control system are shown.**

### 3.2.2. Acquisition parameters

Table 3.1 shows the acquisition parameters of the multichannel seismic survey during Expedition ARA05C. The shooting interval was 50.0 m for most survey lines. Considering a group interval of 12.5 m and 120 channels, a fifteen-fold common-mid-point gather was achieved. Working pressure was about 150 bars. The source depth was 6 m and the streamer depth was set at the same value as the source depth. However, these depths can be slightly variable with weather conditions, currents, and ship speed. Record length and sampling rate were set as 10.0 s and 1 ms, respectively. The recorded data file format was SEG-D. Figure 3.7 shows

field configurations in this seismic survey.

**Table.3.1 - Seismic acquisition parameters.**

| | |
|---|---|
| Shot Interval | 50.0 m |
| Channel Number | 120 |
| Group Interval | 12.5 m |
| Source Depth | 6 m |
| Streamer Depth | 6 m |
| Fold of Coverage | 15 folds |
| Working Pressure | 150 bar |
| Recording Length | 10.0 s |
| Sample Rate | 1 ms |
| Tape Format | SEG-D |

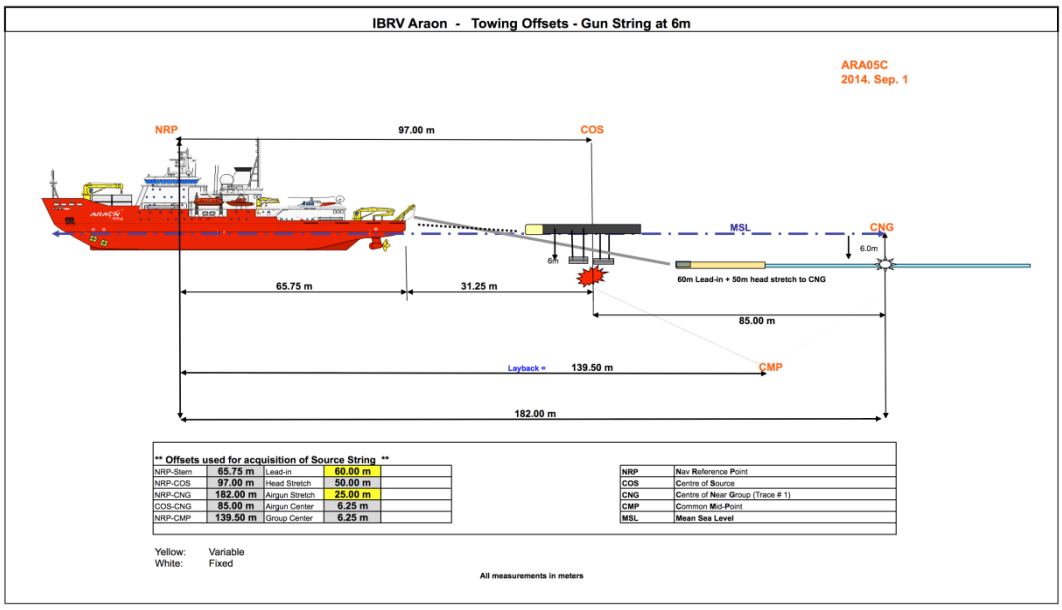


**Figure 3.7 - Field acquisition parameters and layouts.**

## *3.3. Results*

### 3.3.1. Data acquisition

The multichannel seismic data collected during Expedition ARA05C consist of 23 survey lines (20 lines and 3 short transit lines), 998 line-km and 19,962 shot gathers (Table 3.2, Fig. 3.8) from 2nd September to 13th September. The first twenty lines were collected in the Main Seismic Area while the last three lines were acquired in the Western Seismic Area. Some planned survey lines were modified due to proximity to RV Amundsen, weather and sea ice conditions. We collected the first five seismic lines (ARA05C-SS-01 to ARA05C-SS-05) from 2nd to 3rd September. A juvenile bowhead whale entered the 1,000 m radius safety zone, therefore all airguns were turned off for 1.5 hours while the whale cleared the zone resulting in a gap in the shooting sequence in line ARA05C-SS-04. All guns fired well and working pressure was maintained at 150 bar during the first collection period. The total volume of the airgun array was kept 1,200 $in^3$ and the acquired data show nice shot gathers with clear reflections. We retrieved the airgun array and the streamer after ARA05C-SS-05 on 3rd September. We acquired the subsequent fifteen seismic lines from 8th to 10th September. During the recording ARA05C-SS-11, gun #2 with 250 $in^3$ was misfiring, therefore it was turned off resulting in a volume of 950 $in^3$. Due to sea ice conditions, survey lines ARA05C-SS-09, 13, 14, were modified from the original acquisition plan.

**Table 3.2 - Seismic survey line log.**

| Line Name | SOL (Start of Line) | | | | | | | EOL (End of Line) | | | | | | | FGSP | LGSP |
|---|---|---|---|---|---|---|---|---|---|---|---|---|---|---|---|---|
| | SP | Date | Time | Latitude (- / South) | | Longitude (- / West) | | SP | Date | Time | Latitude (- / South) | | Longitude (- / West) | | | |
| ARA05C-SS-01 | 1001 | 2014-09-02 | 03:03:33 | 70.509576 | 70 30.5746 | -134.395013 | -134 23.7008 | 2850 | 2014-09-02 | 13:00:52 | 71.220395 | 71 13.2237 | -135.605767 | -135 36.3460 | 1003 | 2848 |
| ARA05C-SS-02 | 2862 | 2014-09-02 | 14:18:35 | 71.187900 | 71 11.2740 | -135.636357 | -135 38.1814 | 3307 | 2014-09-02 | 16:42:51 | 71.273987 | 71 16.4392 | -135.090929 | -135 05.4557 | 2865 | 3273 |
| ARA05C-SS-03 | 3308 | 2014-09-02 | 17:27:01 | 71.285447 | 71 17.1268 | -135.180022 | -135 10.8013 | 5380 | 2014-09-03 | 04:16:51 | 70.451241 | 70 27.0745 | -134.043227 | -134 02.5936 | 3344 | 5324 |
| ARA05C-SS-04 | 5381 | 2014-09-03 | 05:57:10 | 70.415626 | 70 24.9376 | -134.384226 | -134 23.0536 | 5531 | 2014-09-03 | 06:45:22 | 70.406747 | 70 24.4048 | -134.577830 | -134 34.6698 | 5381 | 5498 |
| ARA05C-SS-05 | 5532 | 2014-09-03 | 06:45:52 | 70.406990 | 70 24.4194 | -134.579712 | -134 34.7827 | 7463 | 2014-09-03 | 17:04:32 | 71.048464 | 71 02.9078 | -136.250708 | -136 15.0425 | 5555 | 7432 |
| ARA05C-SS-06 | 7468 | 2014-09-08 | 01:10:35 | 70.657397 | 70 39.4438 | -135.763156 | -135 45.7894 | 8285 | 2014-09-08 | 05:44:07 | 70.379485 | 70 22.7691 | -135.080881 | -135 04.8529 | 7510 | 8148 |
| ARA05C-SS-07 | 8286 | 2014-09-08 | 07:25:12 | 70.446023 | 70 26.7614 | -135.064814 | -135 03.8888 | 9063 | 2014-09-08 | 11:35:00 | 70.306539 | 70 18.3923 | -135.989311 | -135 59.3587 | 8290 | 9063 |
| ARA05C-SS-08 | 9065 | 2014-09-08 | 13:35:37 | 70.292619 | 70 17.5571 | -135.766219 | -135 45.9731 | 9960 | 2014-09-08 | 18:25:31 | 70.577150 | 70 34.6290 | -136.567480 | -136 34.0488 | 9162 | 9946 |
| ARA05C-SS-09 | 9961 | 2014-09-08 | 18:26:16 | 70.576860 | 70 34.6116 | -136.570113 | -136 34.2068 | 10114 | 2014-09-08 | 19:16:26 | 70.543596 | 70 32.6158 | -136.744754 | -136 44.6852 | 9972 | 10114 |
| ARA05C-SS-10 | 10118 | 2014-09-08 | 19:23:32 | 70.535492 | 70 32.1295 | -136.756053 | -136 45.3632 | 10407 | 2014-09-08 | 20:59:25 | 70.439994 | 70 26.3996 | -136.507125 | -136 30.4275 | 10120 | 10377 |
| ARA05C-SS-11 | 10412 | 2014-09-08 | 21:02:18 | 70.438443 | 70 26.3066 | -136.496304 | -136 29.7782 | 12449 | 2014-09-09 | 07:47:47 | 70.893278 | 70 53.5967 | -134.178805 | -134 10.7283 | 10430 | 12440 |
| ARA05C-SS-12 | 12450 | 2014-09-09 | 07:48:04 | 70.893705 | 70 53.6223 | -134.179345 | -134 10.7607 | 12762 | 2014-09-09 | 09:25:10 | 71.019158 | 71 01.1495 | -134.346122 | -134 20.7673 | 12460 | 12762 |
| ARA05C-SS-13 | 12763 | 2014-09-09 | 09:26:20 | 71.020067 | 71 01.2040 | -134.349923 | -134 20.9954 | 12952 | 2014-09-09 | 10:31:57 | 70.982579 | 70 58.9547 | -134.578023 | -134 34.6814 | 12775 | 12952 |
| ARA05C-SS-13T | 12954 | 2014-09-09 | 10:32:47 | 70.981506 | 70 58.8904 | -134.579338 | -134 34.7603 | 13091 | 2014-09-09 | 11:20:54 | 70.921106 | 70 55.2664 | -134.587996 | -134 35.2798 | 12955 | 13091 |
| ARA05C-SS-14 | 13092 | 2014-09-09 | 11:21:12 | 70.920873 | 70 55.2524 | -134.589187 | -134 35.3512 | 14339 | 2014-09-09 | 17:50:02 | 70.646218 | 70 38.7731 | -136.024463 | -136 01.4678 | 13102 | 14284 |
| ARA05C-SS-14T | 14340 | 2014-09-09 | 17:50:59 | 70.644922 | 70 38.6953 | -136.024162 | -136 01.4497 | 14636 | 2014-09-09 | 19:49:28 | 70.610046 | 70 36.6028 | -135.652660 | -135 39.1596 | 14340 | 14636 |
| ARA05C-SS-15 | 14637 | 2014-09-09 | 20:05:05 | 70.630287 | 70 37.8172 | -135.671902 | -135 40.3141 | 15262 | 2014-09-09 | 23:13:18 | 70.845205 | 70 50.7123 | -136.184159 | -136 11.0495 | 14640 | 15262 |
| ARA05C-SS-16 | 15263 | 2014-09-10 | 00:19:42 | 70.854576 | 70 51.2746 | -135.998226 | -135 59.8936 | 16543 | 2014-09-10 | 07:07:52 | 70.412333 | 70 24.7400 | -134.959218 | -134 57.5531 | 15266 | 16540 |
| ARA05C-SS-16T | 16594 | 2014-09-10 | 07:35:24 | 70.380833 | 70 22.8500 | -134.986491 | -134 59.1895 | 16762 | 2014-09-10 | 08:28:23 | 70.400726 | 70 24.0436 | -135.197376 | -135 11.8426 | 16598 | 16760 |
| ARA05C-SS-17 | 16764 | 2014-09-10 | 10:01:05 | 70.429910 | 70 25.7946 | -135.158416 | -135 09.5050 | 17803 | 2014-09-10 | 15:36:11 | 70.610116 | 70 36.6070 | -133.907749 | -133 54.4649 | 16701 | 17803 |
| ARA05C-SS-18 | 17804 | 2014-09-13 | 00:57:01 | 70.322537 | 70 19.3522 | -136.991595 | -136 59.4957 | 19152 | 2014-09-13 | 08:06:52 | 70.014033 | 70 00.8420 | -138.474672 | -138 28.4803 | 17840 | 19152 |
| ARA05C-SS-19 | 19153 | 2014-09-13 | 08:07:18 | 70.014184 | 70 00.8510 | -138.476272 | -138 28.5763 | 20462 | 2014-09-13 | 14:58:31 | 70.480590 | 70 28.8354 | -139.459768 | -139 27.5860 | 17159 | 20434 |
| ARA05C-SS-20 | 20463 | 2014-09-13 | 14:58:49 | 70.480947 | 70 28.8568 | -139.460021 | -139 27.6013 | 20961 | 2014-09-13 | 17:39:11 | 70.692451 | 70 41.5470 | -139.299194 | -139 17.9516 | 20480 | 20874 |

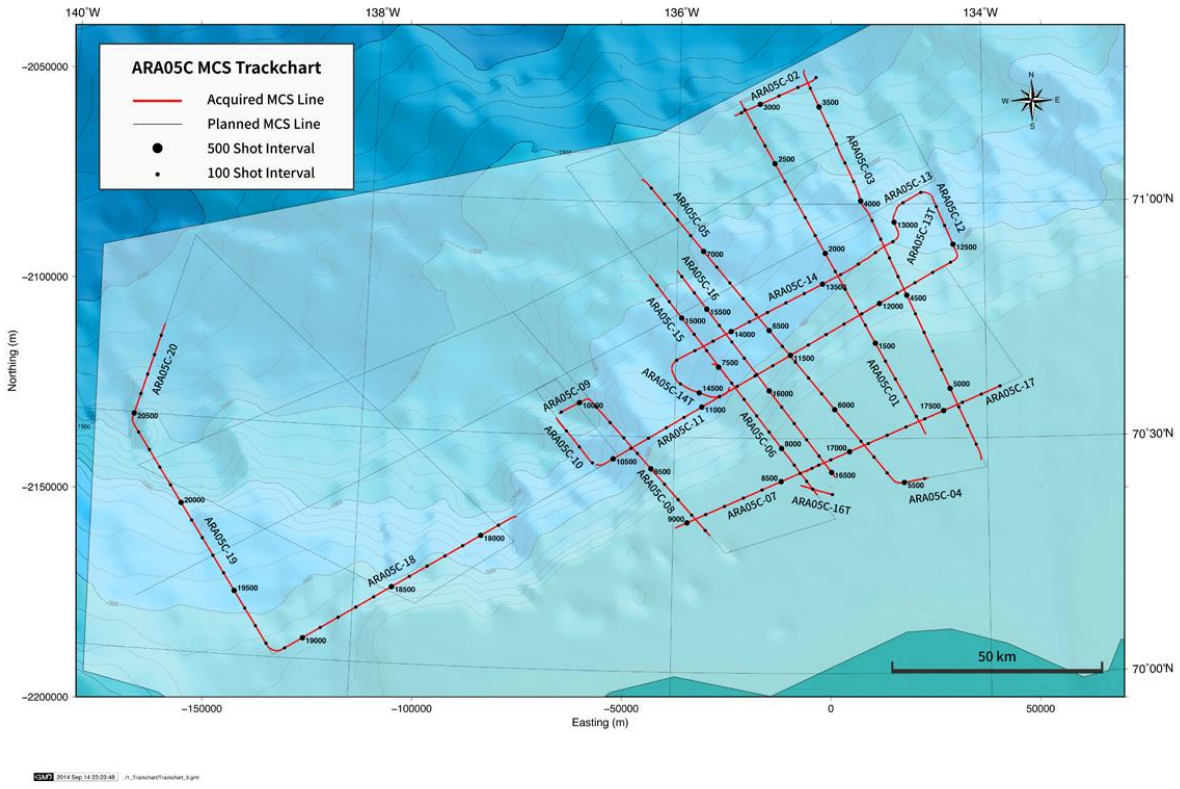


**Figure 3.8 - Track chart of the seismic survey of Expedition ARA05C.**

We collected the final three seismic lines in the Western Seismic Area from 12$^{th}$ to 13$^{th}$ September. The data collection started with ARA05C-SS-18. Airgun #4 had a problem with a bad timing signal so we used a seven airgun configuration with the total volume of 1,000 in$^3$. We acquired seismic data along ARA05C-SS-19, which crosses two sites in IODP pre-proposal #753, with good recording conditions. An air leak developed during the acquisition of ARA05C-SS-20 therefore the seismic survey was concluded at 17:39 on September 13, 2014 as the weather was deteriorating.

### *3.3.2. Data processing and analysis*

Some portions of the acquired seismic data were processed onboard to generate a brute-stack with the seismic data processing software (GEDCO VISTA 10.0). The seismic data processing sequence consists of SEG-D file reading, band-pass filtering, recording delay correction, geometry setting, velocity analysis, normal move out (NMO) correction, and common mid-point (CMP) stacking. Due to very shallow water depth of around 60 m over the majority of the continental shelf in the study area, the direct wave and refracted waves overlapped with primary reflection signals.

The seismic profile ARA05C-SS-05 crosses the shelf edge and slope and shows deep structure and chaotic stratigraphy (Fig. 3.9). High-amplitude seafloor multiples make it difficult to interpret sedimentary sequences and detailed stratigraphy beneath the seafloor. Specialized processing techniques, such as SRME or tau-p transform, are required to remove very strong

multiples. In the deeper part of the section, however, folds and fault structures are clearly shown. In the slope region, major seismic horizons show the characteristics of discontinuity by faults and mud volcanos. The stratigraphy on the slope region may indicate a chaotic paleo-depositional environment.

The seismic profile ARA05C-SS-19 acquired beginning at the mouth of the Mackenzie Trough captured information on detailed stratigraphy and deeper structure (Fig. 3.10). The seismic horizons show good continuities and fold and fault structures beneath the prominent unconformity in the profile. A chaotic and transparent sedimentary sequence is deposited above the unconformity.

For more accurate and detailed seismic sequence interpretation, specialized processing sequences such as multiple attenuation, deconvolution, and migration will be applied after this cruise.

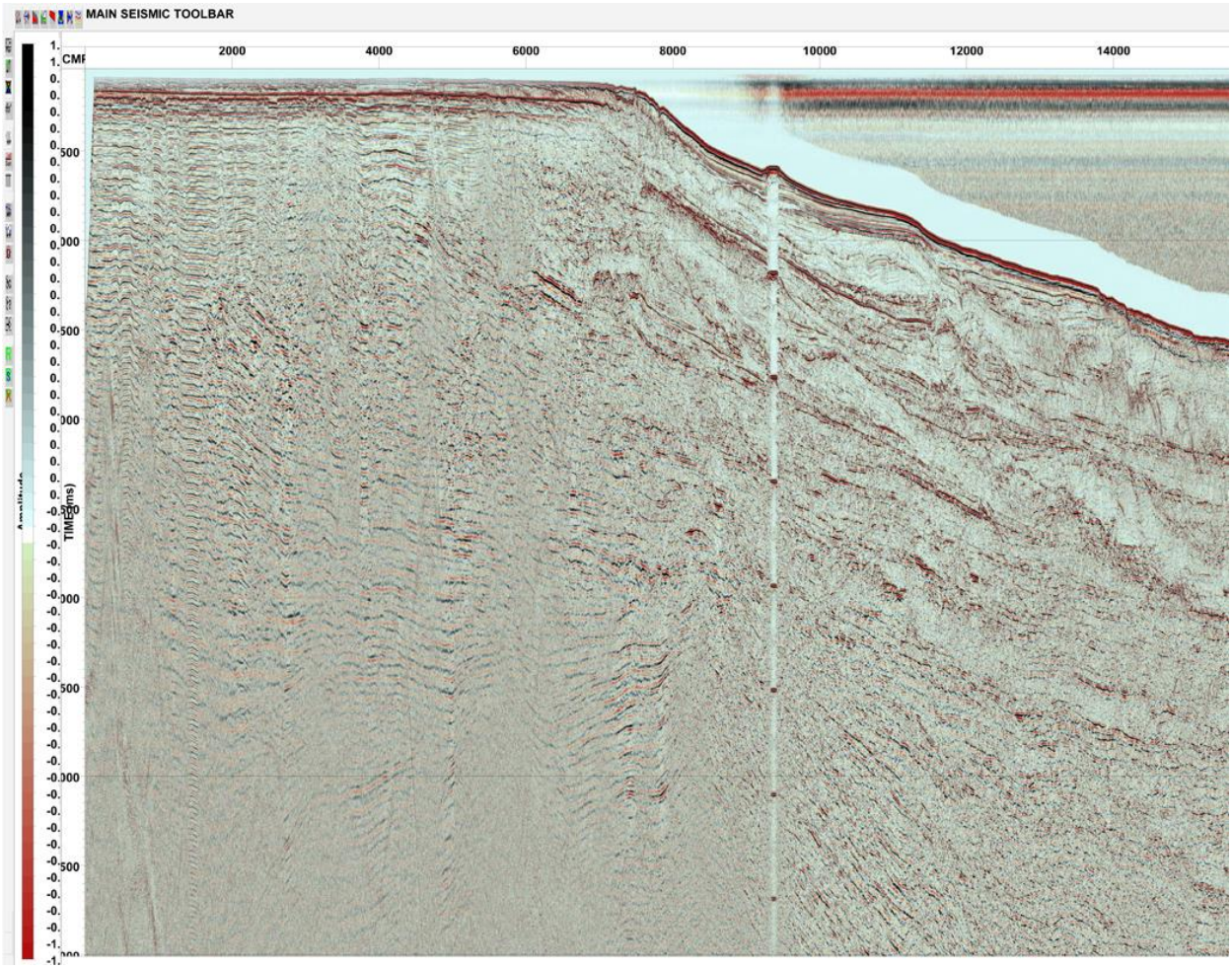


**Figure 3.9 - A brute stack section of ARA05C-SS-05.**

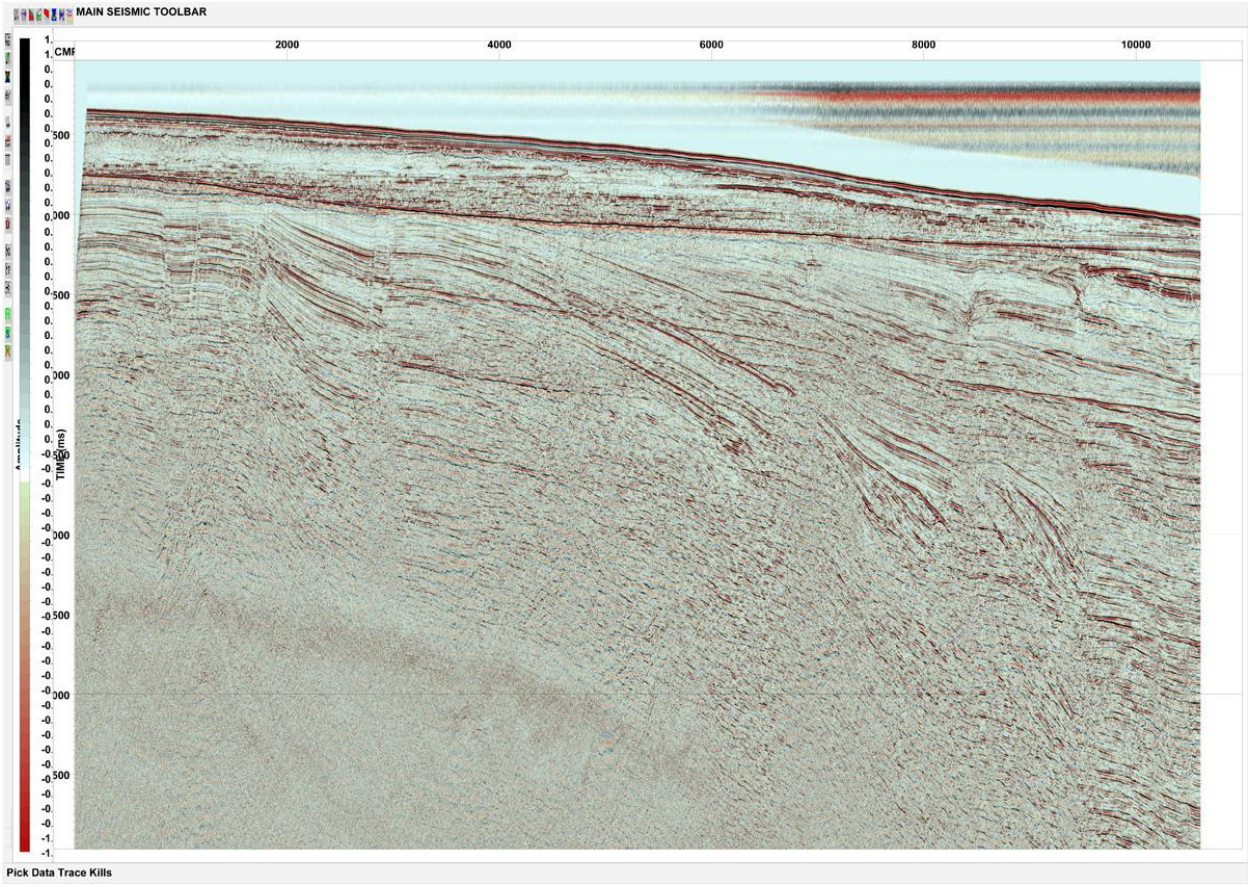


**Figure 3.10 - A brute stack section of ARA05C-SS-19.**

## *3.4. Summary*

Multichannel seismic data were acquired on the outer continental shelf of the Beaufort Sea with 23 seismic lines with 998 line-km and 19,962 shot gathers during 2-13 September, 2014. All seismic equipment operated well, therefore good-quality seismic data were acquired. Most processed seismic profiles show shallow and deep structures clearly. The seismic data will be used for interpretation of permafrost and gas hydrate occurrence and the paleo-depositional environment.

# CHAPTER 4 - Multibeam survey

**H.J. Kim, J.K. Hong, I. Lee and C. Kim**

## *4.1. Introduction*

A swath bathymetry survey was conducted utilizing an EM122 multibeam echosounder. Data acquisition was continued for the whole period of the cruise and the survey area is limited to the international waters in the Beaufort Sea. Sound velocity profiles are updated frequently using the profiles obtained from CTD casting. Acquired bathymetry data were processed onboard using CARIS HIPS&SIPS 7.0 version, a specialized bathymetry processing software, and the results are plotted using Generic Mapping Tools (GMT) software.

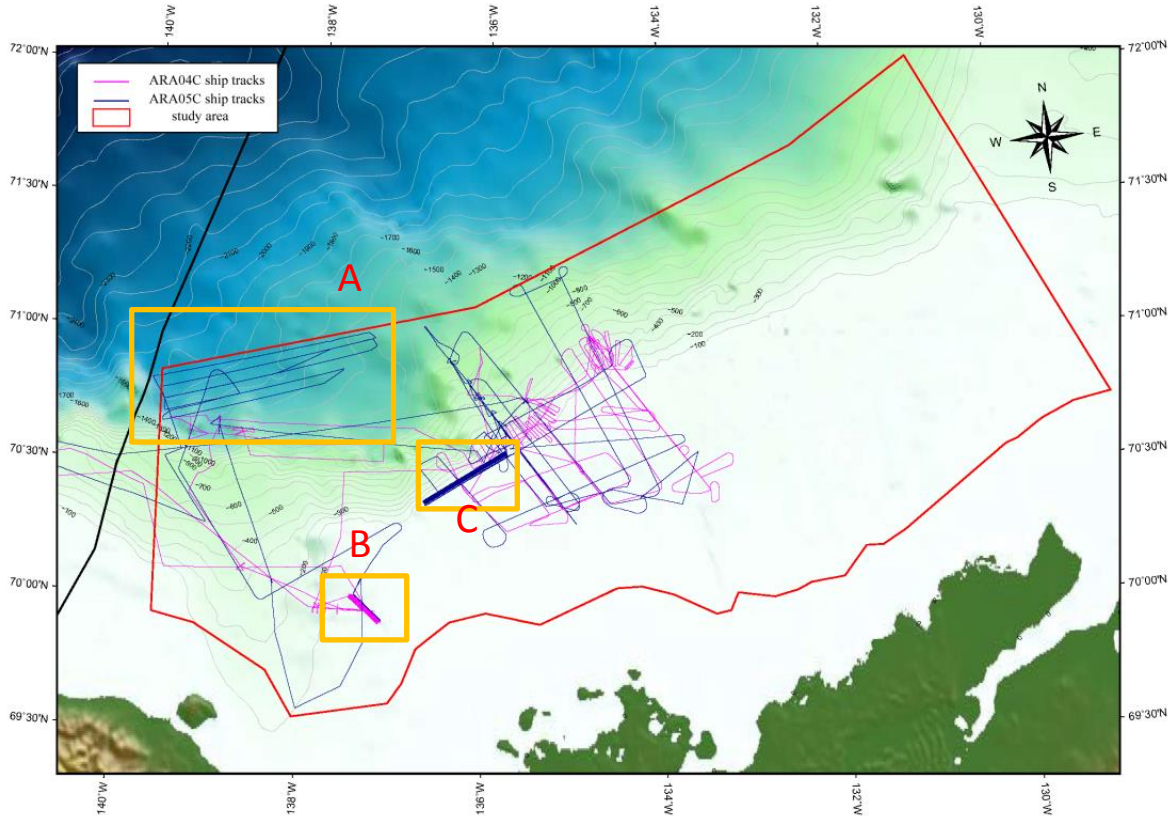


**Figure 4.1 - This figure is shown the ARA04C and ARA05C vessel tracks. Magenta line is ARA04C, blue line is ARA05C. Area A is Northwestern area. Area B is known for many pingo-like features (PLFs), also referred to as "Gary Knolls". Area C is Shallow Edge.**

The major purposes of the multibeam survey are to aid in the regional bathymetric mapping of the study zone, reveal unknown features not previously mapped, and to confirm specific seafloor morphological features of target areas recognized through earlier studies. Processed seafloor bathymetric images were also utilized to determine sites of geological sampling and heat flow measurement. Some of the processed data will also contribute to the international bathymetry data sets (i.e., International Bathymetric Chart of the Arctic Ocean (IBCAO), and General Bathymetric Chart of the Ocean (GEBCO)).

During the survey, recording errors occurred mainly due to malfunctions of the supporting navigation system (Seapath system). When a navigation error occurred, the operator station could not calculate water depth correctly due to wrong navigation information. In most cases the navigation error recovered automatically after several minutes, but sometimes the problem required rebooting of the system, resulting in data gaps of approximately one hour.

### *4.2 - System description & data acquisition*

The multibeam system consists of a hull-mounted transmit and receive transducer, transceiver unit, and operator station (Fig 4.2). EM122 has a wide beam angle (-70 ~ +70 degrees) and a capability of measuring into the deep ocean up to 11,000 meters. The technical specifications of EM122 are listed in Table 4.1.

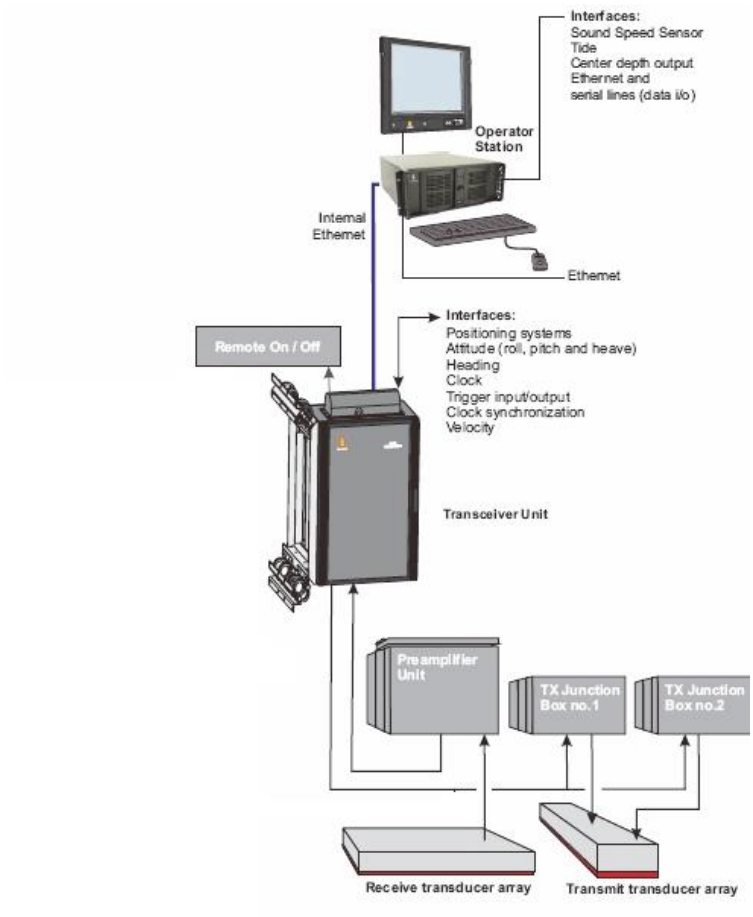


**Figure 4.2 - System diagram of EM122 multibeam system.**

**Table 4.1 - Technical specifications of EM122.**

| | | |
|---|---|---|
| Operating frequency | | 12 kHz |
| Depth range | | 20 – 11000 m |
| Swath width | | 6 × Depth, to approx 30 km |
| Pulse forms | | CW and FM chirp |
| No. of beams | | 288 |
| Swath profiles per ping | | 1 or 2 |
| Motion compensation | Yaw | ± 10 degrees |
| | Pitch | ± 10 degrees |
| | Roll | ± 15 degrees |
| Sounding pattern | | Equi-distant on bottom/equiangular |
| Depth resolution of soundings | | 1 cm |
| High resolution mode | | High Density processing |
| Side lobe suppression | | -25 dB |
| Modular design, beam width | | 0.5 to 4 degrees |

## *4.3. Preliminary results*

### 4.3.1. Northwestern area

This area (Fig. 4.3) is the deepest part in the permitted survey area. During the survey, we experienced strong wind more than 40 knots so that acquired data along SW-NE direction were of poor quality. We designed survey tracks in a NE-SE direction to cover the whole area. Three recording gaps are found due to instrument error.

Newly acquired data were compiled with existing data acquired in 2013. Two noticeable ridges are found in the western part of the figure. The full interpretation will be conducted after the cruise.

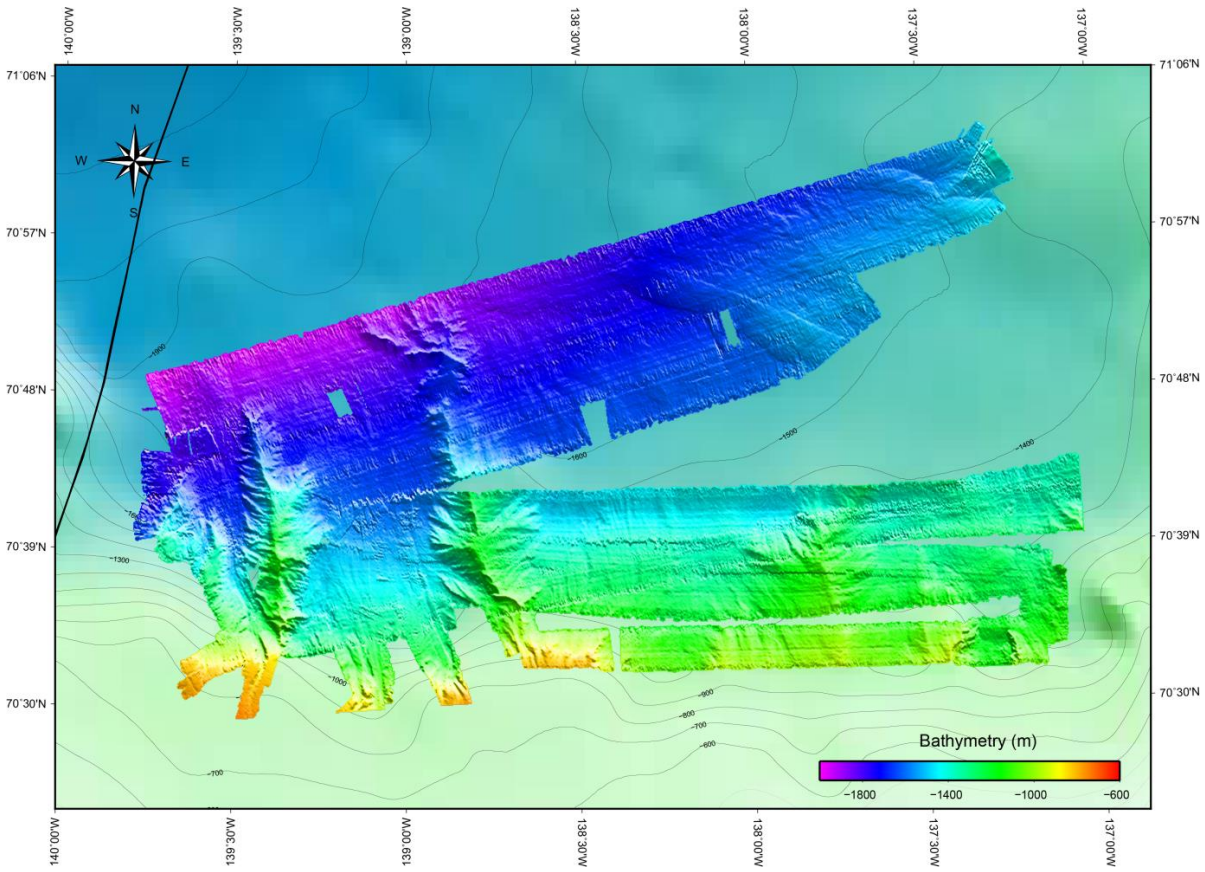


**Figure 4.3 - Bathymetry map showing northwestern part of the study area.**

### 4.3.2 Gary Knolls

After completing the planned station work, we had several hours before starting the seismic survey. Therefore we designed an additional multibeam survey on the PLFs area (Fig. 4.4) to complement data collected in 2013. Two lines of data were added to the existing data. In 2014, we applied different acquisition parameters to obtain a coarser horizontal resolution than the previous year. The main reason for this is to reduce data volume to prevent very slow post-processing. Even though the data have coarser resolution, we can clearly find a topographic high in the southeastern part of the area.

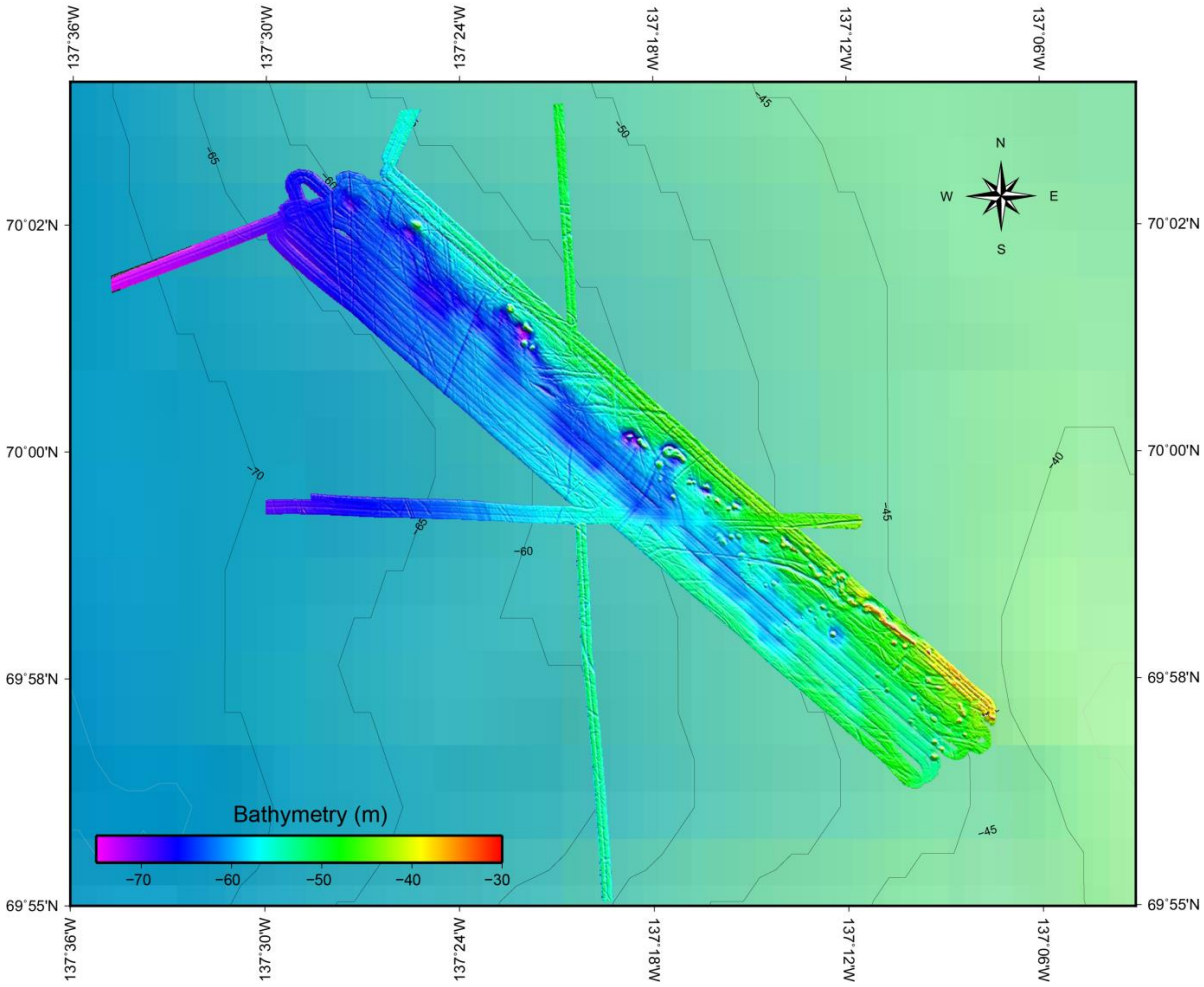


**Figure 4.4 - Bathymetry map showing the PLFs area.**

### 4.3.3. Shallow Edge

On September 5 and 6, we experienced strong winds so we conducted a multibeam survey. Multibeam data were noisy due to waves and swells. This area was not surveyed yet so the data will be added to main data library. Topography is generally flat and we can find many scars ploughed by icebergs (Fig. 4.5).

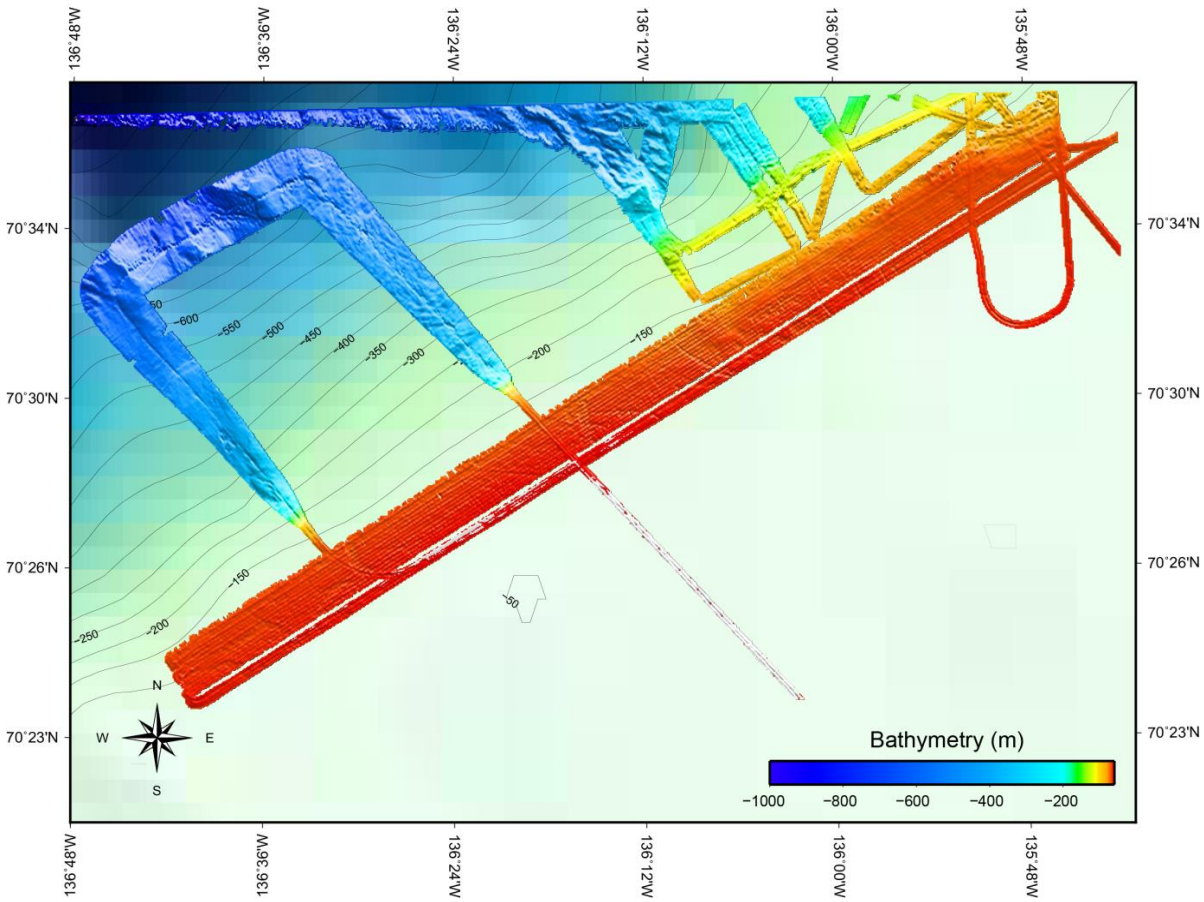


**Figure 4.5 - Bathymetry map showing the shelf edge.**

# CHAPTER 5 - Sub-bottom profiler (SBP) survey

J.K. Hong, H.J. Kim, I. Lee and C. Kim

## *5.1. Introduction*

Subsurface images obtained from sub-bottom profiler (SBP) show precise sediment structure below the surface. Conventional SBP equipment transmits 3.5 KHz acoustic signals and receives reflections. The resolution of SBP is the highest among other reflection methods such as Sparker, Boomer, and air-gun seismic instruments. Theoretically, SBP has vertical resolution of up to 10 cm, depending on the sediment P-wave velocity structure. In most cases, vertical resolution is ~0.5 m.

In the survey area of the Canadian Beaufort Sea, many subsurface structures are closely related to the geologic evolution of permafrost, gas expulsion, landslides and slumps. Sub-bottom images will provide additional insight on these features. Sub-bottom images are also utilized to define the optimum site for sediment coring, CPT and heat flow measurements.

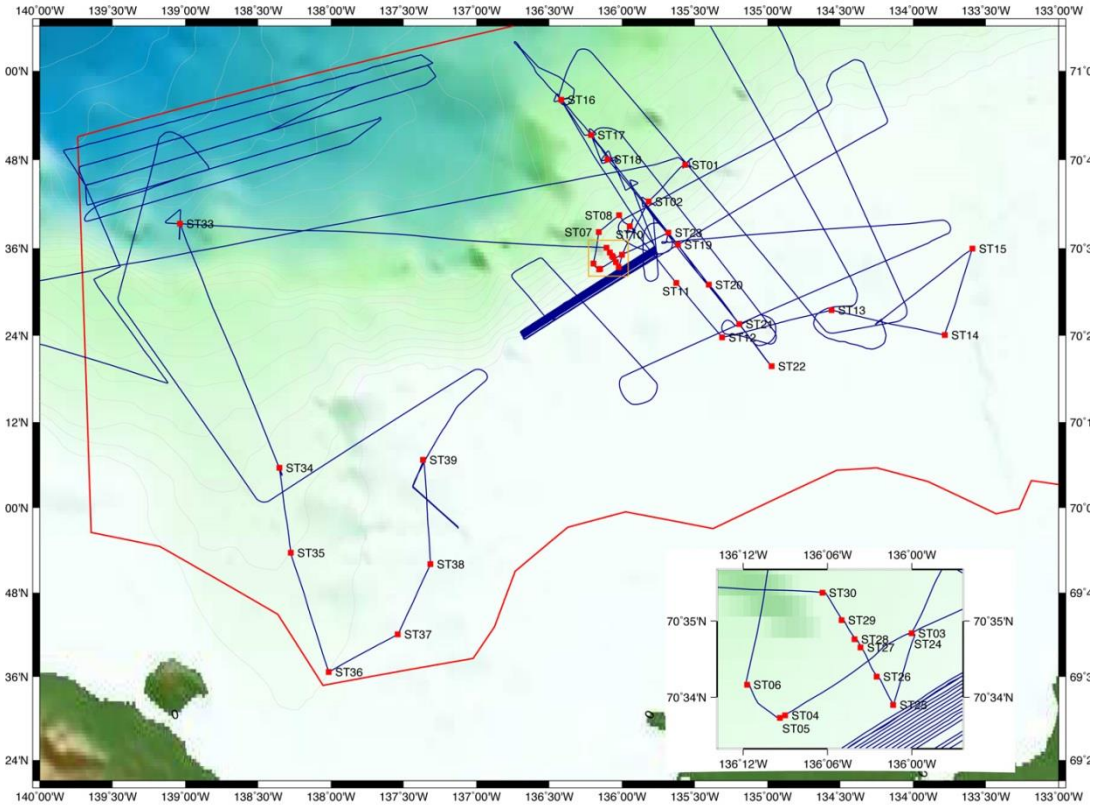


**Figure 5.1 - Ship track chart of the Expedition ARA05C showing all stations. SBP data were recorded when the vessel moved along survey lines, but was stopped when the vessel was on station for coring, CTD, CPT, and heat flow measurements.**

### *5.2. System Description*

The SBP120 sub-bottom profiler installed on the RV Araon is an optional extension to the EM122 multibeam echo sounder. Figure 5.2 shows the SBP system diagram.

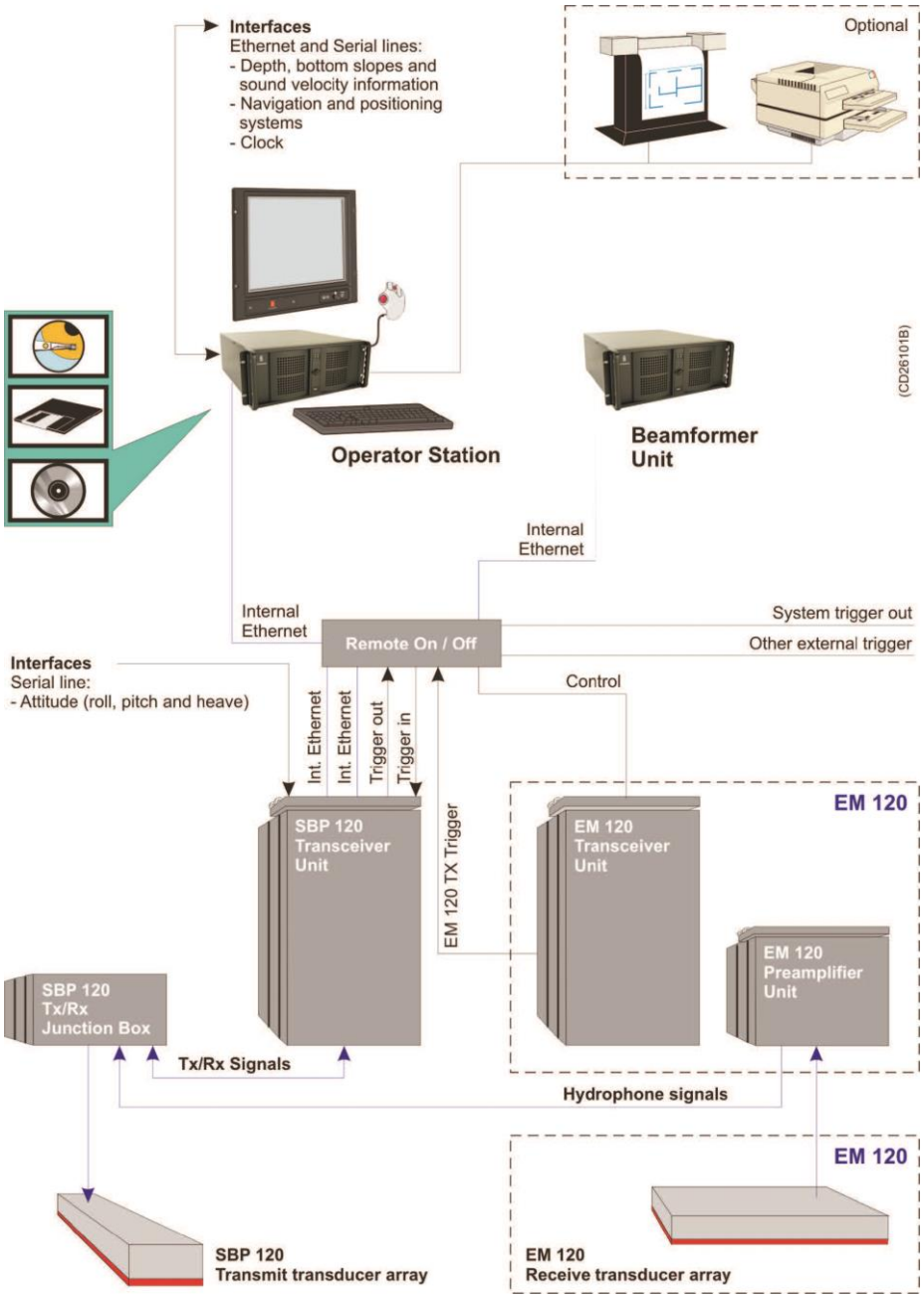


**Figure 5.2 - SBP 120 system units and interfaces.**

The receiving transducer hydrophone array used by the EM122 multibeam system is a broadband system; by adding a separate low frequency transmitting transducer and electronic cabinets and operator stations, the EM122 can be extended to include the sub-bottom profiling capability, as provided by the SBP120. System beamwidth is 12 degrees with 24 transducers, equivalent to a footprint of 20 m in 100 m water depth (or 20% of water depth).

The frequency range of the SBP120 is 2.5 to 7 kHz. The SBP120 beam is electronically stabilized for roll and pitch. It can also be steered to take into account bottom slope. The ping rate is synchronized to that of the multibeam echo sounder transmitter if both are running simultaneously.

The data produced by SBP120 are logged in the Topas .raw format and can be converted to SEG-Y format that allows post-processing by standard seismic processing software packages. During the ARA04C cruise, we used SBP120 settings as summarized in Table. 5.1.

**Table 5.1 - Setting information of SBP 120 during cruise ARA05C.**

| Used Settings | Value | Unit |
|---|---|---|
| Runtime Parameter | | |
| Transmit mode | normal | |
| Synchronization | Fixed ping rate | ms |
| Acquisition delay | manual& automatic mode | ms |
| Acquisition window | 400 | ms |
| Pulse form | Linear chirp up | |
| Sweep low frequency | 2500 | Hz |
| Sweep high frequency | 6500 | Hz |
| Pulse shape | 80 | % |
| Pulse length | 30 | ms |
| Source power | 0 | dB |
| Beam widths Tx | Normal | |
| Beam widths Rx | Normal | |
| Number of Rx beams | 1 | |
| Beam spacing | 3 | 1 deg |
| Calculate delay from depth | X | |
| Delay hysteresis | 30 | % |
| Bottom screen position | 50 | % |
| Automatic slope corrections | On | |
| Gain | 36 | dB |
| Bottom tracker | | |

| | | |
|---|---|---|
| Window start | 40 | ms |
| Window length | 20 | ms |
| Threshold | 80 | % |
| Time Variable Gain | | |
| TVG control | manual | |

### *5.3. Data acquisition and results*

We experienced recording gaps through the whole cruise resulting in a loss of about 20% of the data. However, the system was still useful for determining core sites and investigating shallow structures. We determined coring sites using SBP results. Figure 5.4 shows SBP images for all coring sites

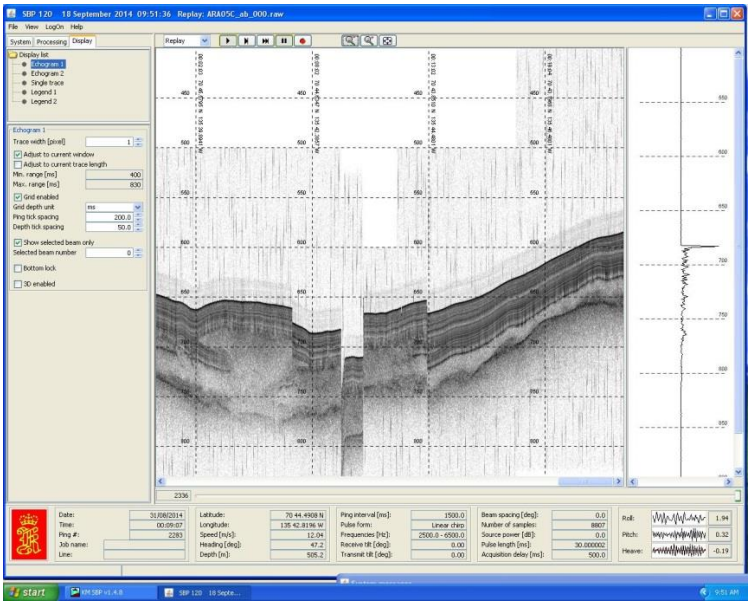

**Figure 5.3 - A Screen image of SBP recorder showing recording gaps. Recording gaps occurred due to an unknown instrumental error and lasted for the whole cruise.**

.

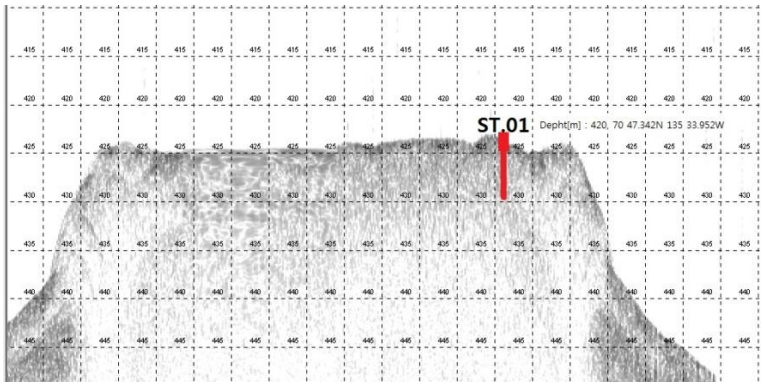
ST.01
Depht[m] : 420, 70 47.342N 135 33.952W

(a)

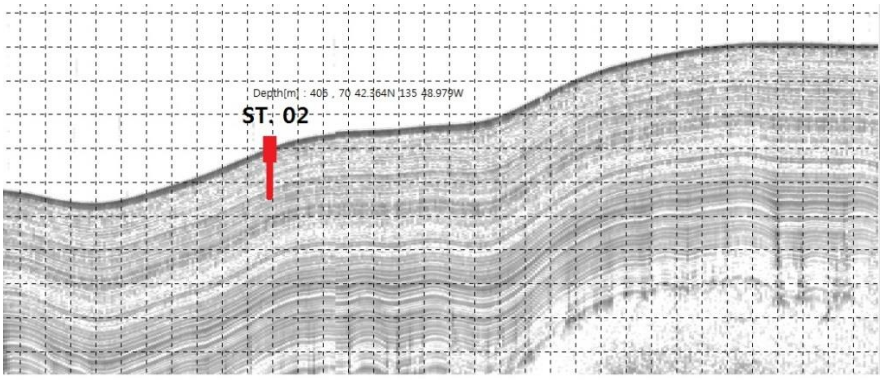
Depth[m] : 405 , 70 42.364N 135 48.979W
ST. 02

(b)

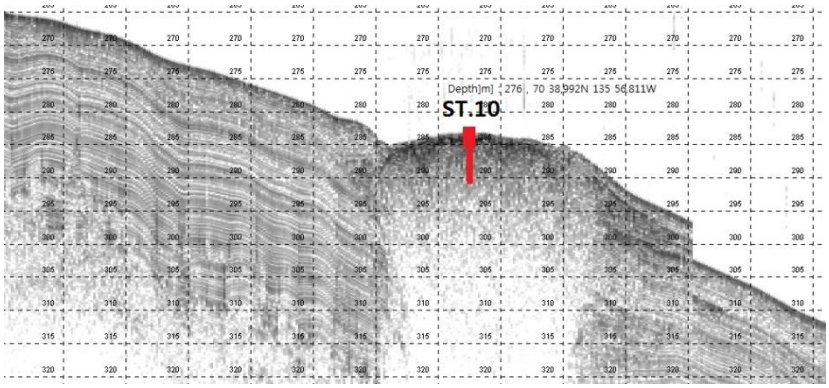
Depth[m] : 276 , 70 38.992N 135 56.811W
ST.10

(c)

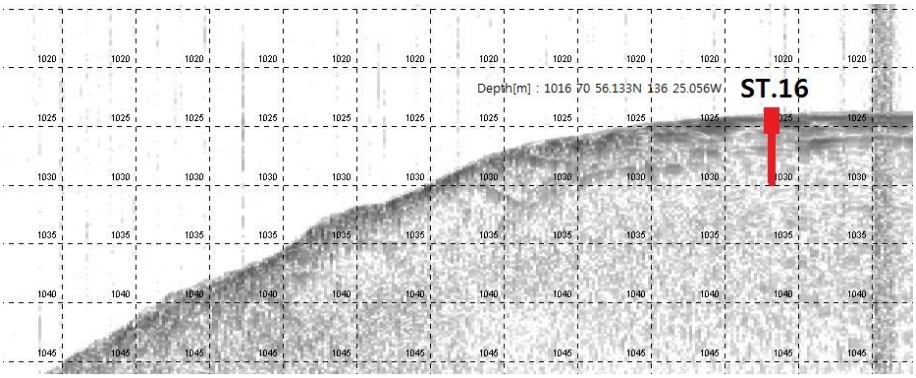
Depth[m] : 1016 70 56.133N 136 25.056W
ST.16

(d)

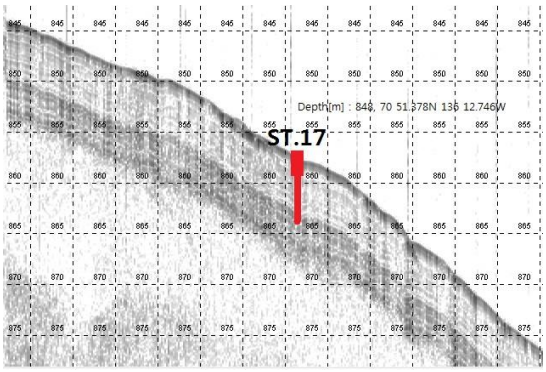


(e)

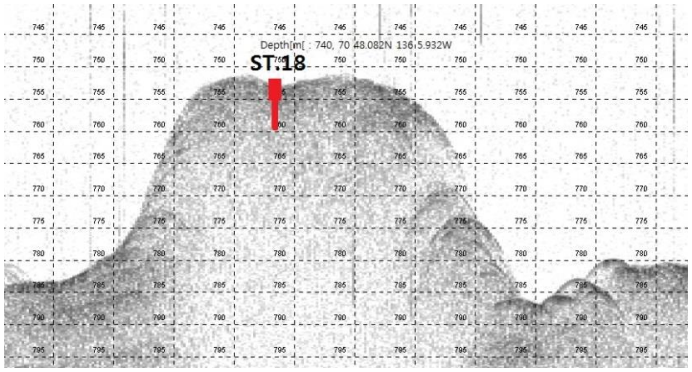


(f)

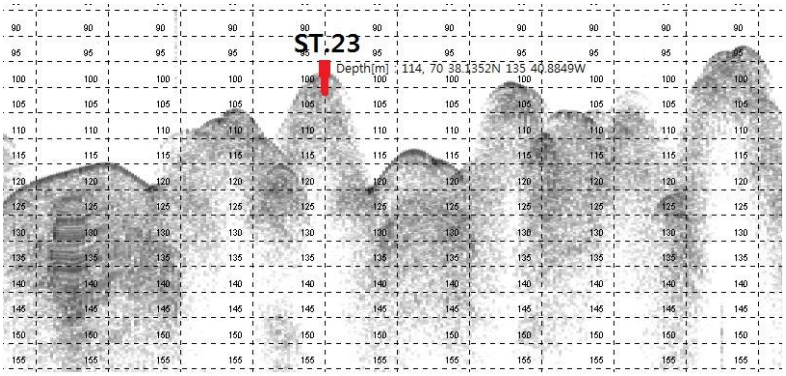


(g)

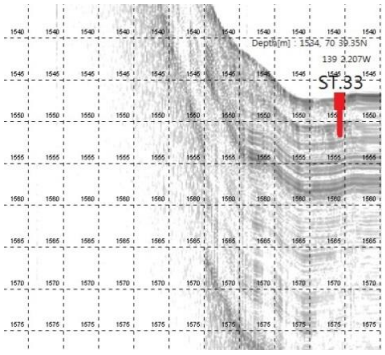


(h)

**Figure 5.4 - SBP images at every core stations. Station numbers and locations are drawn on the image. Red pins are drawn to match the real penetration depth.**

# CHAPTER 6 - Heat flow measurements

**Y.-G. Kim and I. Lee**

## *6.1. Introduction*

Regional heat flow distributions are used to understand the thermodynamics of the Earth's interior as well as surficial process within sediments (e.g., Von Herzen and Uyeda, 1963). Its local distribution may be useful to unravel surficial process such as fluid expulsion from sediments to sea water, and in the detection of ice within sediments, which are expected to occur within the KOPRI study area. Also, defining geothermal gradients is a common approach to estimate the extent of the gas hydrate stability zone (e.g. Yamano et al., 1982; Kim et al., 2010).

During Expedition ARA05C, heat flow measurements were carried out at seven stations to complement data at collected at eight stations during Expedition ARA04C in 2013 (Fig. 6.1; Table 6.1). Three thermal regimes, background, mud volcano, and permafrost area, were defined based on the results of the ARA04C expedition. The main purpose for this work is to collect thermal conductivity data within the KORPI study area as data collection in 2013 was poor as the Lister-type heat probe did not function well in the Arctic conditions.

In this survey, the Lister-type heat probe was used to measure in-situ thermal conductivity as well as geothermal gradients by a single penetration of the probe into the sediments (Table 6.2; Figs 6.2 and 6.3). The probe has mainly been used at two research study sites around Japan and Korea during the past two decades (e.g., Yamano et al., 2008; Kim et al., 2010), but the first attempt during ARA04C provided some confidence that the tool is also useful in polar regions of extremely cold air/water temperature, sea ice, and "sticky" sediments. During the ARA04C expedition, a shock sensor within the data logger, which was designed to detect deceleration when the probe begins to penetrating sediments, did not work properly. Two potential reasons for this malfunction are proposed based on results from the ARA04C and the test cruise in June 2014 in the Ulleung Basin, East Sea: large vibrations (deceleration/acceleration) during deployment from the deck to water, and weak surficial sediments to lead smooth penetration without significant deceleration. In the ARA05C, we have prepared an additional thermal conductivity meter, TK04 thermal conductivity measuring system, to deal with the case where in-situ thermal conductivity was not measured by the probe (Fig. 6.4; Table 6.3).

In order to prevent damage to the probe and to guarantee reliability of the measured data, it is important to choose a site carefully using sub-bottom profiler data obtained prior to any deployment. The dynamic positioning system of the vessel should also be used to maintain station-position during the measurement period (typically 1 hour). The RV Araon fully satisfies these conditions with providing high quality sub-bottom profiler data (See Chapter 5) and dynamic positioning with less than a few meters deviation from the intended location during the heat flow survey.

## *6.2. Method*

### 6.2.1. Lister-type heat flow probe

Marine heat flow is determined by two physical properties: geothermal gradient within a sediment section and thermal conductivity of sediments penetrated. Marine heat flow is observed mainly by inserting a heat probe, which consists of a frame (weight and barrel) and electrical parts (sensors, data logger, and thermistors), into sediments several meters below the seafloor (Fig. 6.2). In general, the data logger containing several kinds of sensor is inserted into the top-weight, and thermistors are attached to the barrel connected below the top-weight. Thus, deployment of the heat probe is very similar to that of a gravity corer.

As with the previous expedition (ARA04C), the Lister-type heat probe was used during the ARA05C. The probe can observe the geothermal gradient and in-situ thermal conductivity simultaneously as heat-generating thermistors as well as passive thermistors are attached on the barrel. The probe has nine thermistor channels in total, with three heating channels and a maximum six normal thermistors. In-situ thermal conductivity is determined based on the speed of heat dissipation on temperature-time curves after a given amount of heat is provided, which is known as the transient method (Von Herzen and Maxwell, 1959; Carslaw and Jaeger, 1959). Shock and tilt sensors to determine appropriate tool-conditions to generate heat after penetration of the probe into the sediments are included (Table 6.2). In addition, a pinger and transponder are used to determine accurate position of the probe in the water column (Fig. 6.2).

The standard procedure to calculate marine heat flow using the Lister-type probe is as follows: deployment of the probe after setup, standby for 10 minutes at several tens of meters above the seafloor, standby for 20 minutes after penetration of the probe into sediments, pull-out and standby for 5 minutes in the water above seafloor, and re-insertion and standby for 15 minutes in the sediments, final removal of the tool and data retrieval from the data logger via RS-232 to a PC. Two measurements at each station are carried out to increase reliability of the measurements (Fig. 6.5). Furthermore, increasing the waiting time by 5 minutes is also adopted to secure enough time for sensors to be thermally equilibrated with surroundings. The raw data observed at the thermistors are transformed into temperature values based on the individual thermistor-calibration functions. The data are quality controlled by screening for erroneous temperature (i.e. resistance) data using simultaneous change of both tension and tilt, and general data trends. The geothermal gradient and in-situ thermal conductivity are then calculated from the temperature-time curves.

### 6.2.2. TK04 thermal conductivity measuring system

One of the lessons learned from the Expedition ARA04C was that we should prepare an additional thermal conductivity meter for the ARA05C. In the ARA04C, we learned that the shock sensor equipped in the data logger recognized the timing of vertically-standing up of the A-frame during deployment instead of the exact penetration timing of the probe into the seafloor. This is mainly because the sediments are so soft/weak that the probe does not ‘feel’ enough shock. In other words, the threshold of deceleration set for the shock sensor to detect as shock from penetration seems to be larger than the actual situation. Thus, in-situ thermal

conductivity was not properly measured in the last expedition. In order to avoid the same situation, we have an additional thermal conductivity meter, instead of adjusting the threshold of deceleration. Adjustment of the shock sensor can be performed by the manufacturer and the current value has been proven as suitable for mid-latitude coarser sediments.

New equipment is the TK04 thermal conductivity measuring system from TeKa, Germany. It is commonly used in thermal conductivity measurements, particularly on marine research vessels collecting sediment cores, such as DV Joides Resolution (e.g. Blume 1997), because the TK04 system is configured with a needle-type probe and it is very handy for cored sediments (Fig 6.4a). Its measuring range of 0.2 to 10 W/m/K is suitable for subsurficial marine sediment ranging from 0.7 to 3 W/m/K with its characteristic of loose packing, high porosity, and muddy to sandy lithology. According to the manufacturer, an additional benefit is that it is not necessary to calibrate the system with standard materials. However, the needle probe is considered to generate higher than true values, thus calibration is recommended. KOPRI uses a standard material of 1.614 W/m/K as well as the TK04 thermal conductivity measuring system with the needle probe for calibration purposes (Fig. 6.4b).

To measure thermal conductivity in the lab, one should be cautious of temperature and humidity change during measurement because those two parameters may result in unexpected measurements. Significant temperature change outside of the sediments can prevent correct temperature response of the sediments with respect to heat generated from a line source, i.e., the needle probe inserted into sediments (Fig. 6.4c and d). Even a small change in temperature can cause longer waiting time to complete the temperature drift control stage prior to the actual measuring stage due to heat generation from the view of TK04 measuring procedure. In order to secure thermal equilibrium status through the targeted sediments, the core is left more than 4-6 hours and the measurement is generally carried out in an iso-temperature room. Unfortunately there is no such laboratory in RV Araon, thus we applied an alternative solution to minimize the temperature disturbance as follows: 1) air ventilation is stopped in the dry lab where the measurement is carried out, 2) access around measurement place is limited, and 3) a wind protector is deployed (Fig. 6.4e and f). For this case, humidity change in the lab is considered negligible. Measurement with the probe is done through a small hole of ~ 2 mm in diameter and the hole is drilled just before insertion of the needle probe (Fig 6.4d). In addition, measured holes are sealed tightly when repeated measurement at different depths are conducted.

Thermal conductivity is the first step of the whole core analysis in the ARA05C because an intact whole core is required for accurate measurement due to sensitivity to the water content of sediments. When a sediment core is retrieved on deck, one section of 1.5 m in length is chosen based on sediment texture and is placed in the Dry Lab for at least 6 hours. Due to the homogeneous lithology through the entire core length (max. ~5 m), one measurement per core appears to be reasonable. The other sections were cut in half and both halves were processed with other analyses such as pore water extraction, subsampling, and fall cone penetration. We followed the default setting of the software package for the TK04 system. It is necessary to increase/decrease the heating power option for the cases where expected thermal conductivity is significantly higher/lower than that of a standard soil of ~1.5 W/m/K, but this was not the case

for expedition study area.

## *6.3. Results*

### 6.3.1. Stations

Eight stations from three thermal regimes, i.e., background, mud volcano, and permafrost area, were visited during the ARA04C, and seven stations from this expedition are chosen to complement data obtained in the last expedition (Figs 6.1 and 6.6; Table 6.1): 1) Stations 01, 10, and 18 are on the flat-top of mud volcanos at 420, 290, and 720 mbsl, respectively, and Station 02 served as reference with respect to all three volcanos, 2) Stations 16 and 33 are in the background area because these two stations are located at the deepest depths and there is no disturbance in sediment layers on a SBP profile by faults or other vertical features which could serve as a conduit for fluid advection, and 3) Station 34 as one component for the transect line of the eastern slope of Mackenzie trough where permafrost degradation in the shelf is shown on a SBP profile (Jin et al., 2014).

Finally thermal conductivity was measured from sediment cores at five stations (01, 02, 16, 33 and 34) distributed in all regimes (Fig. 6.1). Unfortunately, data from sediment cores with moussey or vesicular texture or large voids at Stations 10 and 18, which may be caused by dissociation of gas hydrate, were not collected because such matrix texture is not suitable for laboratory thermal conductivity measurement using a needle probe (see Section 7.4.2). In terms of geothermal gradient, five more stations (02, 10, 16, 18 and 34) were appended.

Because heat flow stations are not far apart in the main study area, data downloading and charging was done after completion of 2 stations for ~10-24 hours. It is useful to check that the logger runs for at least 24 hours after full charge of battery.

### 6.3.2. Heat flow estimation

All eight thermistors attached to the heat probe were fully penetrated into the seafloor at all five stations. The conversion to temperature values was done on-board, although a full analysis of the data is not complete. In addition, thermal conductivity data are not yet calibrated. The results presented in this cruise report are therefore preliminary.

The observed geothermal gradients show typical ranges characteristic of the three thermal regimes (Table 6.1; Fig. 6.7): 517.7 and 104.3 mK/m for the mud volcano (Stations 10 and 18), 75.1 and 44.3 mK/m for the background area (Stations 02 and 16), and -20.6 mK/m for the permafrost area (Station 34). The higher geothermal gradient and the higher seafloor temperature than bottom water temperature (not presented in this report) from the mud volcano indicate the occurrence of intermittent warm fluid expulsion from sediment into the water column at the mud volcanos (Kim et al., 2014). The negative geothermal gradient at the permafrost area confirms the presence of frozen material beneath the seafloor (Kim et al., 2014).

Observed thermal conductivity of marine sediments seems to be slightly higher than true values because readings of standard material 1.614 W/m/K done just after measurement of sediments are higher than the true value of 1.614 (Table 6.1; Fig. 6.8). Even considering

overestimation, thermal conductivity of sediments are reasonable based on the general value for fully-saturated silty mud to mud lithology (e.g. Lowell 1985). In other words, it seems that there are no other particular grain components leading to higher thermal conductivity, such as limestone and quartz which are common in the Queens Elizabeth Island area (Ruediger, 2008).

Background heat flow in the KOPRI study area is in the range of 40-78 mW/m$^2$ based on the data collected during the ARA05C. This preliminary conclusion agrees well with the heat flow of ~58 mW/m$^2$ inferred from a deep borehole of 500-5000 mbsf (Taylor et al., 2013).

#### 6.3.3. Further data process at shore

A number of tasks will be undertaken post-cruise which will assist in the processing, analysis and interpretation of the data collected at sea. The tasks include:

- Check winch tension data to confirm 'good' penetration of the probe.
- Check and adjust difference in depth readings from the CTD and the logger.
- Screen unqualified temperature data then re-determine geothermal gradient.
- Estimate seafloor temperature based on temperature data from the probe and the CTD.
- Calibrate measured thermal conductivity with respect to reading of standard material. If needed, to do room temperature correction.
- Evaluate heat flow in the three thermal regimes by merging data from the two expeditions.
- Compare heat flow values from subsurficial measurements and deep boreholes with Taylor et al. (2013) to delineate thermal field change with depth.
- Calculate gas hydrate stability zone based on newly-defined heat flow values (Tishchenko et al., 2005).

### *6.4. Summary*

Heat flow measurements were carried out successfully during the ARA05C. Seven stations were carefully chosen to reveal three thermal regimes, background, mud volcano, and permafrost area, to complement the work of the previous ARA04C heat flow survey. We collected thermal conductivity data from five stations using the heat probe and geothermal gradient data from five stations using the TK04 thermal conductivity meter. We have prepared the TK04 thermal conductivity meter to observe laboratory thermal conductivity of marine sediment for the case where in-situ thermal conductivity is not measured by the heat probe. Preliminary results suggest thermal conductivity ranges from 0.921 to 1.071 W/m/K (uncorrected to standard value) and geothermal gradients from -20.6 to 517.7 mK/m. Heat flow in the KOPRI study area is estimated to range from 40 to 78 mW/m$^2$. Based on heat flow survey results obtained in these two expeditions, we expect to delineate three thermal regimes and

calculate gas hydrate stability zone in the KOPRI study area.

## *6.5. Issues to be resolved*

### 6.5.1. Visualization of pinger signals from the data logger

A pinger (acoustic modem) installed into the data logger is designed to send information on the status of the logger during operation, such as tilt and heat generation with 12 kHz acoustic signal. The frequency of the signal is also used by most of the echosounders installed in ships. The RV Araon is equipped with a Kongsberg EA600 providing use of both a 12 and 38 kHz frequency. The pinger mode is designed to trace acoustic signals from a moving source, as in the case of the data logger signal. However, the EA600 does not show the signal from the logger for reasons unknown.

Knowing the status of the data logger is of great help in carrying out successful measurements. Currently, two measurements per site are made but before retrieval of the probe we do not know whether the two penetrations were actually done, whether the logger ran without malfunction, and if heat was generated. This is why we did not collect in-situ thermal conductivity data using the probe during the two expeditions. If we know during the operation that heat generation was not done correctly, more attempts to drop the probe could be made.

In the upcoming Antarctic cruise, we hope to use an additional transceiver using 12 kHz frequency.

### 6.5.2. Heat generation when penetration occurs

We need to adjust the current threshold value of deceleration to be suitable for Arctic soft sediments. In order to increase penetration shock, drop height above the seafloor during the ARA05C is set to 30 m above the seafloor, increased by 5-10 m compared to the previous expedition ARA04C. Despite of increase of drop height, the shock sensor still did not recognize the exact penetration timing.

Due to lack of preparation time between cruises, adjustment of the value will be done in spring/summer 2015 after the upcoming Antarctic cruise.

## References

Blum P. 1997. Physical Properties Handbook: A guide to the shipboard measurement of physical properties of deep-sea cores.

Carslaw HS and Jaeger JC. 1959. Conduction of heat in sold. Claredon press.

Jin YK, Riedel M, Hong JK, Nam SI, Jung JY, Ha SY, Lee JY, Kim Y-G, Yoo J, Kim HS, Kim G, Conway K, Standen G, Ulmi M, and Schreker M. 2015. Overview of field operations during a 2013 research expedition to the southern Beaufort Sea on the RV Araon. In: Geological Survey

of Canada, Open File, p 181.

Kim Y-G, Lee S-M, Matsubayashi O. 2010 New heat flow measurements in the Ulleung Basin, East Sea (Sea of Japan): relationship to local BSR depth, and implications for regional heat flow distribution. Geo-Marine Letters **30**:595-603. doi:10.1007/s00367-010-0207-x

Lovell MA. 1985. Thermal conductivities of marine sediments. Quarterly Journal of Engineering Geology and Hydrogeology **18**:437-441. doi:10.1144/gsl.qjeg.1985.018.04.14

Ruediger S. 2008. Arctic Ocean Sediments: Processes, Proxies, and Paleoenvironment. Elsevier

Taylor AE, Dallimore SR, Hill PR, Issler DR, Blasco S, and Wright F. 2013. Numerical model of the geothermal regime on the Beaufort Shelf, arctic Canada since the Last Interglacial. Journal of Geophysical Research: Earth Surface **118**:2013JF002859. doi:10.1002/2013JF002859

Tishchenko P, Hensen C, Wallmann K, Wong CS. 2005. Calculation of the stability and solubility of methane hydrate in seawater. Chemical Geology **219**:37-52. doi:http://dx.doi.org/10.1016/j.chemgeo.2005.02.008

Von Herzen R, Maxwell AE. 1959. The measurement of thermal conductivity of deep-sea sediments by a needle-probe method. Journal of Geophysical Research **64**:1557-1563. doi:10.1029/JZ064i010p01557

Von Herzen RP, Uyeda S. 1963. Heat flow through the eastern Pacific ocean floor. Journal of Geophysical Research **68**:4219-4250. doi:10.1029/JZ068i014p04219

Yamano M, Uyeda S, Aoki Y, Shipley TH. 1982. Estimates of heat flow derived from gas hydrates. Geology **10**:339-343. doi:10.1130/0091-7613(1982)10<339:eohfdf>2.0.co;2

Kim, Y-G, Jin YK, Hong JK, Riedel M, and Lee S-M. 2014. Preliminary results of marine heat flow measurements in the Canadian Beaufort Sea and its implications for intermittent methane fluid expulsion. Proceedings of EGU General Assembly 2014, 27 Apr-2 May, Vienna, Austria. Poster presentation.

**Table 6.1 - Summary of heat flow measurements.**

| St.Name (Prefix: ARA05C) | Lat N (DM) | Lon W (DM) | WD (m) | Geothermal gradient (mW/m) | Thermal conductivity with reading of 1.614 standard material (W/m/K) | Station description | Remarks |
|---|---|---|---|---|---|---|---|
| 01GC3 Sec 1 | 70° 47.342’ | 135° 33.952’ | 286 | NA | 0.921 /1.642 | Mud volcano inside at 420 mbsl | 118.2 cm below section top (cmbst) |
| 02GC3 Sec 3 | 70° 42.334’ | 135° 49.016’ | 406 | NA | 1.019 /1.652 | Reference to mud volcanos at 290 and 420 mbsl | 50 cmbst; |
| 02HF4 | 70° 42.357’ | 135° 49.076’ | 411 | 75.1 | NA | Reference to mud volcanoes at 290 and 420 mbsl | All 8 thermistors penetrated |
| 10HF4 | 70° 38.965’ | 135° 56.758’ | 278 | 517.7 | NA | Mud volcano inside at 290 mbsl | All 8 thermistors penetrated |
| 16GC2 Sec 3 | 70° 56.157’ | 136° 25.124’ | 1016 | NA | 1.001 /1.688 | Background in the main study | 40, 125 cmbst |

| | | | | | | | |
|---|---|---|---|---|---|---|---|
| | | | | | | area | |
| 16HF3 | 70° 56.157’ | 136° 25.124’ | 1016 | 44.3 | NA | Background in the main study area | All 8 thermistors are penetrated |
| 18HF2 | 70° 48.112’ | 136° 5.981’ | 740 | 104.3 | NA | Mud volcano inside at 740 mbsl | All 8 thermistors are penetrated |
| 33GC3 Sec 3 | 70° 39.346’ | 139° 2.145’ | 1534 | NA | 1.071 /1.665 | Background in the KOPRI study area | 75, 120 cmbst |
| 34HF3 | 70° 05.623’ | 138° 21.120’ | 246 | -20.6 | NA | Eastern slope of Mackenzie trough | All 8 thermistors are penetrated |
| 34GC4 Sec 3 | 70° 05.623’ | 138° 21.120’ | 246 | NA | 1.024 /1.703 | Eastern slope of Mackenzie trough | 75, 125 cmbst |

**Table 6.2 - Specifications of heat probe.**

| Part | Specification | |
|---|---|---|
| Data logger | Dimension | 50 kg; Ø144*775 mm |
| | Housing | Up to 6000 m |
| | Measuring channel | #1~#10<br>#10 for fixed resistor as reference |
| | Measuring interval | 30 sec |
| | Measurable resistance | 1500-6500Ω |
| | Depth sensor | Up to 6000 m with accuracy of 1 m |
| | Tilt sensor | Up to ±45 degree on X, Y axes with accuracy of 0.1 degree |
| | Shock sensor | |
| | Memory | 32MB (corresponding to 0.5 million records) |
| | Heat pulse | On/Off<br>When mode 'On', for 12 seconds with 5 V in 6/8/10 minutes after shock |
| | Pinger frequency | 12/13/14/15 kHz |
| | Pinger pulse length | 2/5 ms |
| | Pinger oscillation mode | 3<br>(Heater On/Heater Off/Tilted) |
| | Connectivity | RS-232C |
| | Battery | NiCd 7.2V *1 for measurement<br>NiCd 25.2V *1 for the pinger |
| Thermistor | Length | Up to 6.5 m |
| | Types | 2(Heat-generating/Normal thermistor) |
| | Measurable temperature | ~1500 Ω for 80 degree<br>6000 Ω for 0 degree<br>Accuracy: 0.01 degree |
| Frame | Head | 400 kg ;Ø540*1330 mm |
| | Barrel | ~35 kg/1.5 m<br>Adjustable using 2 units (1.5 m/3.0 m) |

**Table 6.3 - Specifications of TK04 thermal conductivity measuring system.**

| Part | Specification | |
|---|---|---|
| TK04 thermal conductivity meter | Standard | ASTM D 5334-08 |
| | Measuring principle | Transient heat flow (needle probe method) |
| | Measuring range | 0.1 to 10 W/m/K |
| | Accuracy | ±2% |
| | Reproducibility | ±1.5% |
| | Heater current precision | ±0.01% |
| | Duration of 1 measurement | 60/80/240s |
| | Automatic repetitions | Up to 99 measurements per series |
| | Sample size | No upper limit, minimum size probe dependent |
| | Sample shape | Any |
| | Operating temperature | 0 to 45°C |
| | Sample temperature | -25 to 70°C / -25 to 125°C |
| | Power consumption | 40W |
| | Dimensions (W*H*D) | 471 * 160 * 391 mm |
| | Ports | RS232 serial port (COM port) |
| | Connection cable | Standard serial cable, 9 pin |
| Standard VLQ probe | Probe type | Needle probe |
| | Application | Laboratory use |
| | Measuring range | 0.1 to 10 W/m/K |
| | Accuracy | ±2% |

| | | |
|---|---|---|
| | Duration of 1 measurement | 80 s |
| | Dimension (source) | Length: 70 mm, diameter: 2 mm |
| | Dimension (overall) | Length: 150 mm, diameter (max.): 16 mm |
| | Minimum sample size | Diameter: 30 mm, length 75 mm |
| | Sample shape | Any |
| | Maximum sample size | No limit |
| | Sample temperature | -25 to 125°C |
| | Evaluation parameter set | Standard VLQ (VLQ Source 70*2) |

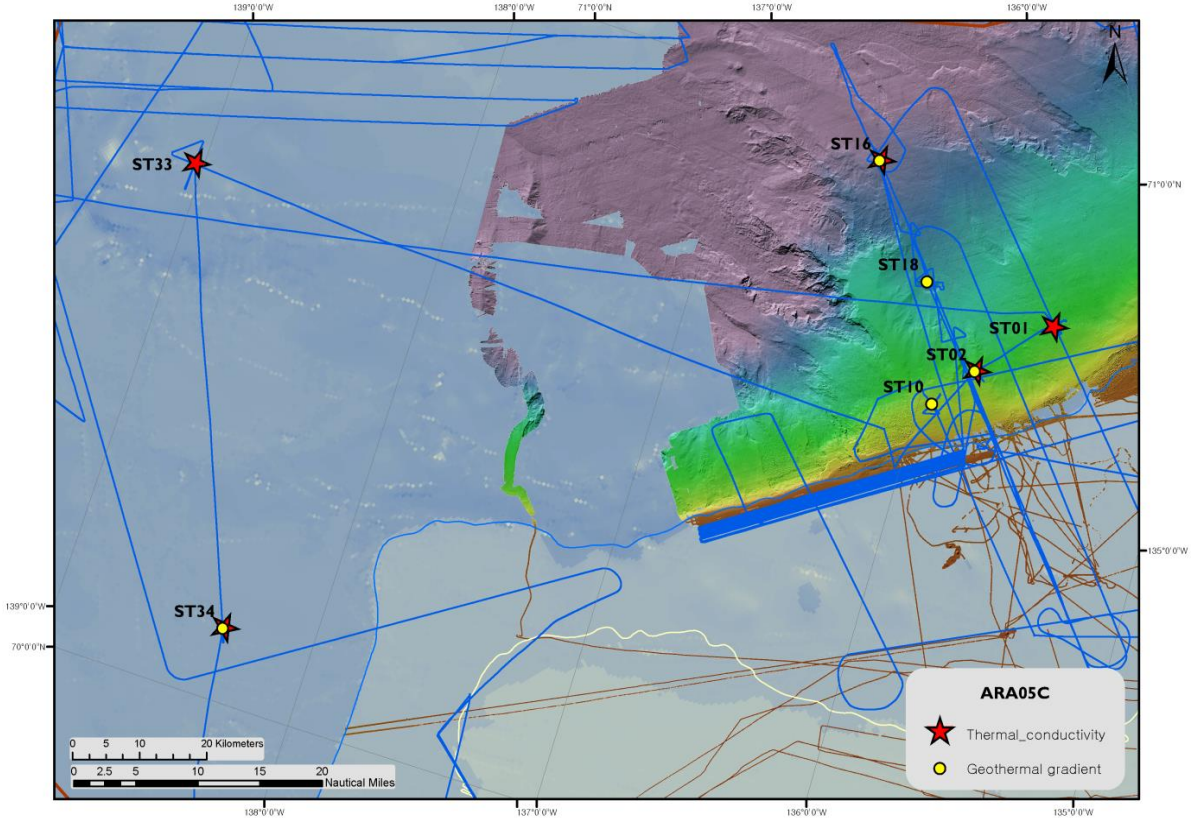


**Figure 6.1 - Locations where geothermal gradient measurements (yellow dots), and thermal conductivity measurements (red stars) were taken. The ship track is indicated by the blue line.**

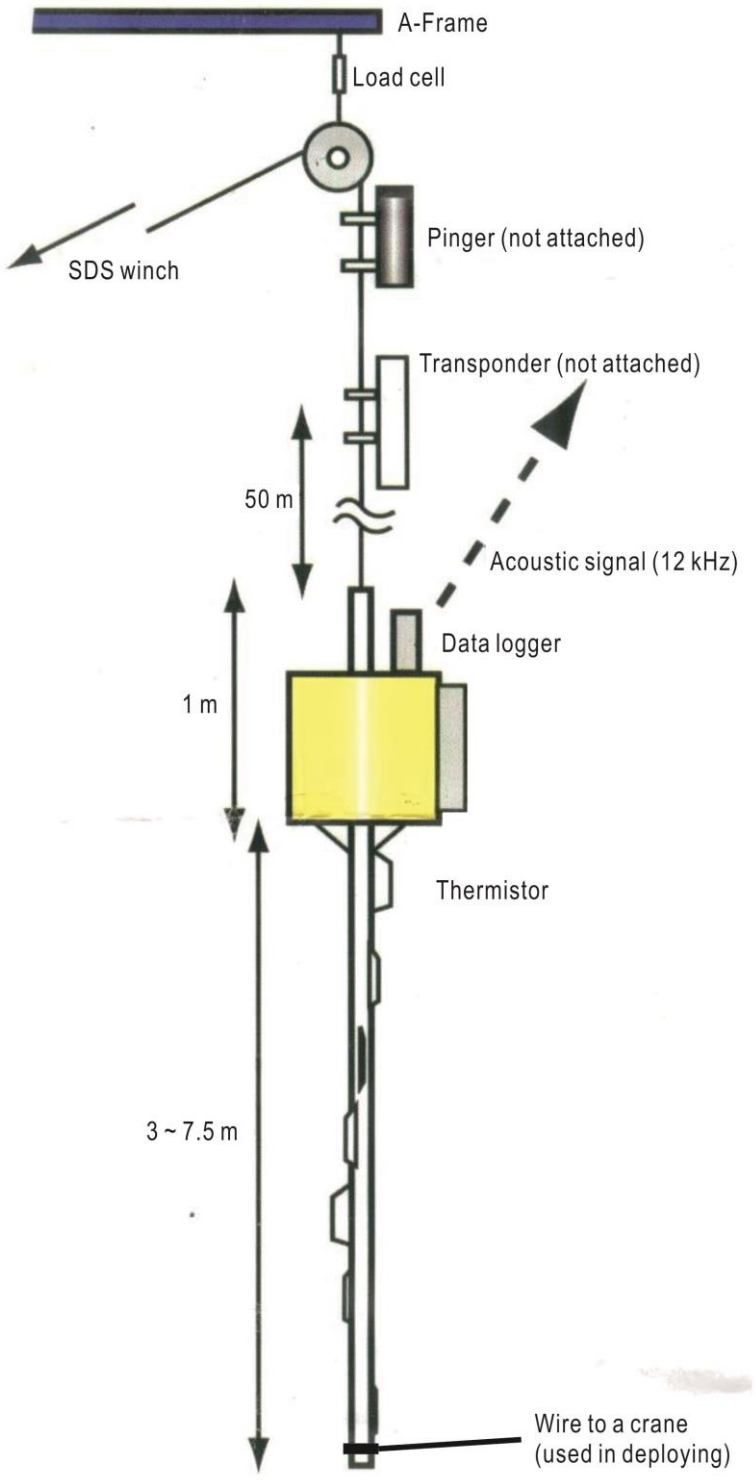


**Figure 6.2 - Schematic diagram of the configuration and deployment of the heat probe. Due to the A-Frame size, the length of the barrel (yellow part) is limited to 4.5 m. A total of 8 thermistors, including maximum 3 heat-generating thermistors, are attached to the barrel. The data logger includes the processing unit, battery, tilt meter, depth meter, shock sensor, connectors to the thermistor, and acoustic modem.**

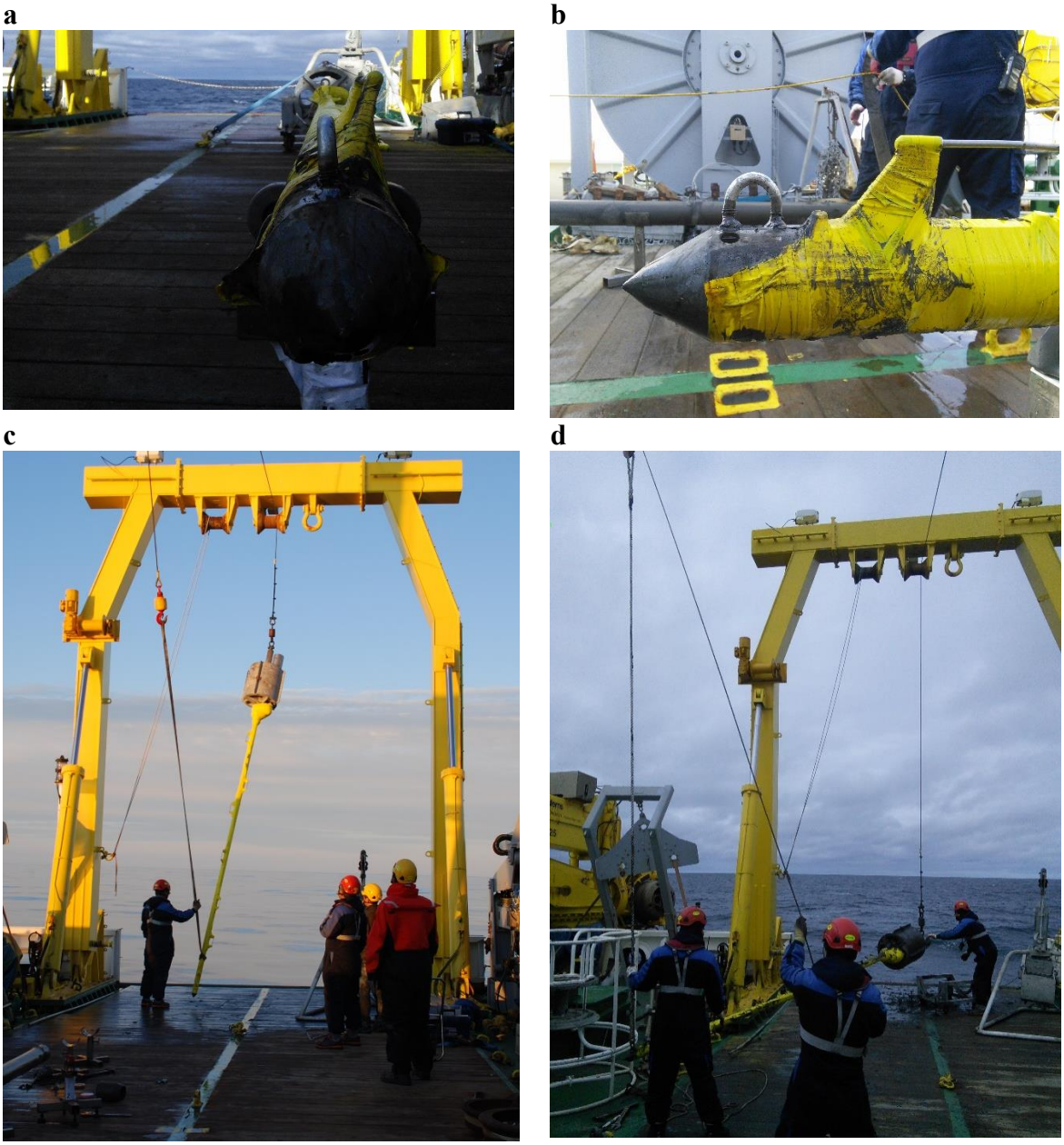


**Figure 6.3 - Photos of heat probe. (a) and (b) a hook is newly attached just above the barrel tip for easy handling during winch operation. Size and direction of the hook is determined not to bother contact of thermistor with sediments when the probe is penetrated into sediments. The probe is deployed and recovered with cooperation of two winches to avoid damage of the thermistors from crush to ship. (c) before and (d) after hook attachment.**

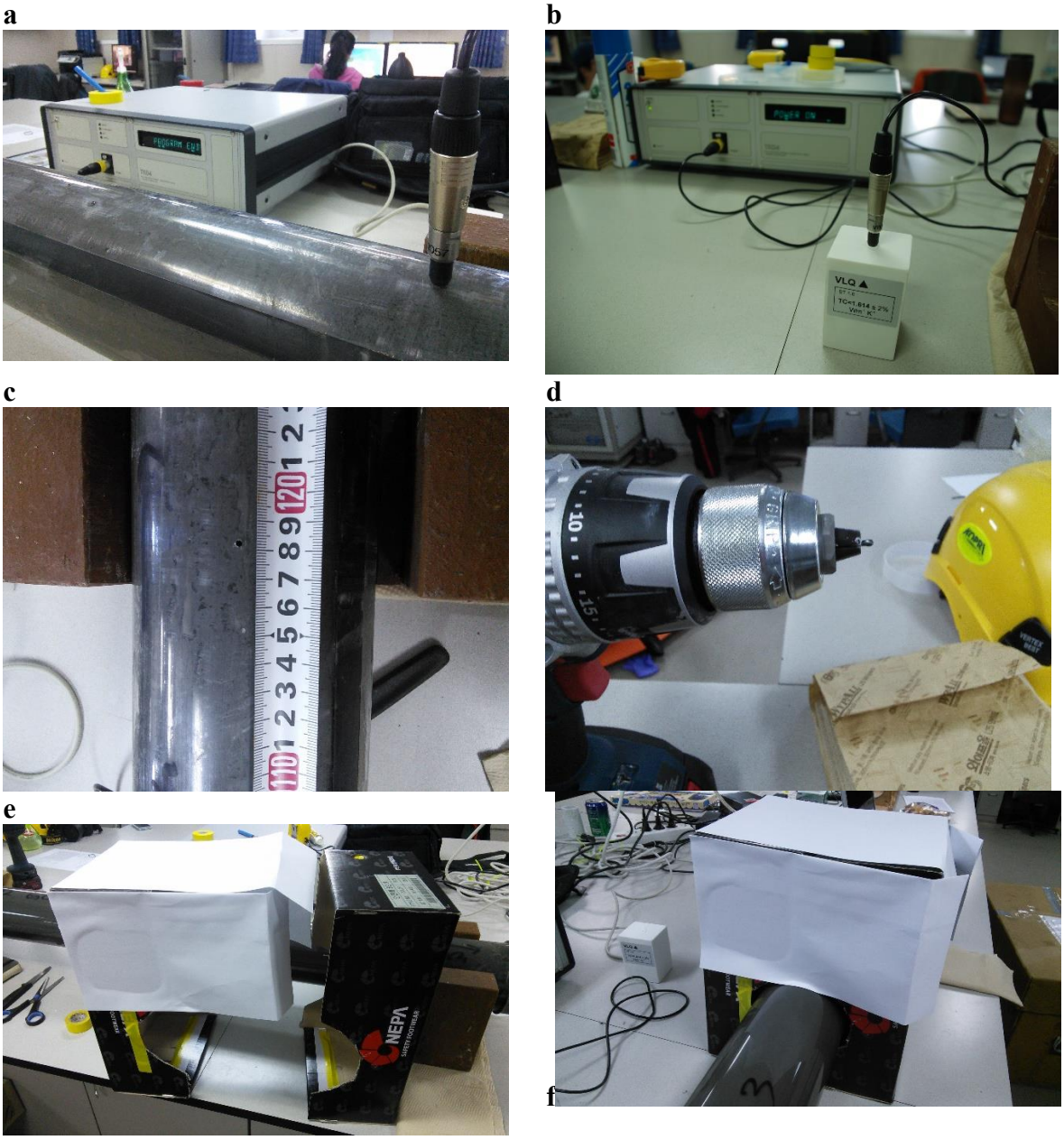


**Figure 6.4 - Photos of thermal conductivity measurement of cored sediment. (a) and (b) measurement procedure is conducted automatically by the software package on a PC connected with the TK04 system after insert of the needle-type probe into sediments and standard material. (c) and (d) the needle probe is inserted through small hole with use of proper drill bit of which length is already adjusted to thickness of a hard core liner to prevent sediment disturbance. (e) and (f) temporarily-made wind protector is useful to shorten waiting time to complete temperature drift stage before actual measuring stage in the measurement procedure.**

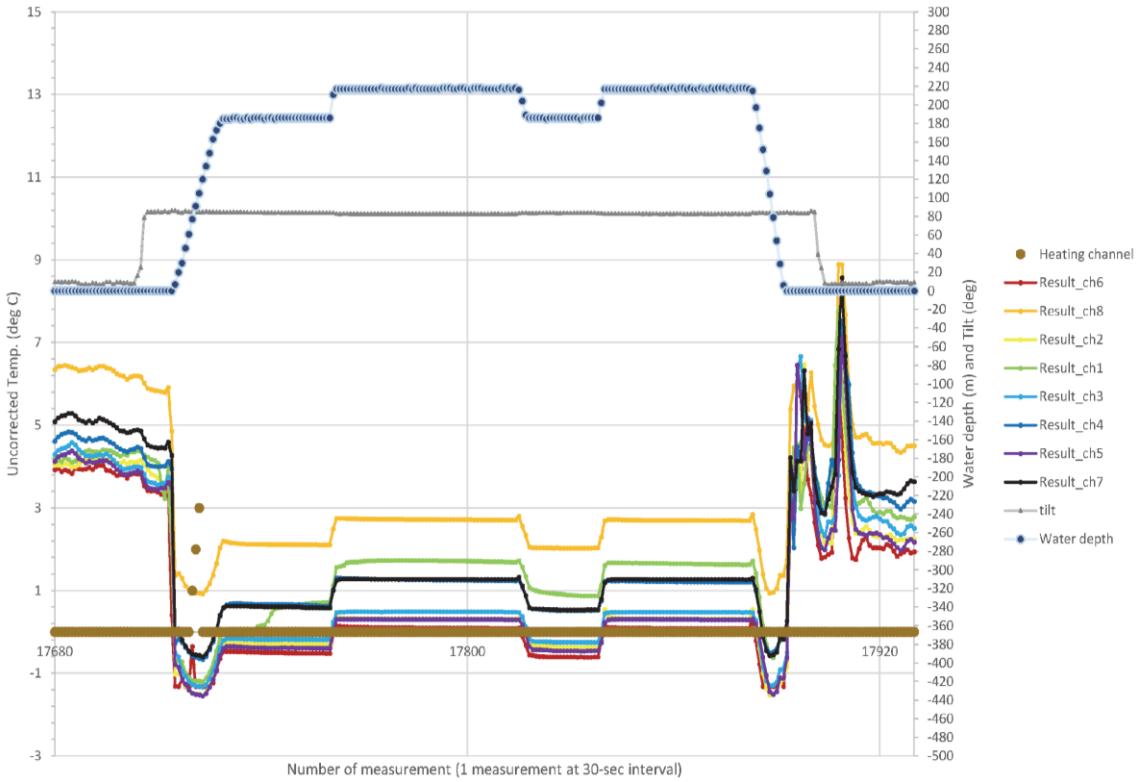


**Figure 6.5 - Temperature-time graph obtained at Station 34. Results 1 to 8 correspond to eight thermistors. Rainbow colors from red to purple are indicative of thermistor location from barrel top to barrel tip. Blue dot-light blue line and black triangle-light black line are depth and angle with respect to the seafloor of data logger, respectively. Gold dot shows heated channel.**

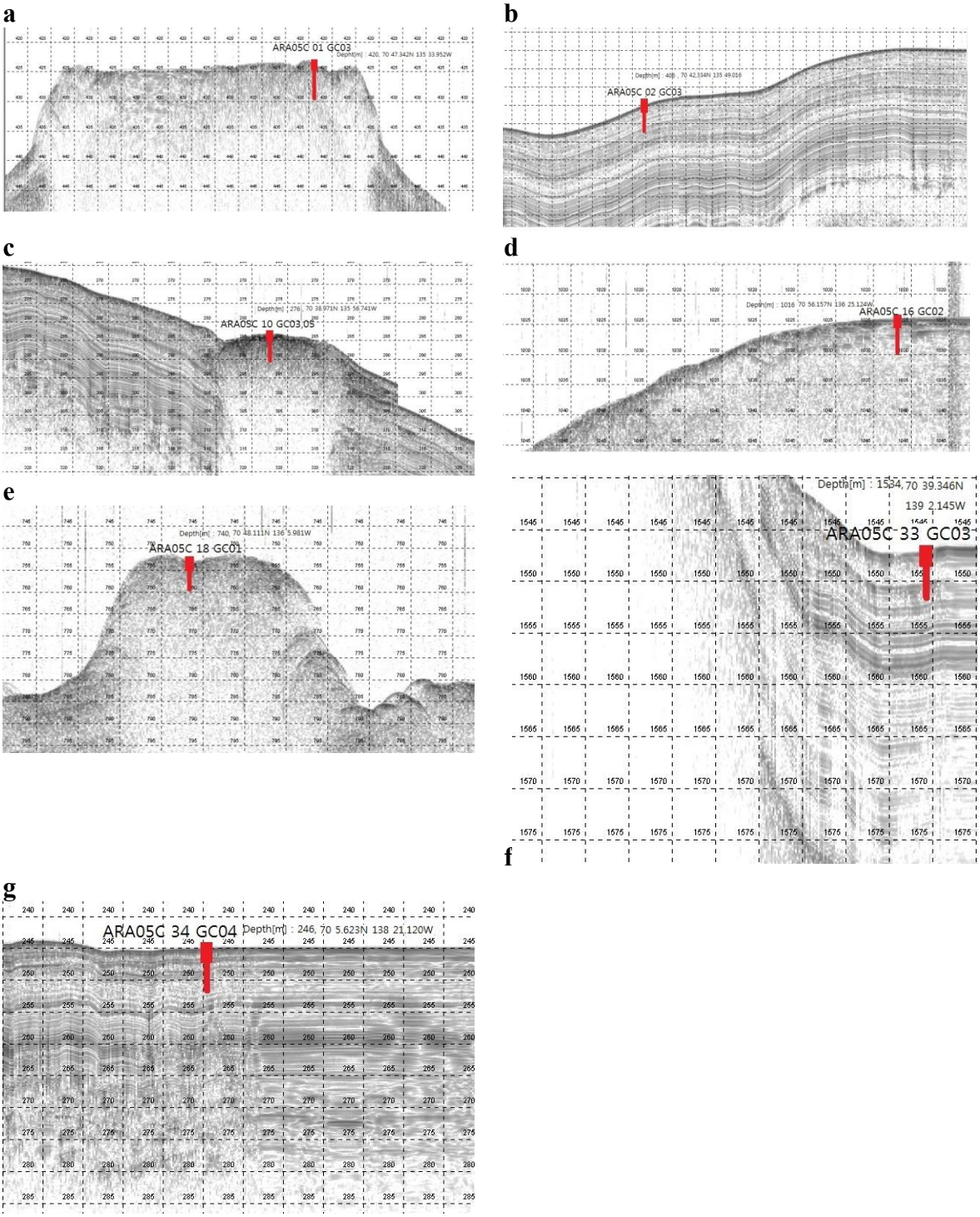


**Figure 6.6 - SBP profiles at seven heat flow measurement stations. Red sign indicates 7 m-long gravity corer. Penetration by the heat probe was made nearly at the same location with gravity coring.**

a

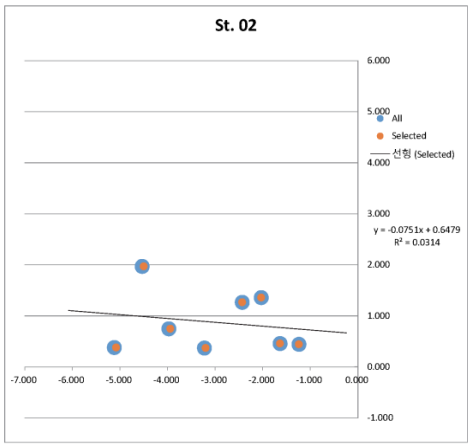


b

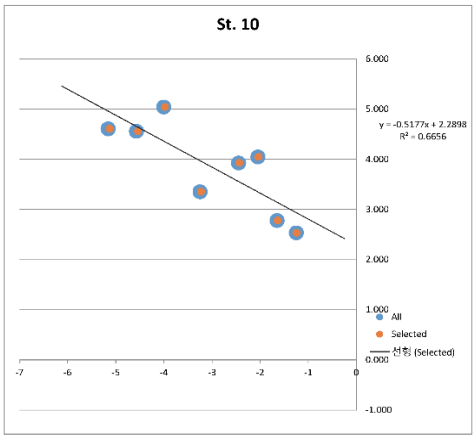


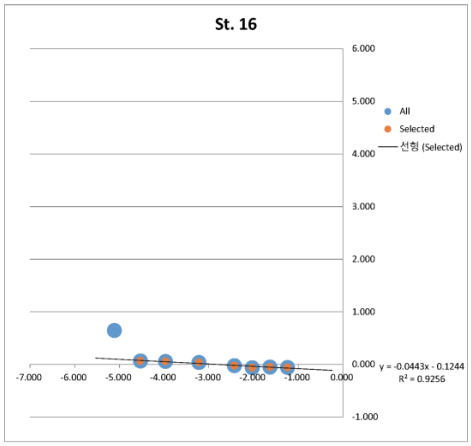


d

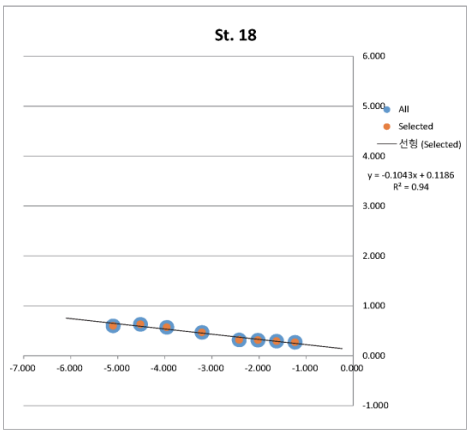


c

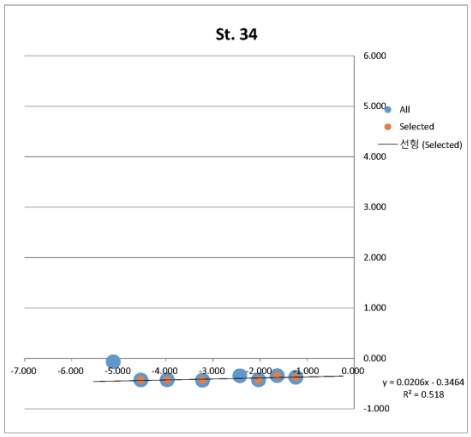


e

**Figure 6.7 -Preliminary results of geothermal gradient from five stations (02, 10, 16, 18 and 34).**

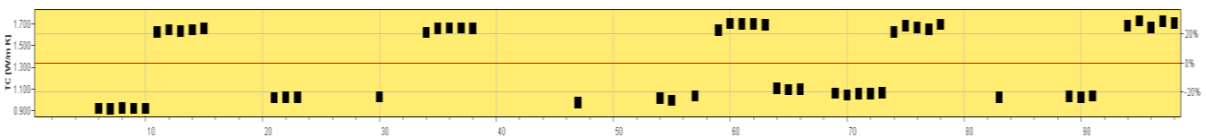

**Figure 6.8 - Preliminary results of thermal conductivity from sediment cores at five stations (01, 02, 16, 33 and 34). Values lower than 1.300 represent thermal conductivities of sediments in the ascending order of stations, and values higher than 1.300 represent thermal conductivities of standard material of 1.614 for calibration.**

# CHAPTER 7 - Sediment coring

**R. Gwiazda, G. Wiemer, D.H. Lee and Y.H. Noh**

## *7.1. Introduction: Scientific Goals*

A coring program was conducted during the ARA05C cruise in the Canadian waters of the Beaufort shelf and slope to meet several scientific objectives: i) Investigate biological processes taking place in methane-rich environments such as the mud volcanoes found on the slope, and contrast them to biological process and microbial populations found in the slope environment away from such features ('slope background'); ii) Complement the existing geographical coverage of cores taken by partnering research institutions in the area of the Beaufort shelf and slope by focusing in regions with the least core sampling, such as the slope background, with the goal of improving our knowledge of the stratigraphy, lithologies and geochemical processes observed in porewaters of this area; iii) Obtain measurements of undrained shear strength in sediments of the shelf edge and slope to assist in the evaluation of geohazards posed by potential landslides, triggered by gas hydrate dissociation or potentially earthquake shaking; iv) Continue the investigation of the regional heat flow regime, initiated in cruise ARA04C, by measuring the thermal conductivity of sediments from areas where thermal gradients had been measured in seafloor sediments.

## *7.2. Background*

Over the last fifteen years, research efforts have been directed to survey the Beaufort Sea, in particular its shelf and slope, because of the realization that terrestrial gas hydrates and permafrost underlying the shelf must be undergoing decomposition and thawing respectively, as a result of warming of the shelf initiated with the sea transgression of the last deglaciation. The thickness of the permafrost north of the Tuktoyaktuk peninsula has been estimated to be ~500 m at its maximum, however seabed temperature measurements at the shelf edge exceeding 0°C indicate that the lateral extent of the permafrost is limited to within the shelf area, and does not extend to the shelf edge proper (Taylor et al., 2013). Freshwater released in permafrost thawing at the base of the permafrost and in terrestrial gas hydrate decomposition at the bottom of the hydrate stability zone under the shelf, may become pressurized and migrate either upwards towards the shelf seafloor, along the permafrost base towards the shelf edge or be channeled along sealed strata towards the slope. Indeed, active gas flow has been identified in areas along the shelf edge. These gas emanations are non-localized but diffuse in their location, and originate in old sources of gas, i.e. not produced biogenically in the present top sediment section. One of the tools at our disposal to identify and track the sources of fluids in the shelf edge and slope, if these were to be identified in the sediment column, is to characterize the porewaters chemical and isotopic composition. As part of the ARA05C cruise coring program, porewaters were collected in sites where information from previous expeditions is lacking or where the geographical coverage is limited, in order to gain a better understanding of the sources and pathways of these fluids. Results to date, which are based on analyses of porewaters from cores collected by the CCGS SW Laurier and the RV Araon in previous expeditions, appear to indicate

that freshwater contributions to porewaters of slope sediments are present in sediments as deep as 800 m water depth, located more than 150 km from shore.

Fluid flow in the shelf edge and slope environments has the potential of destabilizing the sediment column and facilitating slope failures and landslides. Bathymetric maps of the slope document the presence of fresh slope failures morphologies and landslides that attest to the real geohazards that prevail in this region. In this context it is important to document the sediment physical properties in order to evaluate the susceptibility of the shelf edge area to generate spontaneous, fluid initiated, or earthquake triggered slope failures or slumps. The ARA05C coring program tackled this issue with two different and complementary tools: the fall-cone technique was used on collected cores to evaluate the shear strength of the sediment. When possible this was matched by *in-situ* measurements of shear strength using a deployable Cone Penetration Testing device (CPT). For details on the CPT program aboard ARA05C, see Chapter 8: Cone Penetration Test.

One of the main objectives of the ARA05C coring program is to investigate methane-rich environments in order to improve our understanding of the methanotrophic and methanogenic microbial communities that coexist in close proximity in the sea floor in such settings. These two types of communities regulate the production and consumption of methane in sediments. Methanogens generate methane through the assimilation of substrates with low molecular weight such as methylated compounds, and especially through the reduction of carbon dioxide ($CO_2$), which appears to be the most important methanogenic process in the marine environment. In contrast, methanotrophs participate in the consumption of methane by anaerobic oxidation (AOM). The factors that control the distribution and activity of microbial communities that take part in the methane cycle are still poorly defined. To better constrain the environmental conditions that regulate the composition, metabolic pathways and activities of these archeal communities, sediment and porewaters collected in the ARA05C coring program will be analyzed to determine the distribution and carbon isotope values of archeal membrane lipids, and the distribution of specific biomarkers in methane-rich and/or gas hydrate bearing sediments from the Beaufort Sea.

## *7.3. Methods*

Figure 7.1 presents the locations of box-cores and gravity cores collected for this study.

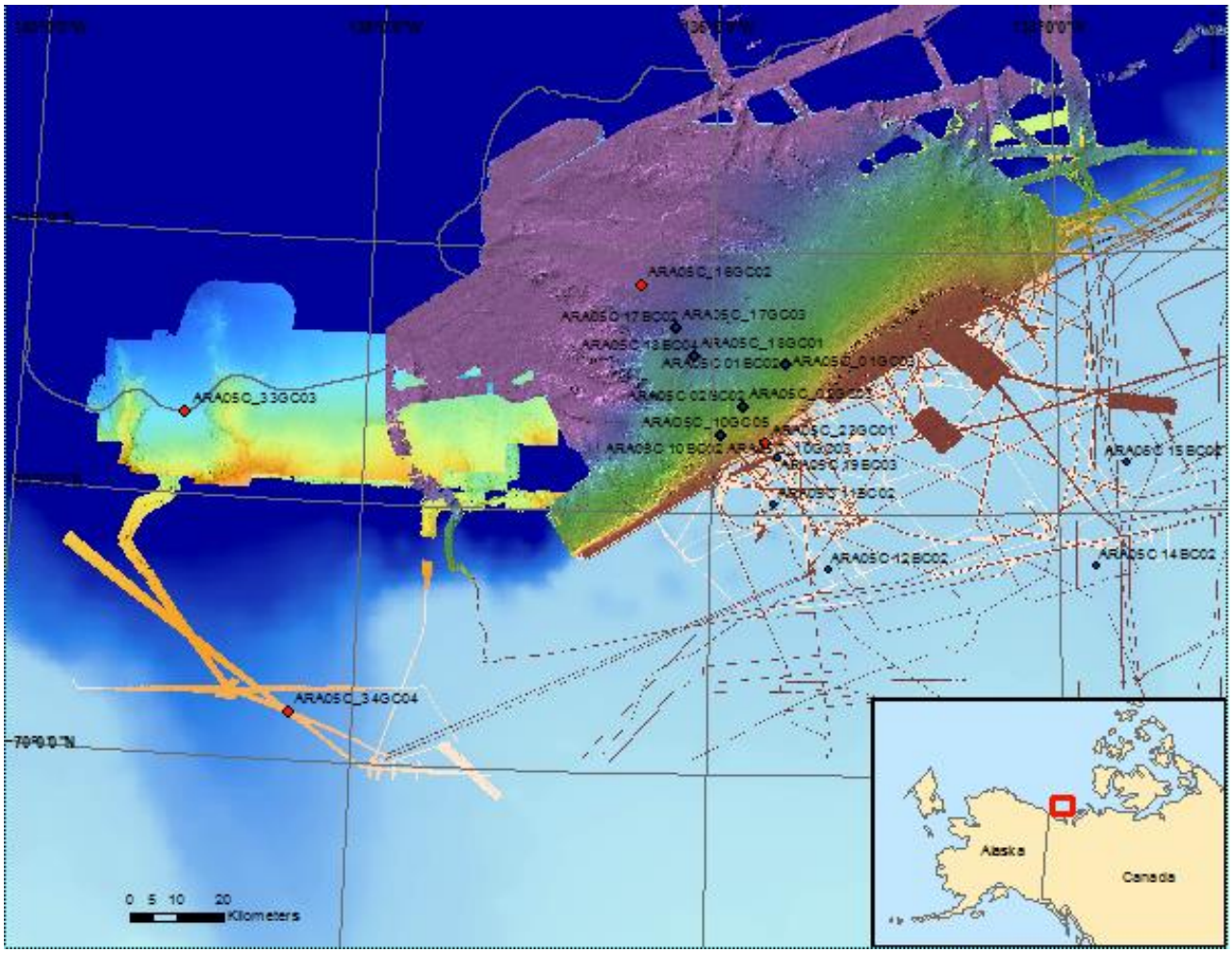


**Figure 7.1 - Map indicating location of box-cores and gravity cores collected during the expedition.**

### 7.3.1. Box-Coring

Box-cores of 60 cm length were collected (Table 7.1). Once on deck the top centimeter of the core was skimmed for organic matter measurements. The box-core was subsampled into several smaller cylindrical cores and the rest of the material left in the box was examined for megafauna presence and then discarded. Biological sampling of box-core material followed the same protocol used with gravity cores, as described in the gravity coring section 7.3.2.

**Table 7.1 – Box-cores collected to study biological communities and processes involved in methane cycling in sediment.**

| Core | Latitude (N) | Longitude (W) | Water depth (m) | Length (cm) |
|---|---|---|---|---|
| ARA05C-01-BC01 | 70°47.342´ | 135°34.047´ | 420 | 47 |
| ARA05C-02-BC02 | 70°42.349´ | 135°34.047´ | 410 | 44 |
| ARA05C-10-BC02 | 70°38.968´ | 135°56.750´ | 277 | 50 |
| ARA05C-11-BC02 | 70°31.217´ | 135°37.545´ | 60 | 36 |
| ARA05C-12-BC02 | 70°23.769´ | 135°18.814´ | 59 | 41 |
| ARA05C-14-BC02 | 70°24.078´ | 133°46.967´ | 56 | 36 |
| ARA05C-15-BC02 | 70°35.922´ | 133°35.529´ | 67 | 40 |
| ARA05C-17-BC02 | 70°51.404´ | 136°12.673´ | 848 | 42 |
| ARA05C-18-BC05 | 70°48.107´ | 136°05.863´ | 740 | 44 |
| ARA05C-19-BC01 | 70°36.519´ | 135°36.922´ | 69 | 24 |
| ARA05C-20-BC02 | 70°31.012´ | 135°24.137´ | 60 | 28 |

### 7.3.2. Gravity Coring

Coring was performed with a gravity coring device consisting of a headstand weighing 1.5 metric tons and a 6 meter long core barrel. The core liner consisted of two clear plastic tubes 10 cm in diameter and 3 meter long each, assembled together for a potential core recovery of 6 meters. The coring tool was deployed from the A frame in the stern using the Deep Sea Traction (DST) winch with spectra rope. Winch velocity on impact was ~72 m/min.

Coring was accurately targeted owing to the Dynamic Positioning System that allowed the RV Araon to position the gravity corer before it is launched within a few meters of the desired coring location. Selection of the targets was a two-step process, where the general location of the site was decided in broader terms (deep slope background site, mud volcano, etc.) but the precise location where the gravity corer was deployed was decided when the site was reached by examining the feed of the CHIRP sub-bottom profiler. Once on deck, if no gas filled gaps were visible, the liner was cut in 1.5 m long sections, which were numbered in sequential order starting at the top. If the core had large gaps in the sediment fill, the liner was pierced with a custom-made tool and the gas was pumped using a large volume syringe to a gas collection bag. In selected cores, thermal conductivity measurements were done in the bottom section before further processing of this section (see Chapter 6, Heat Flow Measurements). Otherwise, sections were opened longitudinally by slicing the liner with an electrical saw. One half designated ‘archive’ was photographed, in most cases in intervals of 30 cm. Subsequently, porewaters were extracted from this half in intervals ranging from 15 to 35 cm, by drilling the plastic liner and inserting a rhizon (i.e. a cylindrical membrane with <1 µm pore space) that was connected to an

evacuated syringe. Ten milliliters of porewaters were collected. Once ashore these waters will be analyzed for major anion and cation concentrations, and oxygen and hydrogen isotopic composition. An aliquot of maximum 2 ml porewaters was taken for the analysis of nutrient and dissolved inorganic carbon (DIC) as part of the biological goals of this cruise. Core descriptions were done on the archive half before sealing the core for storage. The other half was designated 'working' half. Fall-cone tests were carried out on the working half of all gravity cores except on cores ARA05C 10GC03 and ARA05C 10GC05. In these cores the expansion of gas bubbles has disturbed the sediment internal structure to such extent that the measurement of undrained shear strength is not applicable.

The undrained shear strength ($s_u$) along the sediment cores was determined in 5 cm intervals according to British Standards Institutions (BS1377, 1975) using a Wykeham-Farrance cone penetrometer WF 21600 (Fig. 7.2).

In this measurement, the metal cone is brought to a point exactly on the split core face (Wood, 1985). Free-fall penetration of the cone into the sediment is triggered manually. The penetration depth is measured using a displacement transducer that is operated with a precision of 0.01 mm. The undrained shear strength of sediment is a function of the mass of the falling cone (m), gravity (*g*), penetration depth *d* and the cone factor *k* (Hansbo, 1957), which depends on the tip angle of the cone (Wood, 1985). Wood (1985), calculated average values of cone factors from fall-cone and miniature vane tests. $s_u$ was calculated using the following equation:

$s_u = (k*m*g)/d^2$

Here we used k=0.85 for a cone with a 30° tip angle and a mass of 80.51 g.

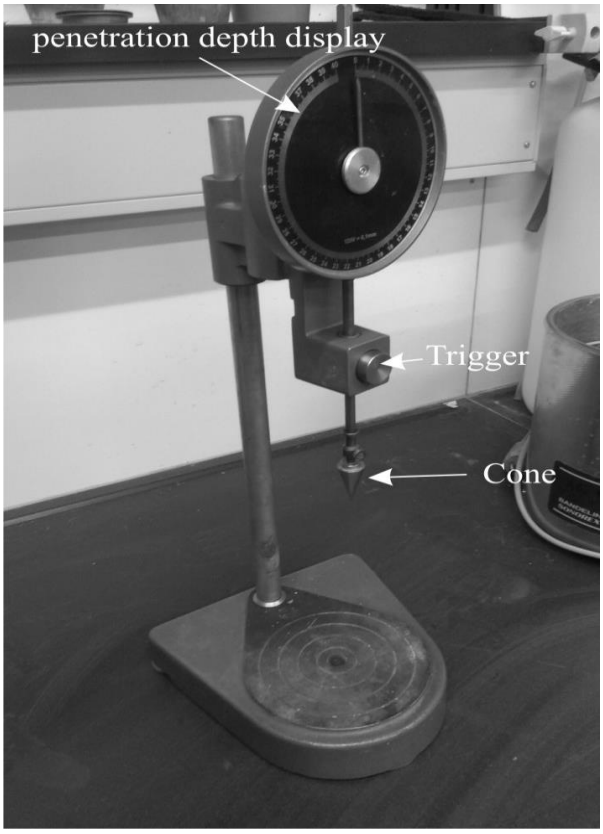


**Figure 7.2 - Fall-cone penetrometer.**

Shore-based laboratory testing will include ring shear experiments as well as direct shear tests to obtain residual strength and rate-dependent frictional properties.

For biological sampling sediment plugs of 5 cc volume were taken every 25 cm from the working half, and stored in sealed serum vials to determine the volatile hydrocarbons concentrations. Additional aliquots of sediment were taken and stored at -20°C to determine the concentration in bulk sediment of total organic carbon, total nitrogen, C/N ratio, $CaCO_3$ content and carbon isotopic composition, and the $\delta^{13}C$ values of methane-related lipid biomarkers (crocetane, PMI, archaeol, *sn*-2-hydroxyarchaeol, GDGTs, IPLs) in the laboratory at Hayang University. The same biological sampling protocol was followed in box-core sampling.

After biological sampling was completed, sediment samples for grain size analysis were taken from the "working' half at intervals of 25 cm before sealing it for refrigerated storage onboard.

## *7.4. Results*

Descriptions of the core lithologies, sedimentary structures, fall-cone measurements and ancillary core information are found at the end of the chapter in Appendix A.8.1: Core descriptions and ancillary information.

Cored sites fit three broad categories: slope background, slope mud volcanoes, and heat-flow measurements-related sites. In addition one site was targeted in order to sample the Cyan unit. This unit is an approximately 40 m thick interval with no acoustic reflectors that as visualized in SBP profiles displays a plastic behavior where it pierces through the overlying unit, the Yellow unit, in particular along the shelf edge. It has been hypothesized that this unit may be a glacial deposit.

### 7.4.1. Slope background sites

Three sites in the Beaufort Sea slope and one in the Mackenzie trough (Table 7.2) were selected with the goal of characterizing the physical and biological properties of the sediment and obtain porewaters, away from the slope mud volcanoes, where it may be possible to verify the presence and characterize the magnitude and identity of freshwater sources flowing into slope sediments.

**Table 7.2 - Slope background gravity cores.**

| Core | Latitude (N) | Longitude (W) | Water depth (m) | Length (cm) |
|---|---|---|---|---|
| **ARA05C 02GC03** | 70°42.364´ | 135°48.979´ | 406 | 425 |
| **ARA05C 16GC02** | 70°56.133´ | 136°25.056´ | 1,016 | 385 |
| **ARA05C 17GC03** | 70°51.378´ | 136°12.746´ | 850 | 373 |
| **ARA05C 33GC03** | 70°39.35´ | 139°2.207´ | 1,534 | 367 |

Slope background core ARA05C 16GC02 from 1,016 m water depth, slope background core ARA05C 17GC03 from 850 m water depth, and core ARA05C 18GC01 collected at the 740 m water depth mud volcano, all line along the multichannel seismic track ARA05C-15.

The sub-bottom profile of the sediments cored at the slope background site at 1,016 m water depth shows that upper sediments have little internal structure and no strong reflectors (Fig. 7.3). In the 850 m water depth site layered sediments are apparent in the sub-bottom profile (Fig. 7.4).

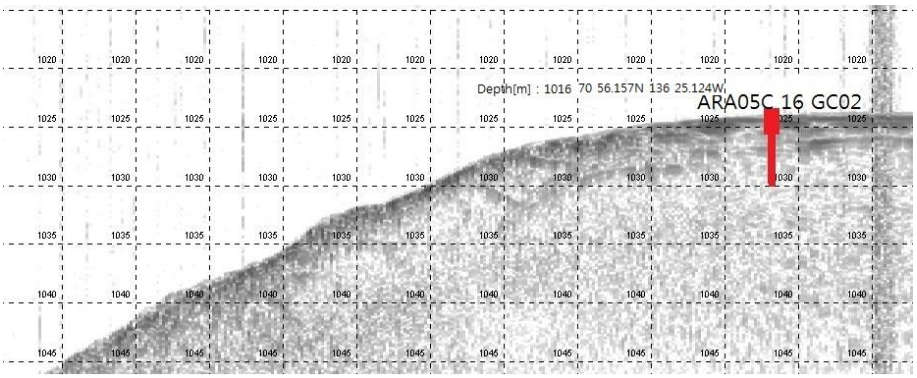


**Figure 7.3 - Sub-bottom profile of the slope background at 1,016 m water depth where core ARA05C 16GC02 was taken. Red icon represents location of the core, not actual core length.**

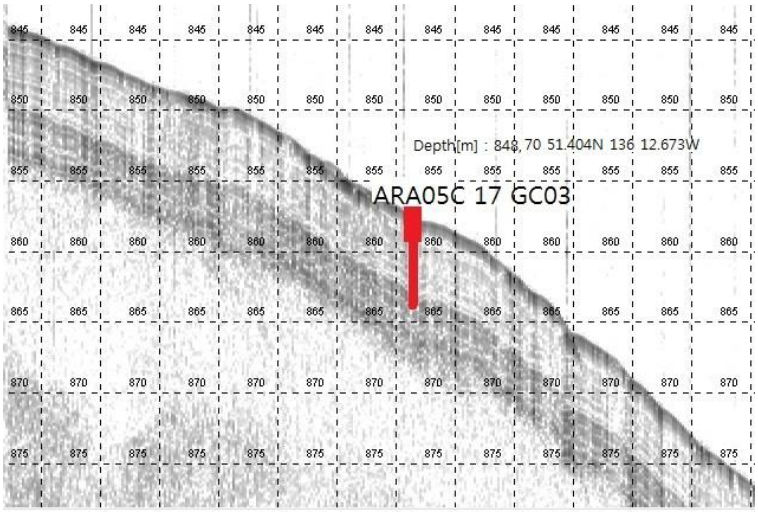


**Figure 7.4 - Sub-bottom profile of the slope background at 850 m water depth where core ARA05C 17GC03 was taken. Red icon represents location of the core, not actual core length.**

The core materials found at both sites are fairly similar, both showing the presence of allochthonous mud clasts less than 2 mm size at the bottom of the core and perhaps indicating that the core was collected on a mass transport deposit. This is further supported by measurements of undrained shear strength obtained with the fall cone method: $s_u$ shows a sudden increase in undrained shear strength at the core depth where allochthonous mud clasts were observed and slumping is hypothesized. Note that $s_u$ of cores ARA05C 16GC03 and ARA05C 17GC03 do not increase with depth in the intervals 0 - 2.4 mbsf and 0 - 2.1 mbsf, respectively. The sediment of the top sections of both cores shows slight over-consolidation, if a linear increase of shear strength with depth is estimated to be 20-40% effective overburden stress, and sediment bulk density is ~1.6 g/cc (for bulk density values of sediment measured in the Beaufort Sea, see Cruise report of ARA04C).

Furthermore, examination of the bathymetry appears to show that the location of the core from 1,016 m water depth is within a mass wasting event filled scour (Fig. 7.5). The evidence in the bathymetric map for the presence of a landslide deposit at the 850 m water depth core site is more equivocal.

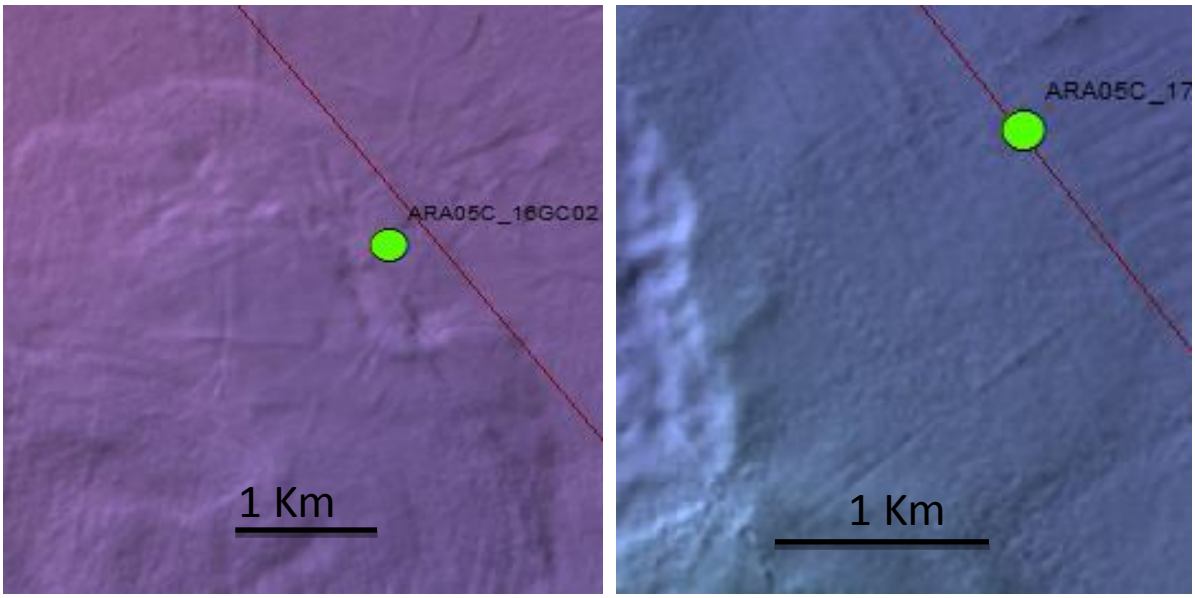


**Slope background 1,016 m** **Slope background 850 m**

**Figure 7.5 - Bathymetric maps of the locations in the slope background where cores ARA05C 16GC02 (1,016 m water depth), and ARA05C 17GC03 (850 m water depth) were taken.**

A third core from the slope background was collected at 406 m water depth in a site roughly equidistant from the mud volcanoes at 420 m and 290 m water depths. The undrained shear strength of the cored sediment increases linearly with depth within a range expected for normally consolidated sediment. Only the upper most sediment section (0-70 cm) shows slightly higher shear strength than expected in normal consolidation, which could be related to compaction effects of the coring method. The lowest shear strength relative to overburden stress is observed in the interval from 270 -290 cm. The sub-bottom profile shows layered sediments at the site of this core (Fig. 7.6).

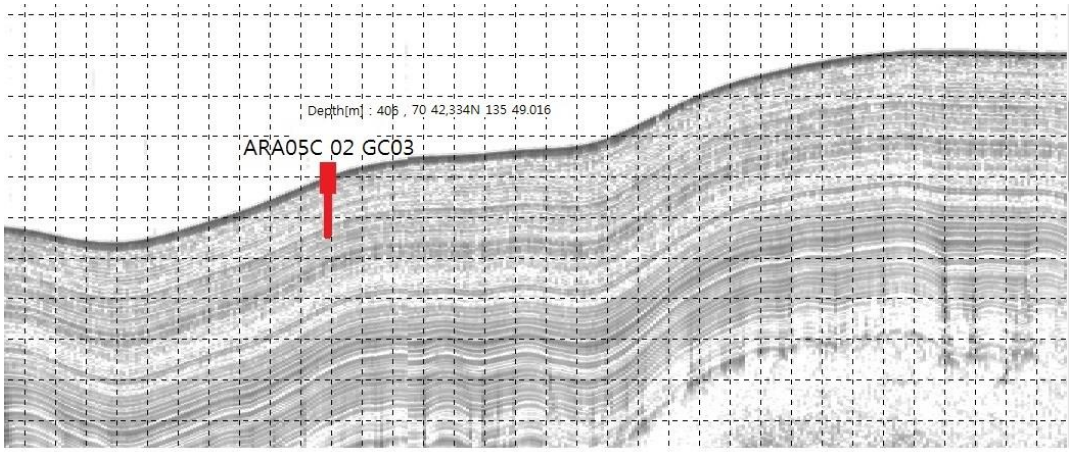


**Figure 7.6 - Site of a slope background core at 406 m water depth. Red icon represents location of the core, not actual core length.**

One core was collected in the Mackenzie trough at approximately the same location where core ARA04C-39GC001 had been collected during cruise ARA04C. Thermal conductivity measurements were done on the lower section of this core to complement thermal gradient measurements performed at this site during cruise ARA04C. In terms of undrained shear strength the sediment shows a slight decrease from ~5 to 2.5 kPa in the uppermost section. Within the second section the sediment shear strength increases linearly with depth as expected in normally consolidated sediment. Towards the bottom of the section II and all along section III (~1.5 -3.72 mbsf) the shear strength scatters from ~6 kPa to ~12 kPa. This may be related to the presence of mud clasts and discontinuous layering, which might indicate the presence of a mass transport deposit, although more data would be needed for confirmation.

### 7.4.2. Slope mud volcanoes

In cruise ARA05C, the three mud volcanoes found in the slope at approximate water depths of 290 m, 460 m, and 740 m, were successfully cored with core recovery averaging 268 cm (table 7.3). Over-penetration of the gravity corer headstand into the seafloor was noticed, probably owing to the soft gassy nature of the sediment.

**Table 7.3 - Mud volcanoes gravity cores.**

| Core | Latitude (N) | Longitude (W) | Water depth (m) | Length (cm) |
|---|---|---|---|---|
| **ARA05C 01GC03** | 70°47.342´ | 135°33.952´ | 420 | 272 |
| **ARA05C 10GC03** | 70°38.992´ | 135°56.811´ | 277 | 280 |
| **ARA05C 10GC05** | 70°38.992´ | 135°56.811´ | 278 | 221 |
| **ARA05C 18GC01** | 70°48.082´ | 136°5.932´ | 740 | 300 |

Two cores were collected at the 280 m water depth mud volcano site, which is captured in the sub-bottom profiler as an acoustic homogenous chimney with no internal reflectors (Fig. 7.7).

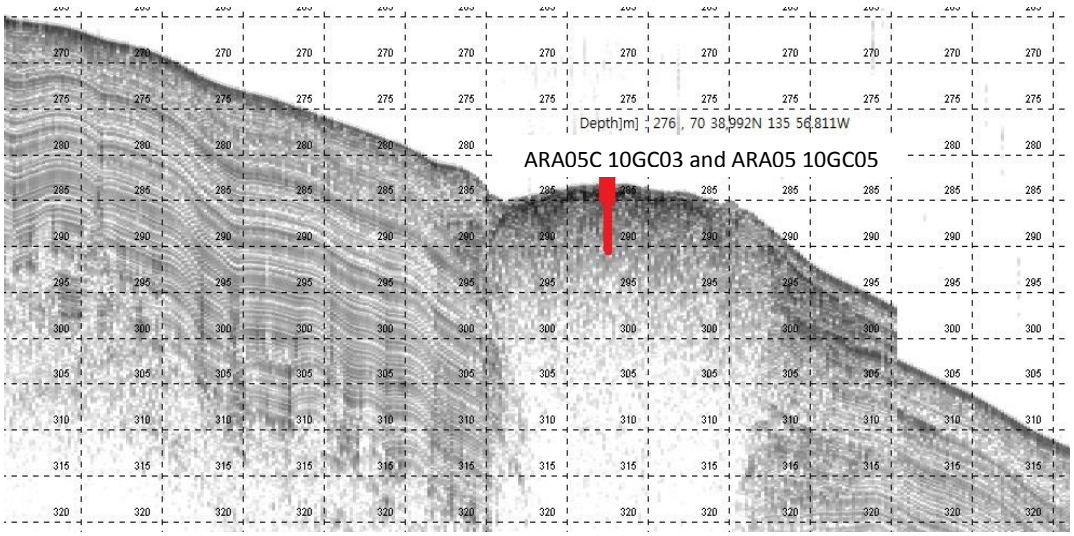


**Figure 7.7 - Sub-bottom profiler image of the 280 m water depth mud volcano. Red icon represents location of the core, not actual core length.**

Upon recovery large voids were visible through the liner, presumably the result of gas-hydrate decomposition and gas expansion that completely displaced the sediment leaving a gap in the sediment material. The gas in the void was sampled in core AR05C 10GC03. Both cores had the so-called "moussey texture" interpreted to be the result of the large abundance of methane bubbles, probably related to gas-hydrate decomposition (Fig. 7.8).

**Figure 7.8 - Moussey texture in core ARA05C 10GC05.**

Core ARAO5C 01GC03 was recovered at the 420 m water depth mud volcano (Fig. 7.9). It also displayed a moussey texture. The undrained shear strength ranges from 1 to 2 kPa within the upper most 80 cm. Down core $s_u$ increases to a maximum of ~5.5 kPa at 2.5 mbsf.

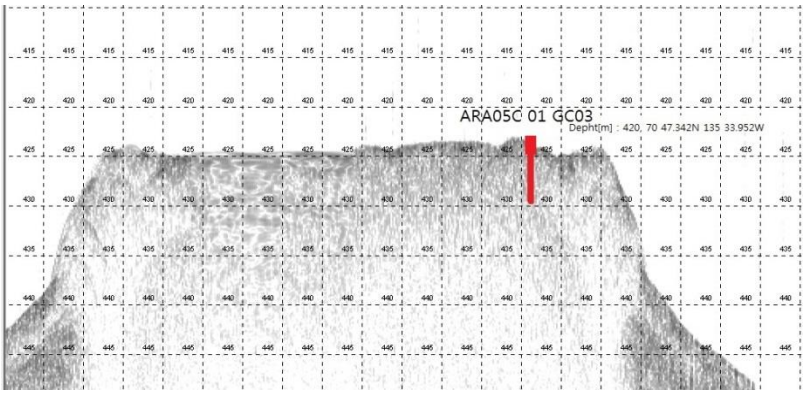


**Figure 7.9 - Sub-bottom profile visualization of the 420 m water depth mud volcano.**

The mud volcano at 764 m water depth (Fig. 7.10) was also sampled via gravity and box-coring.

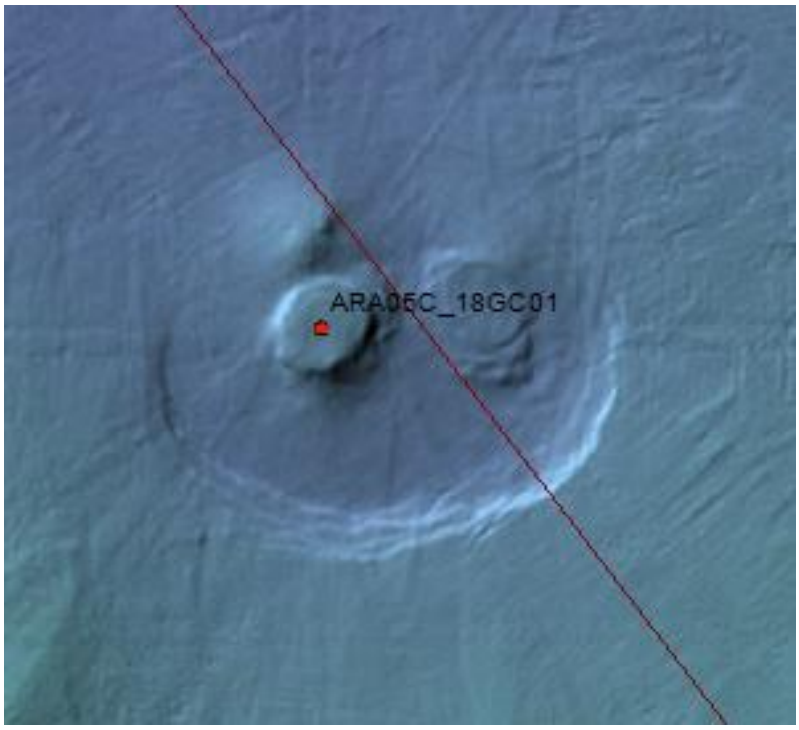


**Figure 7.10 - Map of the 740 m water depth mud volcano on the slope. The W-E extent of this feature is 2.8 km. Location of core ARA05C 18GC01 and seismic line ARA05C-15 are highlighted.**

Core ARA05C 18GC01 was collected at this feature. The core had several gas filled gaps were sediment was completely displaced. Gas from this void was sampled by piercing the liner. Gas hydrates were found in this core. This finding is the first time that gas hydrates are proved to be present and recovered from this mud volcano. Gas hydrates were present in the core catcher and embedded in the sediment in crystals no larger than 2 cm and in smaller crystals along a sediment crack (Fig. 7.11). Although the sediment internal structure supposedly has been greatly disturbed by gas expansion, the undrained shear strength was determined on sediment portions encountered in each section. The uppermost section presents higher shear strength ($s_u$ = 6-18 kPa) than the lower second section ($s_u$ ~ 2-7 kPa). A possible explanation for the reverse increase in shear strength could be the higher amount of gas hydrates and inherent melt water

towards the bottom of the core. Note that shipboard measurements of *in-situ* gas bearing sediment are to be carefully interpreted. Measurements of *in-situ* shear strength (Chapter 8: Cone Penetration Test) should help to clarify this issue.

**Figure 7.11 - Gas hydrates in core ARA05C 18GC01 from the 740 m water depth mud volcano.**

### 7.4.3. Cyan Unit

The stratigraphy of the Beaufort Sea slope is defined by the distinct acoustic response of different lithological units in seismic profiles. The upper sedimentary column of the slope is composed of three units: the Orange unit drapes underlying occasionally deformed and normally fractured sediments of the Yellow unit, which appears in sub-bottom profiles as a package of alternating weak and strong reflectors. Below this unit, the Cyan unit, of approximately 40 m thickness, has an acoustically homogeneous appearance and in many instances displays a plastic behavior where it pierces and fractures the sedimentary Yellow unit above it. It has been proposed that the Orange unit has been deposited during the Holocene. The Yellow unit is thought to be a glacio-marine deposit of late glacial age, and the Cyan unit a diamicton predating the last glacial maximum. The Cyan unit is normally covered by the upper units, however in proximity to the shelf edge, erosion process may have exposed it, and it may be possible to sample it with gravity coring. During ARA04C, this unit was targeted but the core recovery was short in three attempts: 26, 52, and 81 cm. The sediments found in those instances were described as a stiff lithology below 30 cm of soft mud.

The targeting of the Cyan unit was based on the sub-bottom profile acquired when seismic line ARA05C-06 was obtained (Fig. 7.12), where the disruption of the upper units by the plastic cyan unit is clearly visible on the shelf edge. In multibeam sonar images, the protrusions produced by the Cyan unit appear as mounds of less than 200 m length along their longer axis and less than 30 m higher than the surrounding seafloor (Fig. 7.13).

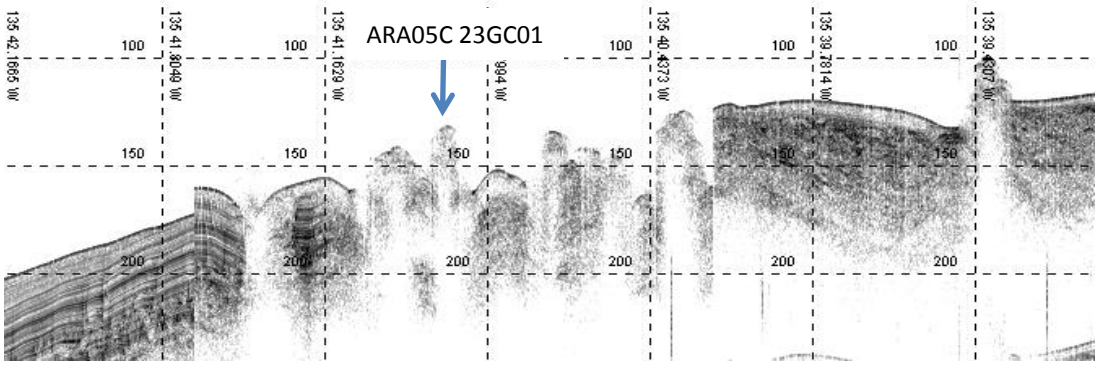


**Figure 7.12 - Sub-bottom profile of the yellow unit on the left breached by upwards flow of the Cyan unit.**

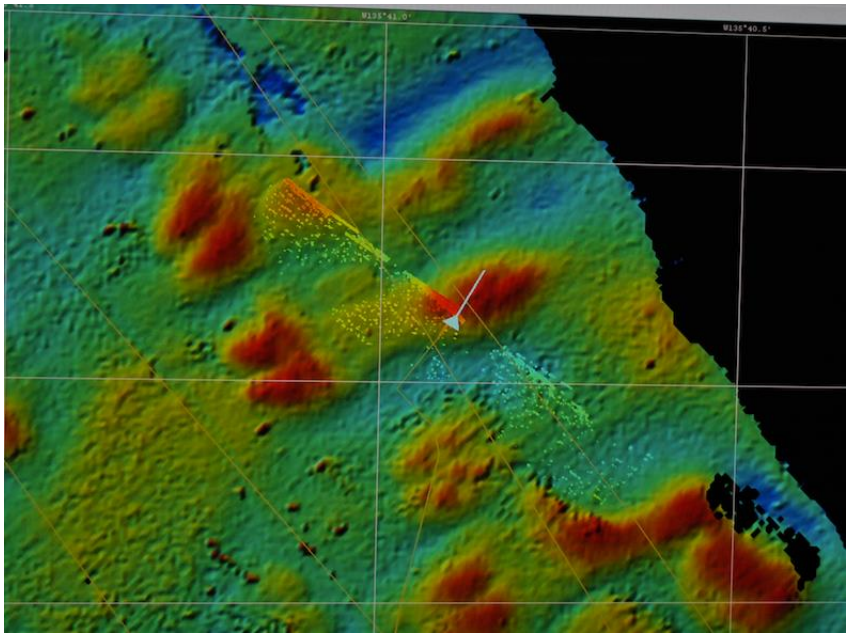

**Figure 7.13 - Multibeam image of mounds believed to be produced by upward flow and breaching of upper sedimentary units by the Cyan unit. The ship icon is above the mound where core ARA05C 23GC01 was collected.**

The recovery of core ARA05C 23GC01 collected on this site was 183 cm. Several rock fragments of different lithologies were found on the surface of the sliced core including a large pink sandstone (Fig. 7.14a) and pebbles of mafic composition. A piece of woody material was noticed, which could be radiocarbon dated to provide an absolute datum to the seismostratigraphic units. The core catcher contained a large piece of clear angular ice (Fig. 7.14b). This finding suggests that this rock unit contains freshwater of unknown origin and age. The undrained shear strength determined via fall-cone testing shows a linear increase with depth at a rate significantly higher than expected in normally consolidated sediment. The sediment found at this location where the Cyan unit was cored could be regarded as highly over-consolidated. The distinct peaks in undrained shear strength are related to the presence of mud clasts that are an order of magnitude stiffer than the surrounding matrix. The fall-cone may also have hit sand size rock fragments of sandstone or mafic rock.


**Figure 7.14 - (a, left) Sandstone rock found in ARA05C 23GC01. (b, right) Ice found in core catcher of ARA05C 23GC01, at 183 cm depth. The ice was angular before it was cleaned for photo documentation.**

## *7.5. Summary*

The coring program during the ARA05C cruise in the Beaufort Sea was highly successful in managing to retrieve cores in all the environments that were considered high priority for this expedition. In addition to collecting slope background cores that will complement the core database compiled in the shelf, shelf edge and slope by partnering research organizations in the past, this expedition is the first to directly sample gas-hydrates at the 740 m water depth mud volcano. Furthermore, the discovery and sampling of sediment and ice in the Cyan unit may provide key information to increase our understanding of the sources and pathways of freshwater flow in the shelf and slope. Physical properties measurements on collected cores will assist in the evaluation of geohazards since geomorphological evidence from the shelf edge and slope shows these areas have experienced mass wasting events.

# Appendix A.7.1: Core descriptions and ancillary information

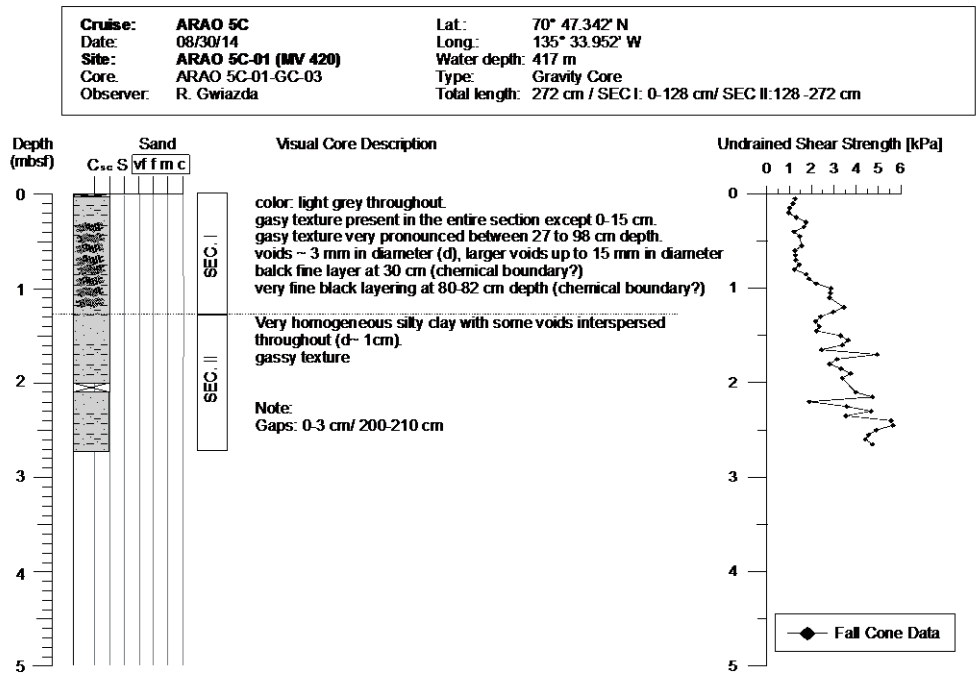


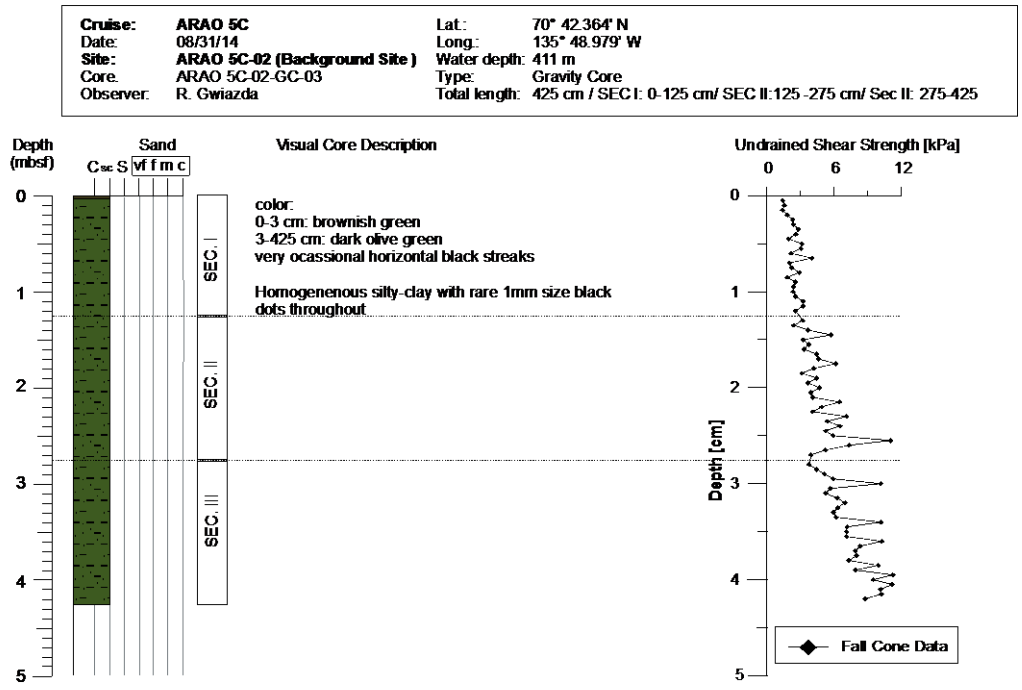

| | | | |
|---|---|---|---|
| **Cruise:** | **ARAO 5C** | Lat.: | 70° 38.992' N |
| Date: | 08/31/14 | Long.: | 135° 56.811' W |
| **Site:** | **ARAO 5C-10 (MV 290/ Coke Cap )** | Water depth: | 277 m |
| Core: | ARAO 5C-10-GC-03 | Type: | Gravity Core |
| Observer: | R. Gwiazda | Total length: | 280 cm / SEC I: 0-130 cm/ SEC II:130 -280 cm |

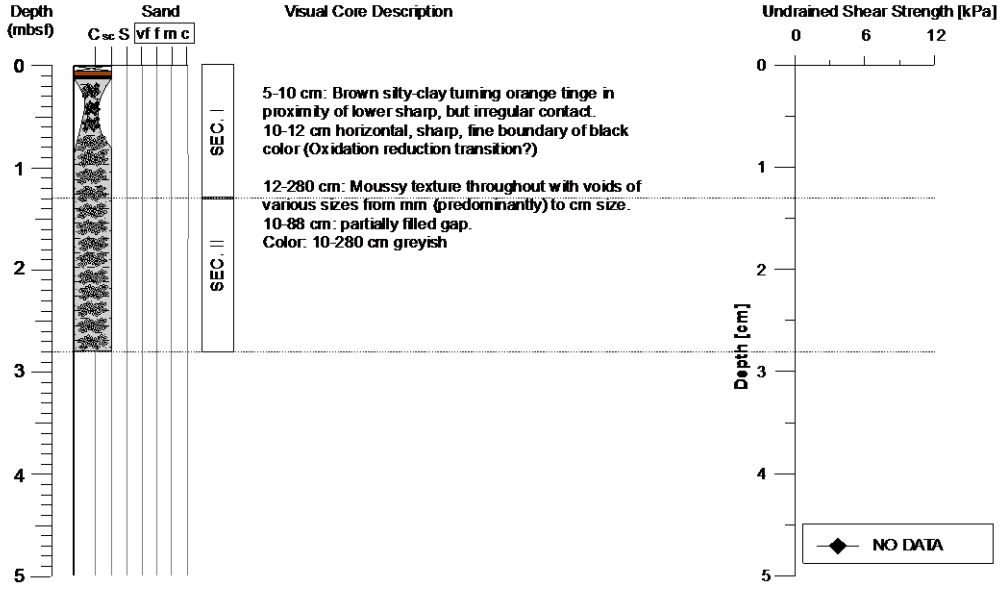


| | | | |
|---|---|---|---|
| **Cruise:** | **ARAO 5C** | Lat.: | 70° 38.992' N |
| Date: | 08/31/14 | Long.: | 135° 56.811' W |
| **Site:** | **ARAO 5C-10 (MV 290/ Coke Cap )** | Water depth: | 278 m |
| Core: | ARAO 5C-10-GC-05 | Type: | Gravity Core |
| Observer: | R. Gwiazda | Total length: | 221cm / SEC I: 0-69 cm/ SEC II:69 -221 cm |

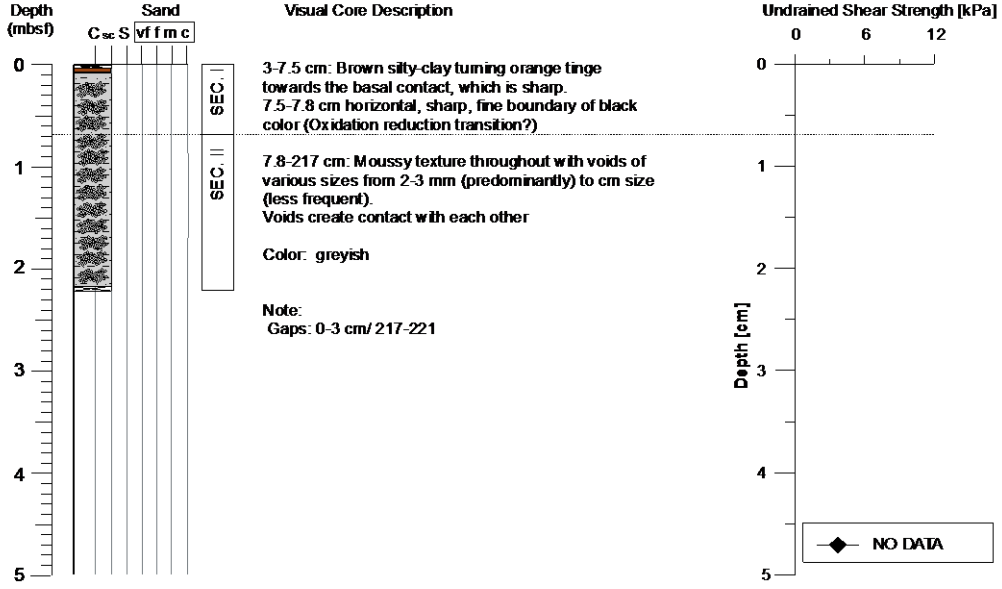

| | | | |
|---|---|---|---|
| **Cruise:** | **ARAO 5C** | Lat.: | 70° 56.133' N |
| Date: | 09/06/14 | Long.: | 136° 25.056' W |
| **Site:** | **ARAO 5C-16 (Deep Background Site )** | Water depth: | 1016 m |
| Core. | ARAO 5C-16-GC-02 | Type: | Gravity Core |
| Observer: | R. Gwiazda | Total length: | 385 cm / SEC I: 0-85 cm/ SEC II:85 -235 cm/ Sec III: 235-385 |

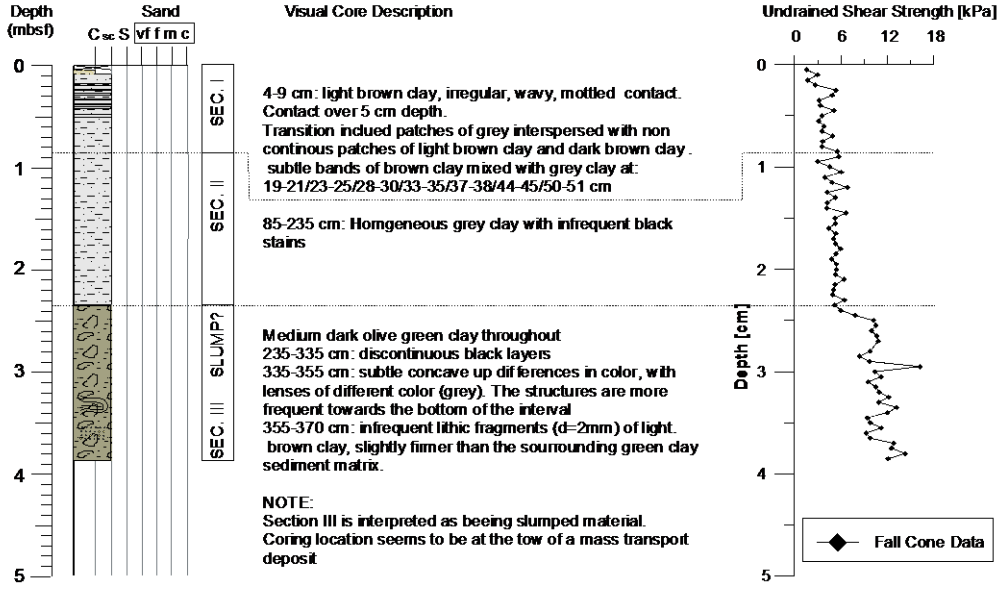


| | | | |
|---|---|---|---|
| **Cruise:** | **ARAO 5C** | Lat.: | 70° 51.378' N |
| Date: | 09/06/14 | Long.: | 136° 12.746' W |
| **Site:** | **ARAO 5C-17 (Background Site )** | Water depth: | 850 m |
| Core. | ARAO 5C-17-GC-03 | Type: | Gravity Core |
| Observer: | R. Gwiazda | Total length: | 373 cm / SEC I: 0-73 cm/ SEC II:73 -223 cm/ Sec III: 223-373 cm |

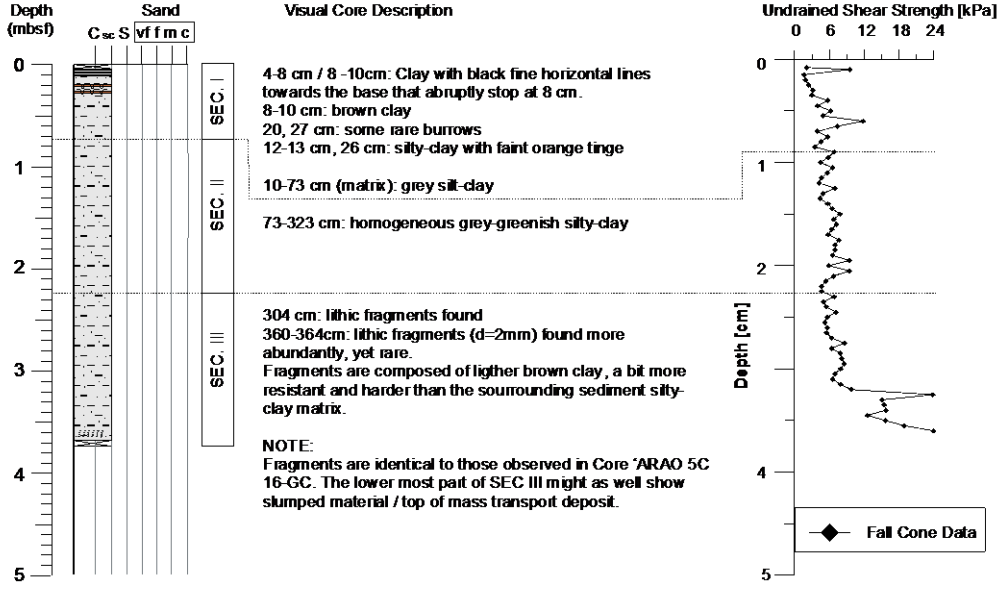

| | | | |
|---|---|---|---|
| **Cruise:** | **ARAO 5C** | Lat.: | 070° 48.082' N |
| Date: | 09/07/14 | Long.: | 136° 05.932' W |
| **Site:** | **ARAO 5C-18 (MV 760 m)** | Water depth: | 740 m |
| Core: | ARAO 5C-18-GC-01 | Type: | Gravity Core |
| Observer: | R. Gwiazda | Total length: | 300cm / SEC I: 0-177 cm/ SEC II:177 -300 cm |

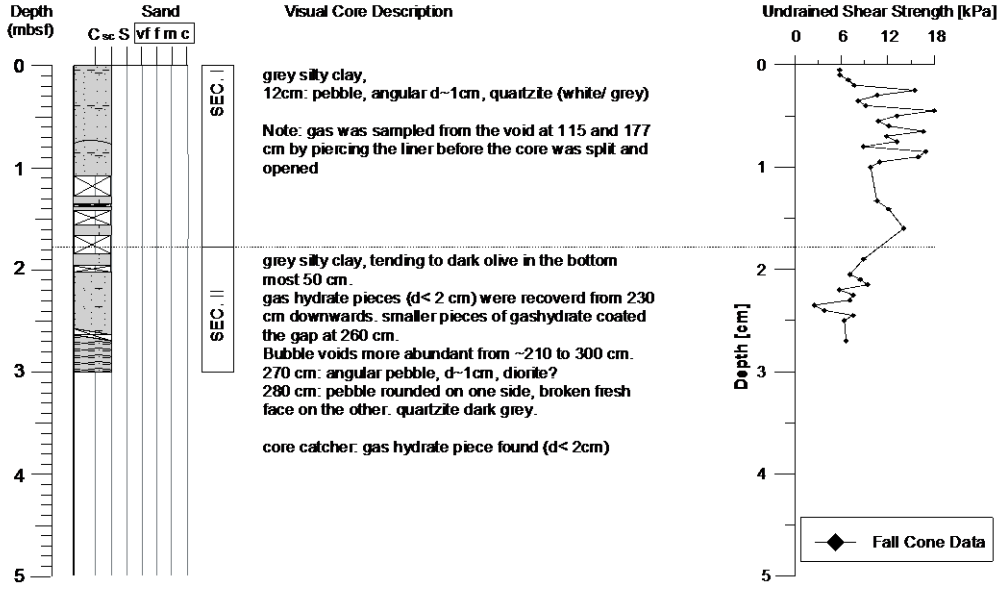


| | | | |
|---|---|---|---|
| **Cruise:** | **ARAO 5C** | Lat.: | 070° 38.1352' N |
| Date: | 09/10/14 | Long.: | 135° 40.8849' W |
| **Site:** | **ARAO 5C-23 (CYAN UNIT)** | Water depth: | 114 m |
| Core: | ARAO 5C-23-GC-05 | Type: | Gravity Core |
| Observer: | Gauvain Wiemer | Total length: | 189cm / SEC I: 0-189 cm |

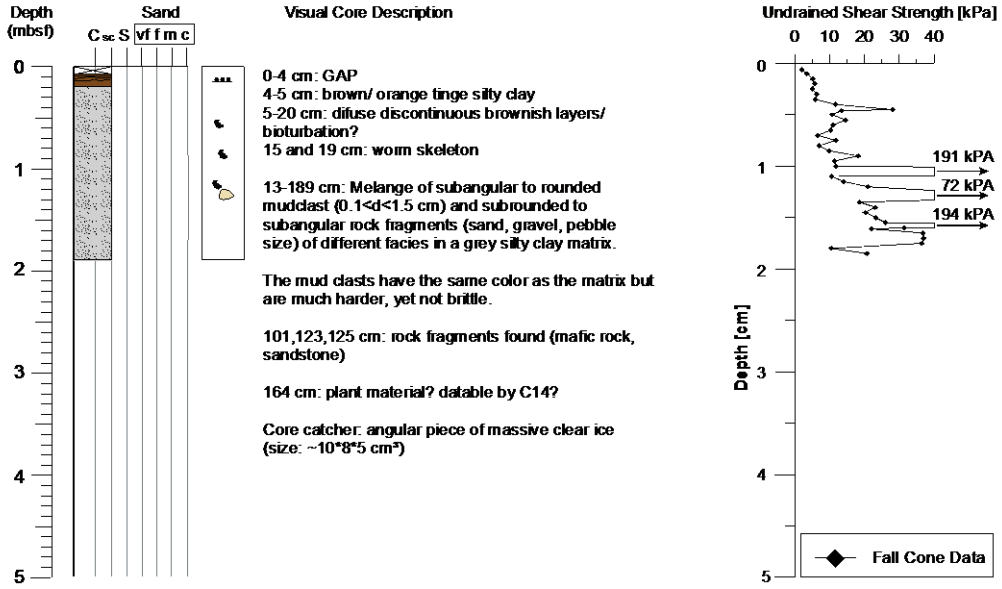

| | | | |
|---|---|---|---|
| **Cruise:** | **ARAO 5C** | Lat.: | 70° 39.35' N |
| Date: | 09/11/14 | Long.: | 139° 2.207' W |
| **Site:** | **ARAO 5C-33 (Mackenzie Trough )** | Water depth: | 1534 m |
| Core. | ARAO 5C-33-GC-03 | Type: | Gravity Core |
| Observer: | G. Wiemer | Total length: | 367 cm / SEC I: 0-67cm/ SEC II:67 -217 cm/ Sec II: 217-367 cm |

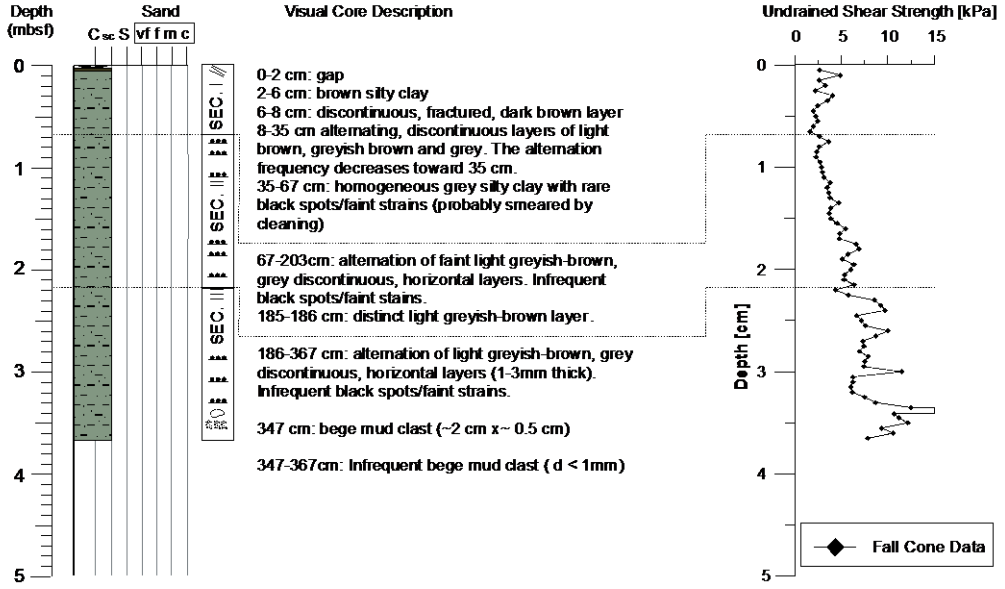


Visual Core Description

0-2 cm: gap
2-6 cm: brown silty clay
6-8 cm: discontinuous, fractured, dark brown layer
8-35 cm alternating, discontinuous layers of light brown, greyish brown and grey. The alternation frequency decreases toward 35 cm.
35-67 cm: homogeneous grey silty clay with rare black spots/faint strains (probably smeared by cleaning)

67-203cm: alternation of faint light greyish-brown, grey discontinuous, horizontal layers. Infrequent black spots/faint stains.
185-186 cm: distinct light greyish-brown layer.

186-367 cm: alternation of light greyish-brown, grey discontinuous, horizontal layers (1-3mm thick). Infrequent black spots/faint strains.

347 cm: bege mud clast (~2 cm x~ 0.5 cm)

347-367cm: Infrequent bege mud clast ( d < 1mm)

| | | | |
|---|---|---|---|
| **Cruise:** | **ARAO 5C** | Lat.: | 70° 5.624' N |
| Date: | 09/12/14 | Long.: | 138° 21.215' W |
| **Site:** | **ARAO 5C-34 (Mackenzie Trough )** | Water depth: | 246 m |
| Core. | ARAO 5C-34-GC-04 | Type: | Gravity Core |
| Observer: | G. Wiemer | Total length: | 417 cm / SEC I: 0-116cm/ SEC II:117 -267 cm/ Sec II: 267-417 cm |

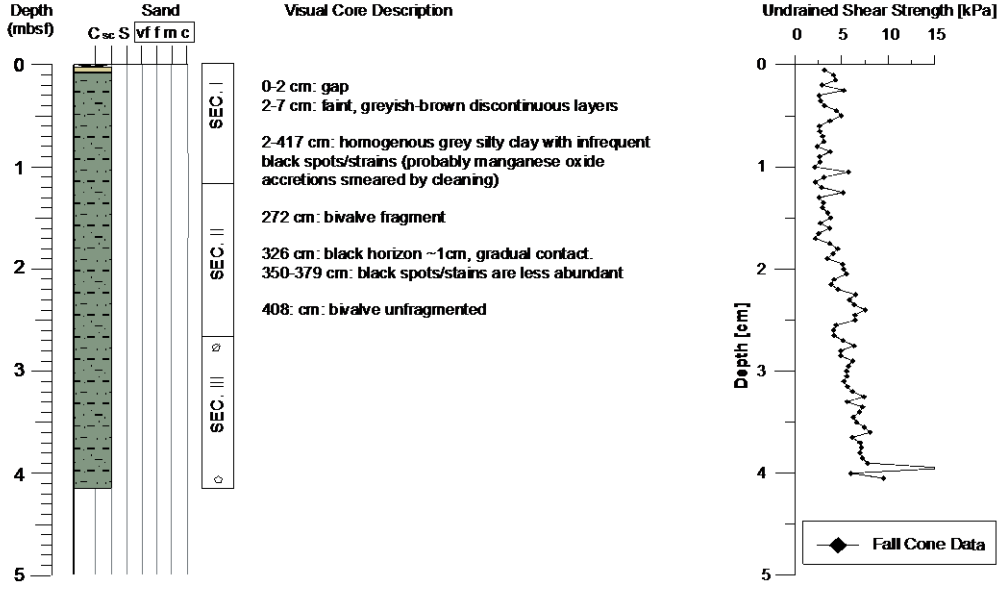


Visual Core Description

0-2 cm: gap
2-7 cm: faint, greyish-brown discontinuous layers

2-417 cm: homogenous grey silty clay with infrequent black spots/strains (probably manganese oxide accretions smeared by cleaning)

272 cm: bivalve fragment

326 cm: black horizon ~1cm, gradual contact.
350-379 cm: black spots/stains are less abundant

408: cm: bivalve unfragmented

# CHAPTER 8 - Cone penetration testing

G. Wiemer

## *8.1. Introduction*

Cone Penetration Testing (CPT) is a common *in situ* onshore and offshore measuring technique to determine key physical parameters of the sediment (Lunne et al., 1997). The MARUM- Shallow-Water-Free-Fall-CPTU (SWFF-CPTU) (Stegmann et al., 2006) (Fig. 8.1) has been deployed during the course of ARA05C cruise. The centrepieces of the instrument are i) an industrial 15 cm² piezocone cone and ii) an aluminium pressure-tight housing containing a microprocessor (Avisaro AG), logging unit, including a standard secure digital memory card (SD), power supply (battery package), tilt meter, accelerometer and data communication unit. The maximum water depth at which this SWFF-CPTU can be operated is 500 m. The instrument is modular and can be adapted in length from 1.5 m - 8.5 m depending on the encountered geological setting and expected penetration depth. The SWFF-CPTU is lowered through the water column either with the help of a winch or in free-fall until it is decelerated by the penetration of the sediment column. Analogue to the length, weights may be added to reach higher penetration. The total weight can vary from minimum 45 kg (manually operational) to maximum 200 kg (winch needed) in its longest and heaviest configuration. The piezocone located at the tip of the CPT, measures cone resistance ($q_c$), sleeve friction ($f_s$), pore pressure (u) and inclination. Further, deceleration and inclination sensors are placed in the housing of the instrument. Data recording takes place at 1 kHz.

**Figure 8.1 - SW-CPTu instrument on A-frame of RV Araon prior to deployment on cruise ARA05C.**

Figure 8.2 illustrates the processing steps needed to obtain the *in situ* undrained shear strength ($s_u$) from the recorded dynamic parameters deceleration, cone resistance ($q_c$) and pore pressure (u) obtained during penetration of the sea floor. Post-processing includes double integration of the deceleration data and implementation of the inclination which allows determining penetration depth accurately with a precision of 2 % of the maximum penetration depth. At that point, cone resistance, sleeve friction and pore pressure along the profile are dynamic parameters, i.e. they are velocity dependent. In order to obtain quasi-static parameters comparable to static CPTu tests these parameters need to be corrected for strain-rate (Lunne et al., 1997; Stegmann et al., 2006; Steiner, 2013). The *in situ* undrained shear strength ($s_u$) is a function of the strain-rate and pore pressure corrected cone resistance ($q_{t,quasi\text{-}stat}$), the effective

overburden stress ($\sigma'_{v0}$) and an empirically determined cone penetration resistance factor ($N_{k,t}$) which is related to $q_{t,quasi\text{-}stat}$ (Lunne et al., 1997). $s_u$ can be determined by applying the following geotechnical solution:

$$s_{u,\ quasi\text{-}stat} = \frac{q_{t,\ quasi\text{-}stat} - \sigma'_{v0}}{N_{k,t}}$$

Once cone resistance has been corrected for pore pressure and strain rate, cone resistance data are comparable to static industrial CPTU tests. The vertical resolution of a CPTu profile is ~1cm at penetration velocities < 10 m/s (Steiner, 2013). A detailed description of the MARUM SWFF-CPT equipment including technical details, data processing and data-processing is given in (Steiner, 2013).

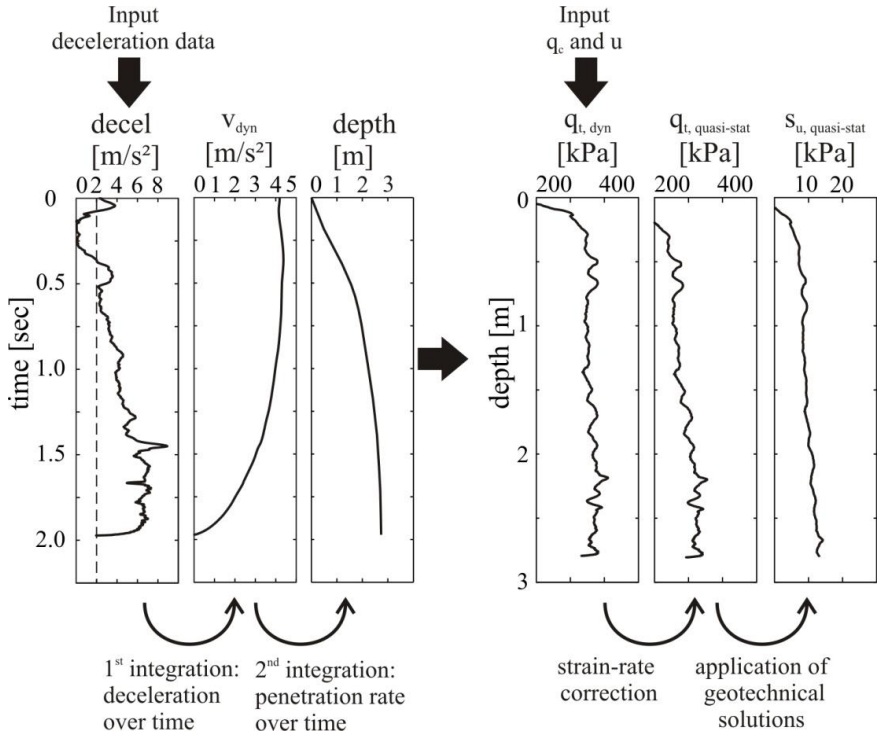


**Figure 8.2 - By integration of the deceleration data over time, penetration velocity (vdyn) is obtained. A second integration over time results in the penetration depth over time. The cone resistance data (qc) is corrected for pore pressure (u) and becomes qt,dyn. $q_{t,\ quasi\text{-}stat}$ is the strain-rate corrected $q_{t,dyn}$ and is comparable to cone resistance from static pushed CPTU data. $s_{u,quasi\text{-}stat}$ is the *in situ* undrained shear strength obtained by resolving equation 4.1 (modified after Steiner (2013)).**

## *8.2. CPT Targets*

CPT measurements conducted in the Beaufort Sea on ARA05C cruise had three main goals:

i) To investigate the in situ geotechnical properties and state of pore water pressure of slope sediment and slope failure involved sediment (see ARA04C cruise report). Gas hydrate

dissociation and/or ice melding in ice-bound sediment are expected to reduce slope sediments resistance to shear failure. Submarine landslides are therefore regarded as a potential future geohazard in the region.

ii) To revisit sites that were measured within the mud volcanoes at 420 m water depth during the Sir Wilfrid Laurier CCGS cruise in 2013 in order to measure potential differences in sediment stiffness and relate them to local/general changes in mud volcano activity.

iii) To determine the geotechnical properties and state of pore water pressure of slope background sediment for reference.

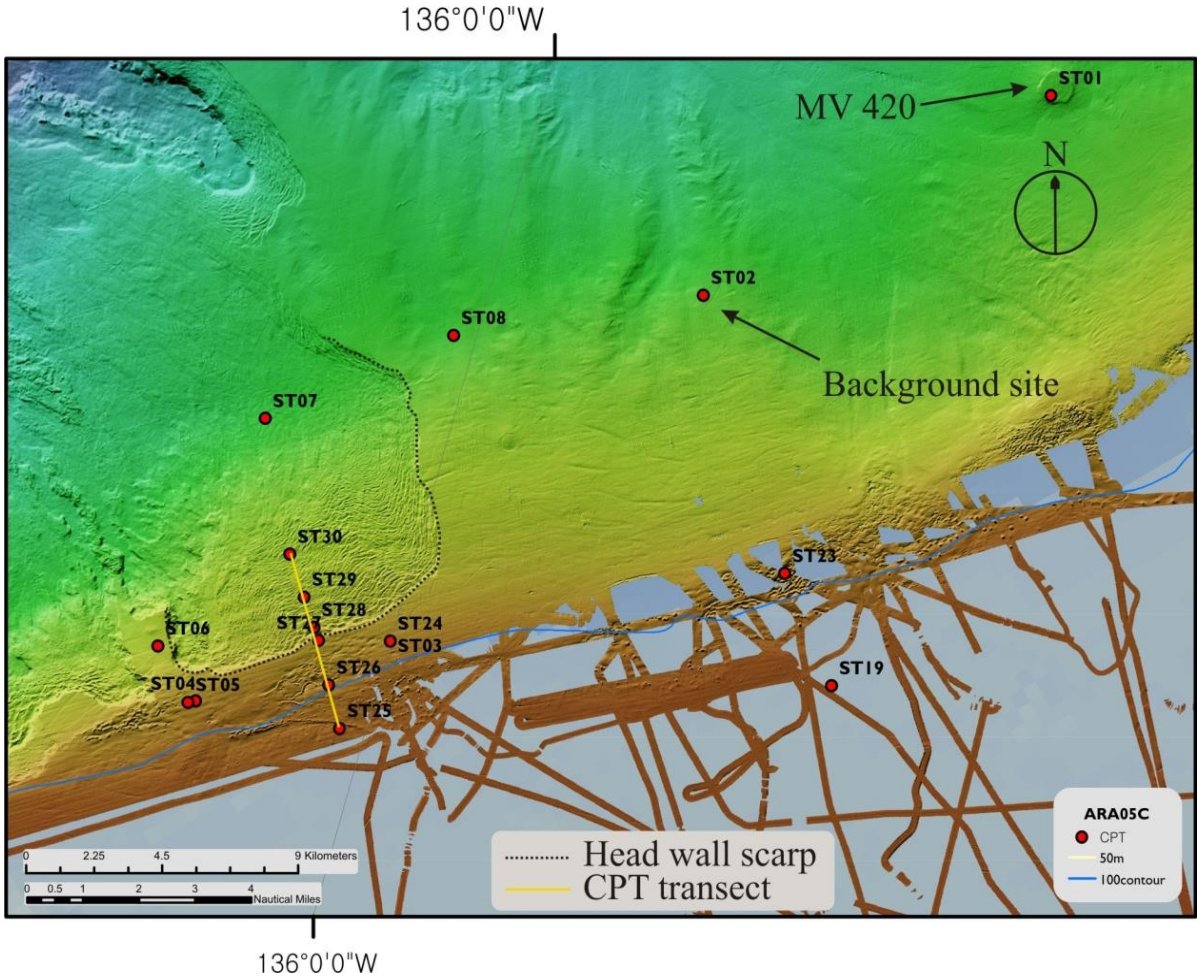


**Figure 8.3 - Locations and station numbers of CPT deployments on ARA05C cruise.**

## *8.3. Data acquisition*

The MARUM SWFF-CPTu was deployed with two different winches available on RV Araon, namely i) Small Deep Sea (SDS) (maximum winch speed: 50 m/min) and ii) Deep Sea Traction (DST) (maximum winch speed: 72 m/min). The CPT was set up to a total length of 4.5 m for the stations ARA05C-01 to ARA05C-08, ARA05C-19 and ARA05C-23. At the following CPT stations the CPT was set to total length of 3.5 m. The pore pressure port was located at the 'u2 position' for each deployment.

Figure 8.3 shows the geologic settings and stations of all CPT deployments conducted during this cruise. Deployment sites dedicated to the determination of sediment physical properties in the slope failure region and slope stability evaluation were chosen a) at positions where the RV Sir Wilfrid Laurier is planning to take piston cores in Sept. 2014 and b) on a down slope transect perpendicular to the head wall of the slide. This CPT transect was started during RV Sir Wilfrid Laurier CCGS cruise 2013, but could not be fully accomplished due to bad weather conditions. During ARA05C cruise we achieved to complete this transect of CPT measurements. The mud volcano located at 420 m water depth (MV 420) was revisited in the course of station ARA05C-01. This position coincides with one station visited during Sir Wilfrid Laurier cruise CCGS 2013. The characterization of the slope background sediment was conducted at station ARA05C-02 (Fig. 8.3).

### *8.4. Preliminary Results*

After the first measurement period (08/30/2014, 20:26 UTC – 08/31/2014, 14:23 UTC) and preliminary data processing we found that the speed of the DSD winch was highly variable. The CPT constantly experienced velocity changes or acceleration and deceleration on its way through the water column, and also when sediment penetration had already started. Variation of CPT-acceleration/deceleration attributed to technical problems of the winch majorly influences the deceleration measurement of the CPT that should be entirely related to sediment penetration.

As a consequence we used the DST winch at station ARA05C-19 to test the second available winch on RV Araon. This winch operates with a neutral buoyancy rope and reaches higher maximum velocities than the SDS winch. Preliminary results of processed data obtained at station ARA05C-19 (see Appendix) shows that the variability of acceleration/deceleration of the CPT attributed to the technical properties of this winch are minor, even negligible. However, due to safety issues, CPT station ARA05C-23 was the last station at which the DST winch could be operated. Hence, all further measurements were conducted with the DST winch although the expected data quality is significantly lower.

In total the CPT was deployed at 17 Stations with a total of 35 drops. Table 8.1 shows the station, station coordinates, CPT setup (number of rods and weights), water depth measured on board, water depth of the CPT at the start of sediment penetration, operated winch, winch speed that was aimed at on board, winch speed of the CPT at the start of sediment penetration and final penetration depth of the CPT.

| CRUISE | STATION | SITE | Lat | Long | RODS | WEIGHTS | Pressure port | DROP | WATER DEPTH CPT (m) | WINCH SPEED (BOYAN ROPE) | WINCH SPEED (AIM) (m/min) | WINCH SPEED (m/s) | PENETRATION [m] |
|---|---|---|---|---|---|---|---|---|---|---|---|---|---|
| ARAO 5C | 01 | MV 420 | 70° 47.342 N | 135° 33.952' W | 3 | 3 | U2 | 1 | 426 | X | 50 | 0,8 | 1,8 |
| ARAO 5C | 01 | MV 420 | 70° 47.342 N | 135° 33.952' W | 3 | 3 | U2 | 2 | 424 | X | 50 | 0,78 | 2,5 |
| ARAO 5C | 01 | MV 420 | 70° 47.342 N | 135° 33.952' W | 3 | 3 | U2 | 3 | 424 | X | 50 | 0,43211 | 1,47 |
| ARAO 5C | 02 | BACKGROUND SITE SLOPE | 70° 42.36362' N | 135° 48.97940' W | 3 | 3 | U2 | 1 | 415 | X | 50 | 0,73 | 3,03 |
| ARAO 5C | 02 | BACKGROUND SITE SLOPE | 70° 42.36362' N | 135° 48.97940' W | 3 | 3 | U2 | 2 | 415 | X | 50 | 0,5226 | 2,77 |
| ARAO 5C | 03 | AMUNDSEN_PC1 | 70° 35.11302' N | 136° 0.00600' W | 3 | 3 | U2 | 1 | X | X | X | X | X |
| ARAO 5C | 03 | AMUNDSEN_PC1 | 70° 35.11302' N | 136° 0.00600' W | 3 | 3 | U2 | 2 | 112 | X | 50 | 0,4-0,68 | 1,20 |
| ARAO 5C | 04 | AMUNDSEN_PC6a | 70° 33.17406' N | 136° 9.01572' W | 3 | 3 | U2 | 1 | 123 | X | 50 | 0,6 | 1,05 |
| ARAO 5C | 04 | AMUNDSEN_PC6a | 70° 33.17406' N | 136° 9.01572' W | 3 | 3 | U2 | 2 | 118 | X | 50 | 0,789 | 1,06 |
| ARAO 5C | 05 | AMUNDSEN_PC6b | 70° 33.11376' N | 136° 9.38730' W | 3 | 3 | U2 | 1 | 128 | X | 50 | 0,55 | 0,91 |
| ARAO 5C | 05 | AMUNDSEN_PC6b | 70° 33.11376' N | 136° 9.38730' W | 3 | 3 | U2 | 2 | 124 | X | 50 | 0,64 | 0,75 |
| ARAO 5C | 06 | AMUNDSEN_PC5 | 70° 33.89664' N | 136° 11.72303' W | 3 | 3 | U2 | 1 | 239 | X | 50 | 0,66 | 3,04 |
| ARAO 5C | 06 | AMUNDSEN_PC5 | 70° 33.89664' N | 136° 11.72303' W | 3 | 3 | U2 | 2 | 238 | X | 50 | 0,72-1 | 3,45 |
| ARAO 5C | 07 | AMUNDSEN_PC3 | 70° 38.20542' N | 136° 9.57186' W | 3 | 3 | U2 | 1 | 477,5 | X | 50 | 0,6-0,81 | 2,1 |
| ARAO 5C | 07 | AMUNDSEN_PC3 | 70° 38.20542' N | 136° 9.57186' W | 3 | 3 | U2 | 2 | 476,8 | X | 50 | 0,75 | 2,59 |
| ARAO 5C | 08 | AMUNDSEN_PC2 | 70° 40.49796' N | 136° 1.17234' W | 3 | 3 | U2 | 1 | 442 | X | 50 | 0,95-1 | 3,38 |
| ARAO 5C | 08 | AMUNDSEN_PC2 | 70° 40.49796' N | 136° 1.17234' W | 3 | 3 | U2 | 2 | 442 | X | 50 | 0,84-1,2 | 3,39 |
| | | | | | | | | | | | | | |
| ARAO 5C | 19 | Test of buyont rope winch | 70° 36.48400' N | 135° 36.92300' W | 3 | 3 | U2 | 1 | 73 | 60 | X | 0,8 | 0,24 |
| ARAO 5C | 19 | Test of buyont rope winch | 70° 36.48400' N | 135° 36.92300' W | 3 | 3 | U2 | 2 | 71,8 | 72 | X | 1,2 | 0,29 |
| | | | | | | | | | | | | | |
| ARAO 5C | 23 | SHELF: CAYAN UNIT | 70° 38.13000' N | 135° 40.78500' W | 3 | 3 | U2 | 1 | 108,8 | 60 | X | 1,18 | 1,1 |
| ARAO 5C | 23 | SHELF: CAYAN UNIT | 70° 38.13000' N | 135° 40.78500' W | 3 | 3 | U2 | 2 | 108,8 | 72 | X | 1,18 | 0,91 |
| | | | | | | | | | | | | | |
| ARAO 5C | 24 | AMUNDSEN_PC1 | 70° 35.11302' N | 136° 0.00600' W | 2 | 4 | U2 | 1 | 85 | X | 30 | 0,39 | 1,18 |
| ARAO 5C | 24 | AMUNDSEN_PC1 | 70° 35.11302' N | 136° 0.00600' W | 2 | 4 | U2 | 2 | 85 | X | 40 | 0,7 | 0,59 |
| ARAO 5C | 25 | START DOWN SLOPE CPT PROFILE | 70° 33.41808' N | 136° 1.32558' W | 2 | 4 | U2 | 1 | X | X | X | X | X |
| ARAO 5C | 25 | START DOWN SLOPE CPT PROFILE | 70° 33.41808' N | 136° 1.32558' W | 2 | 4 | U2 | 2 | X | X | X | X | X |
| ARAO 5C | 26 | STAT_112 LAURIER 2013 | 70° 34.08966' N | 136° 2.49936' W | 2 | 4 | U2 | 1 | 111,5 | X | 40 | 0,6 | 2,30 |
| ARAO 5C | 26 | STAT_112 LAURIER 2013 | 70° 34.08966' N | 136° 2.49936' W | 2 | 4 | U2 | 2 | 100,9 | X | 60 | 1 | 2,50 |
| ARAO 5C | 27 | SHELF: HEADWALL EDGE | 70° 34.77732' N | 136° 3.64782' W | 2 | 4 | U2 | 1 | 139,8 | X | 40 | 0,6 | 2,1 |
| ARAO 5C | 27 | SHELF: HEADWALL EDGE | 70° 34.77732' N | 136° 3.64782' W | 2 | 4 | U2 | 2 | 130,3 | X | 60 | 1 | 2,15 |
| ARAO 5C | 28 | SLOPE: FOOT OF HEADWALL | 70° 34.97070' N | 136° 4.06992' W | 2 | 4 | U2 | 1 | 184 | X | 40 | 0,58 | 2,10 |
| ARAO 5C | 28 | SLOPE: FOOT OF HEADWALL | 70° 34.97070' N | 136° 4.06992' W | 2 | 4 | U2 | 2 | 180 | X | 60 | 1 | 1,18 |
| ARAO 5C | 29 | SLOPE: INSIDE FAILURE_1 | 70° 35.42154' N | 136° 4.99830' W | 2 | 4 | U2 | 1 | 227 | X | 40 | 0,4-0,7 | 2,1 |
| ARAO 5C | 29 | SLOPE: INSIDE FAILURE_1 | 70° 35.42154' N | 136° 4.99830' W | 2 | 4 | U2 | 2 | 222 | X | 60 | 1 | 2 |
| ARAO 5C | 30 | SLOPE: INSIDE FAILURE_2 | 70° 36.07098' N | 136° 06,2575' W | 2 | 4 | U2 | 1 | 270 | X | 40 | 0,6 | 2,60 |
| ARAO 5C | 30 | SLOPE: INSIDE FAILURE_2 | 70° 36.07098' N | 136° 6.36132' W | 2 | 4 | U2 | 2 | 267 | X | 60 | 0,8-1,3 | 2,58 |

**Table 8.1 - Overview of CPT stations, geologic setting (site), station coordinates, CPT setup, employed winch, winch speed (shipboard), winch speed obtained from CPT data processing and penetration depth.**

Partially processed CPT data are presented in the Appendix of this chapter. For each station, the data of acceleration/deceleration, velocity, pore water pressure (u), dynamic cone resistance ($q_c$), dynamic cone resistance corrected for pore water pressure ($q_t$) and sleeve friction of the first drop are presented against penetration depth. The data are not strain-rate corrected and are preliminary. In post-processing of the data, the influence of the winch will be filtered and corrected for. More data processing is required before formal interpretation is undertaken.

Note, that no data were recovered from station ARA05C-25-CPT-1 because the CPT was stopped by the winch operator before penetration. Reasons for that are obscure, but are likely related to technical issues with the winch.

The following paragraph presents the data obtained at station ARA05C-01-CPT-04 exemplarily (see Appendix ARA05C-01-CPT-04):

The first plot presents deceleration and velocity of the CPT with penetration depth. It is shown that the deceleration fluctuates between maximum amplitudes of -1.5 and +1.5 m/s² at the beginning of penetration. The amplitude of fluctuation decreases with depth and reaches ~ 0 at the end of penetration. The velocity profile follows this trend with a phase difference of ~$\pi h$ /4. The pore water pressure signal starts at 4.26 MPa and increases near linearly to 4.32 MPa. The start value (4.26 MPa) corresponds to the hydrostatic pressure at the beginning of penetration. From this value we deduce a water depth of ~426 m assuming water at a density of 1.02 g/cc. The pore pressure increases with a rate higher than hydrostatic pressure. With pore water pressure corrected, dynamic cone resistance increases with depth from 0-35 kPa from the sediment-water interface to ~ 0.4 mbsf. From 0.4 mbsf to ~0.7 mbs qc does not increase. At ~1.8 mbsf qc reaches its maximum at about 125 kPa. Sleeve friction increases linearly from 0-3.5 kPa in the depth interval of 0-1 mbsf. From 1 mbsf to 1.5 mbsf sleeve friction increases to ~10 kPa. With further penetration to 1.8 mbsf sleeve friction stays steady.

## Appendix 8. Drop data of all CPT stations

ARAO5C -01-CPT-04

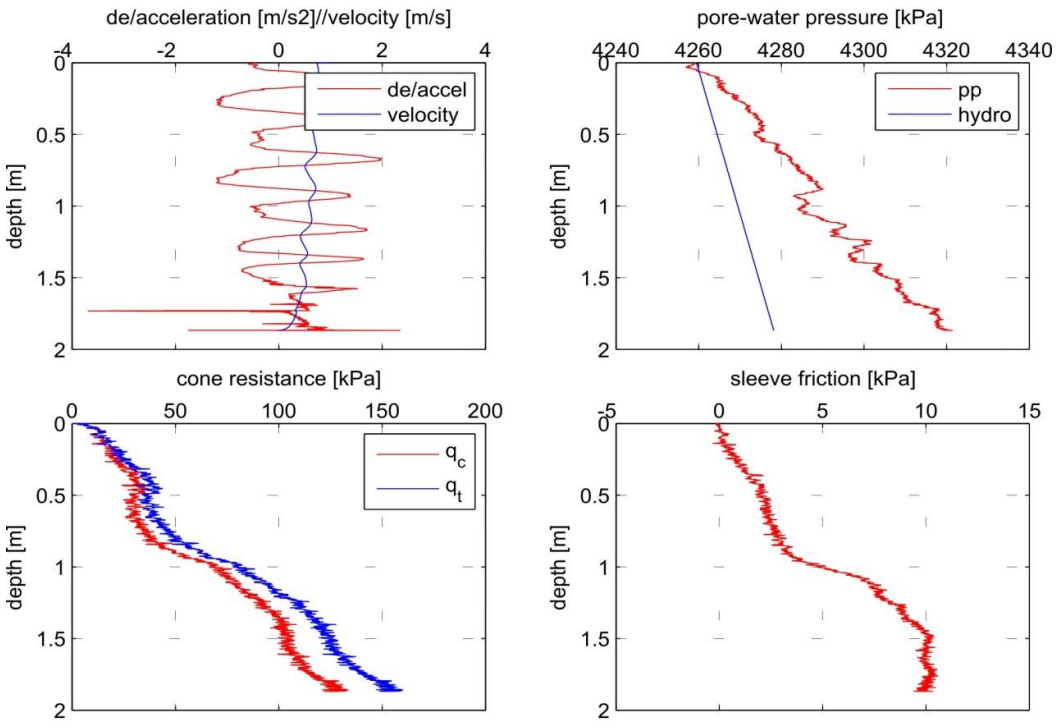


ARAO5C -02-CPT-04

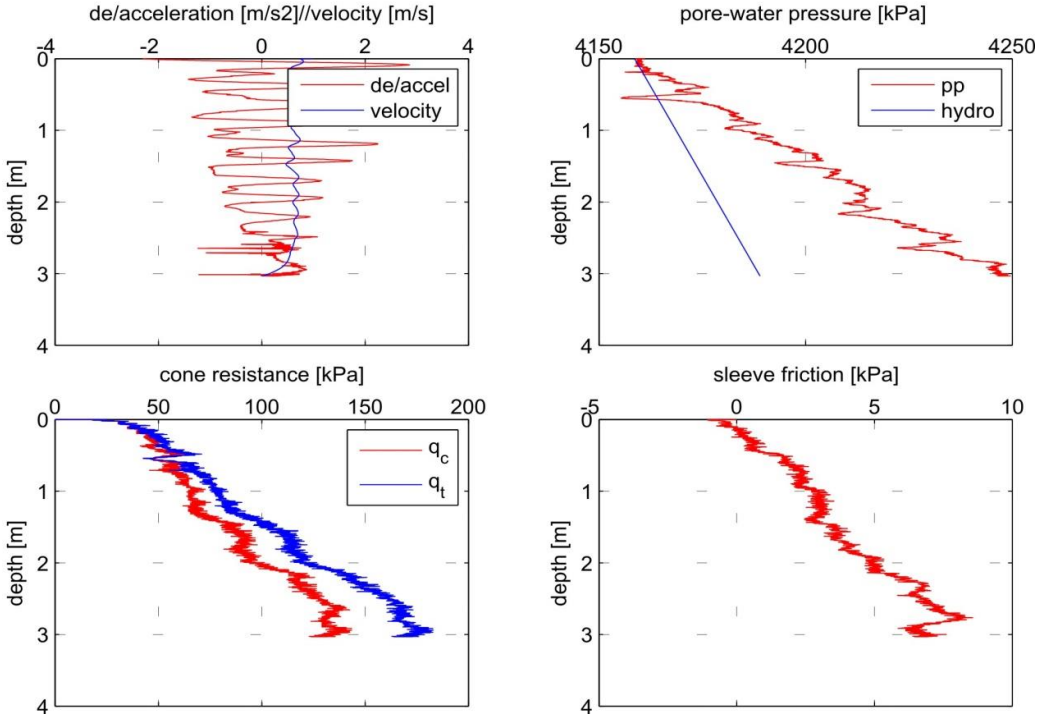

ARAO5C -03-CPT

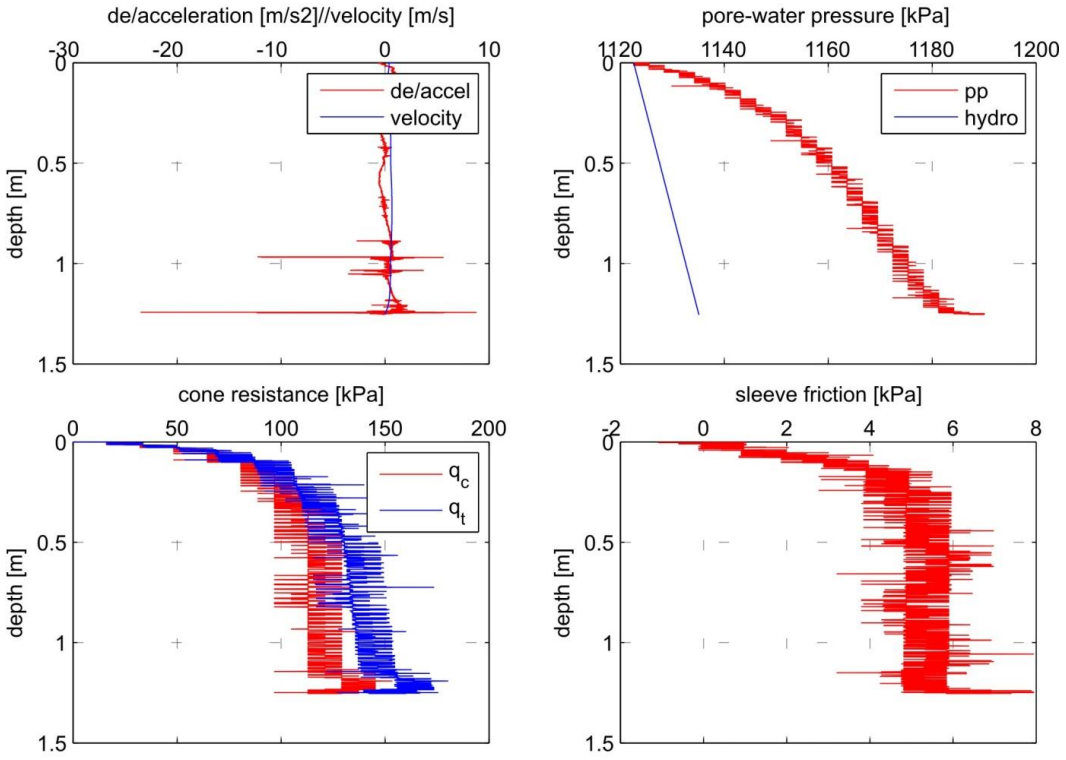


ARAO5C -04-CPT

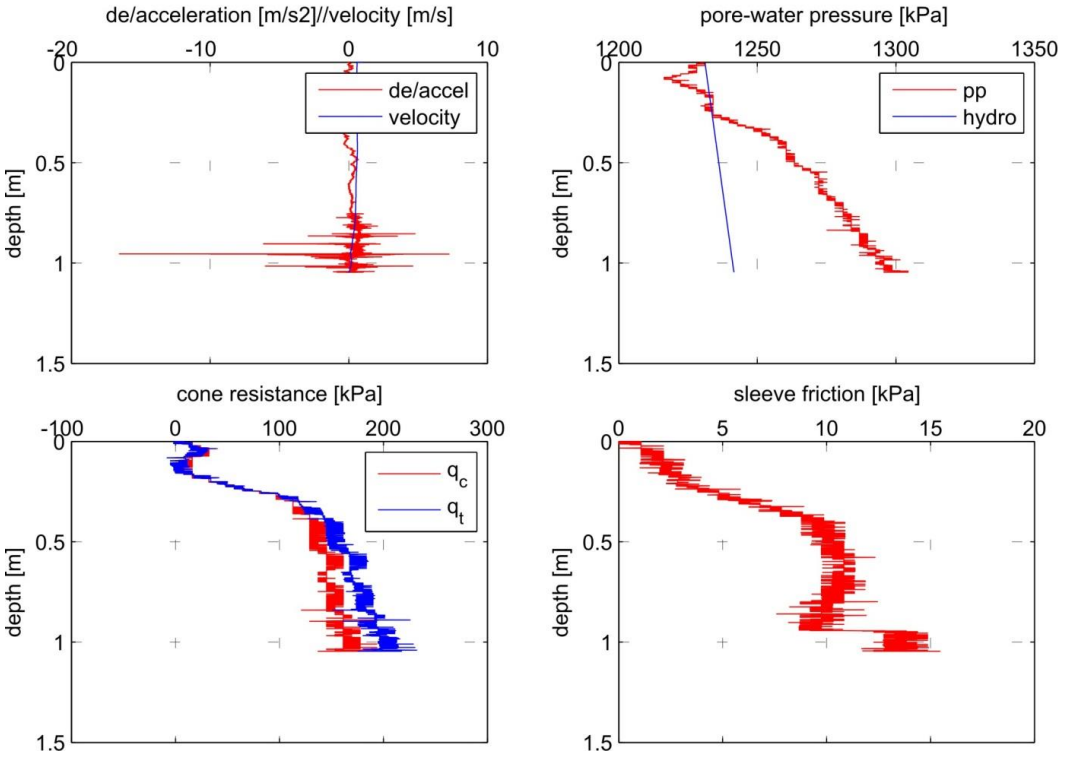

ARAO5C -05-CPT

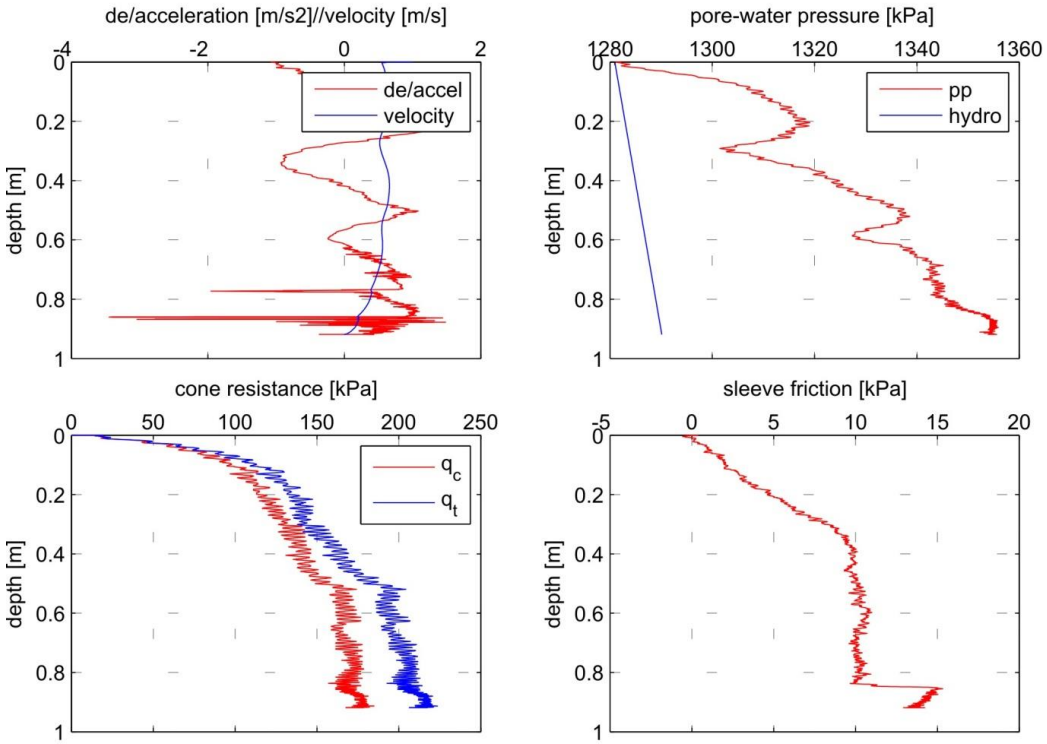


ARAO5C -06-CPT

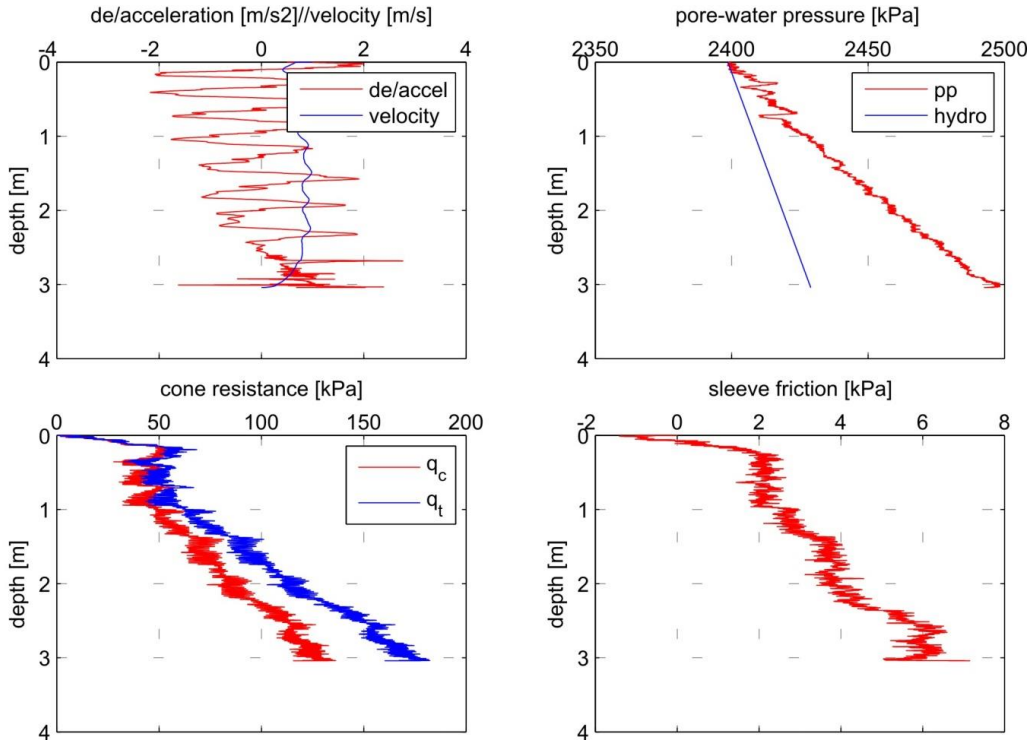

ARAO5C -07-CPT

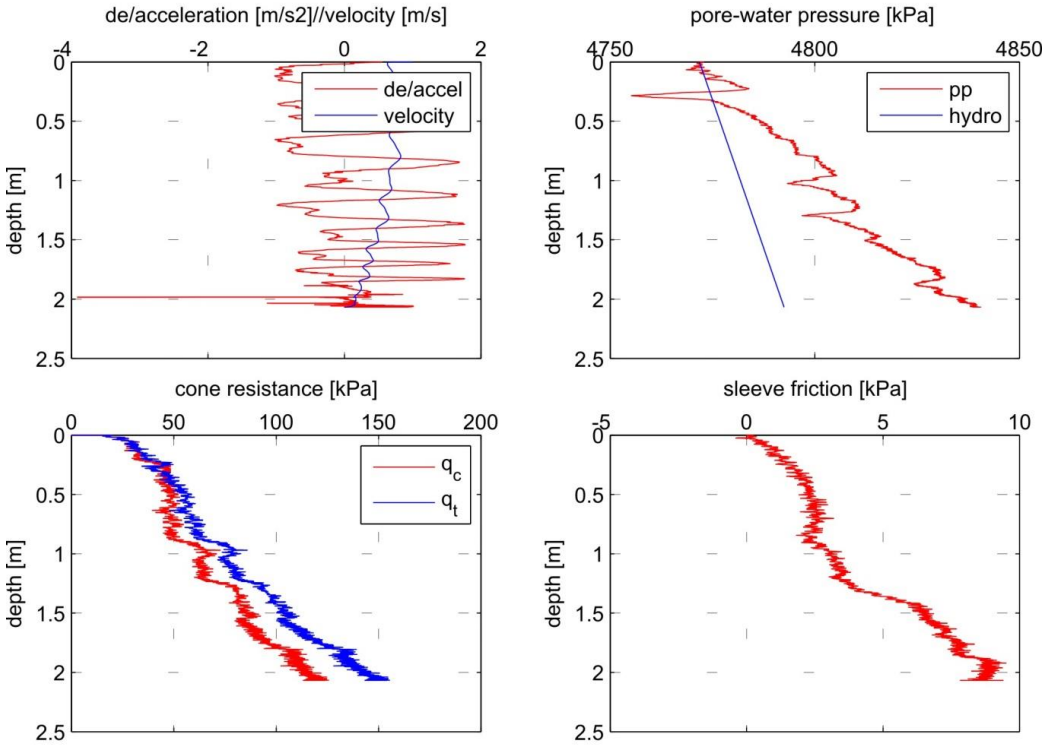


ARAO5C -08-CPT

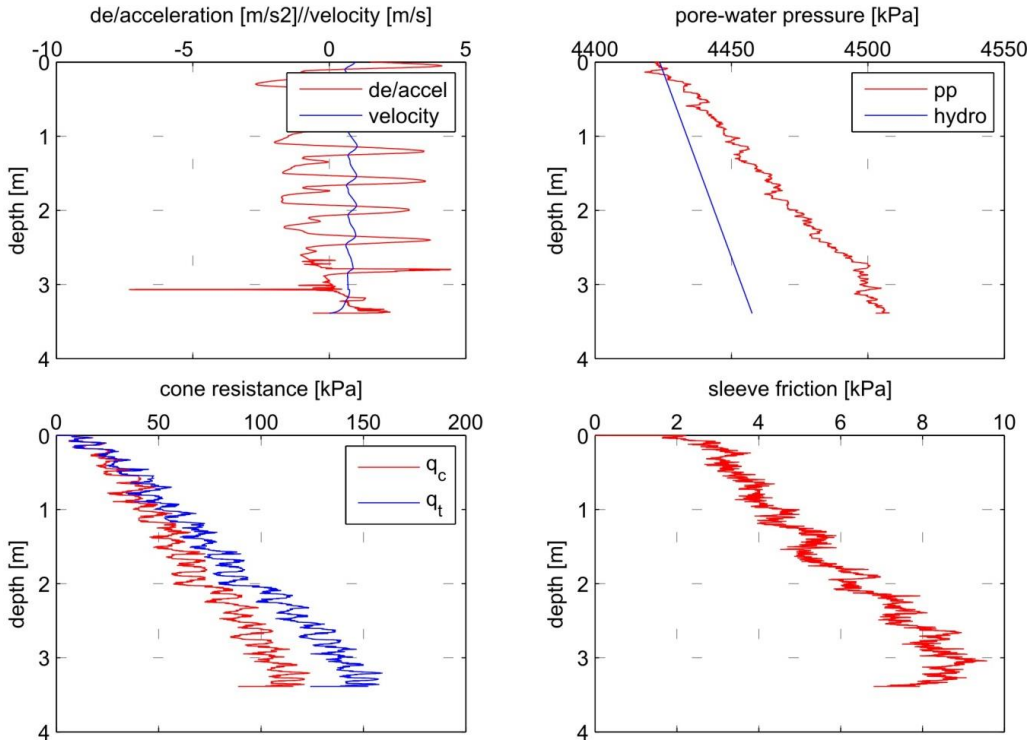

ARAO5C -19-CPT

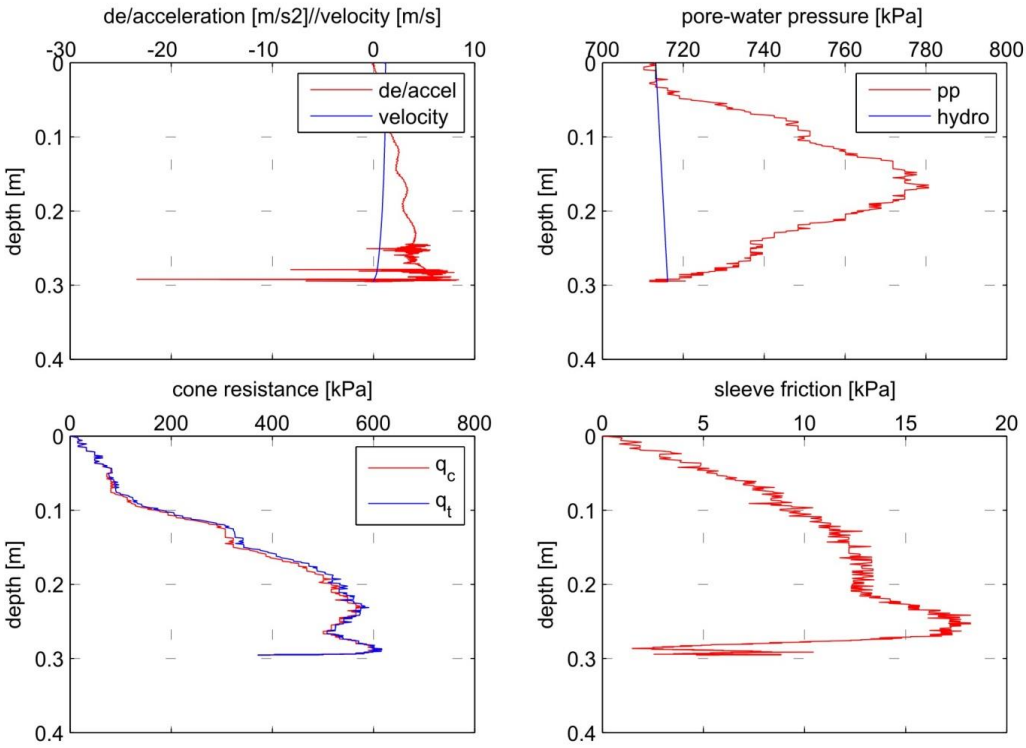


ARAO5C -23-CPT

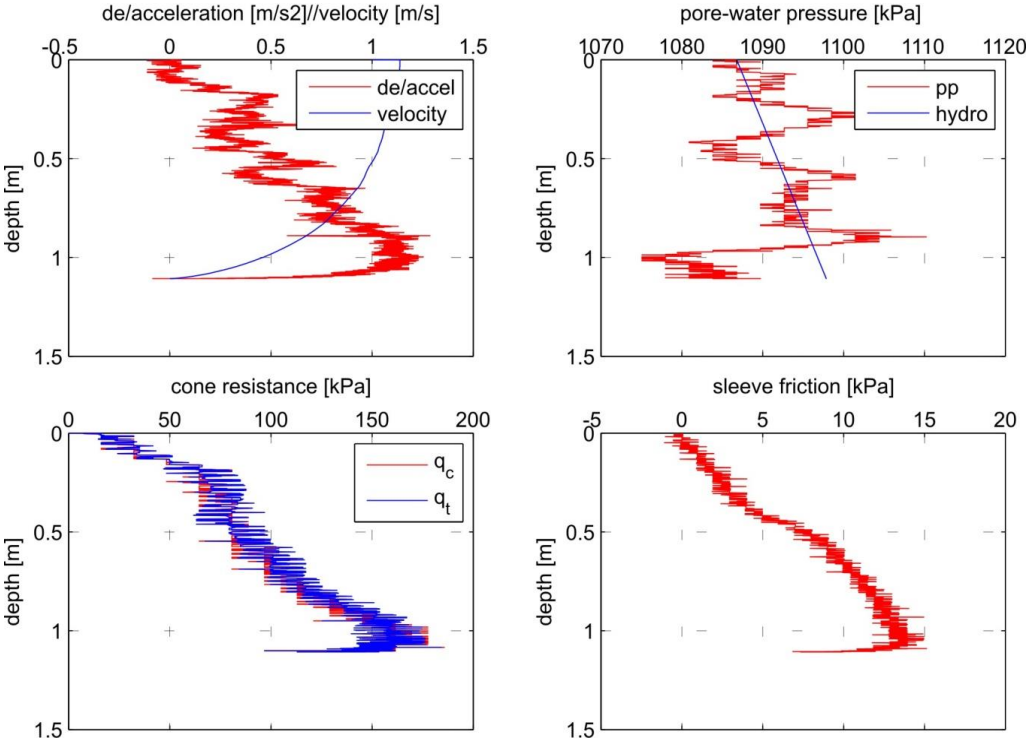

ARAO5C -24-CPT

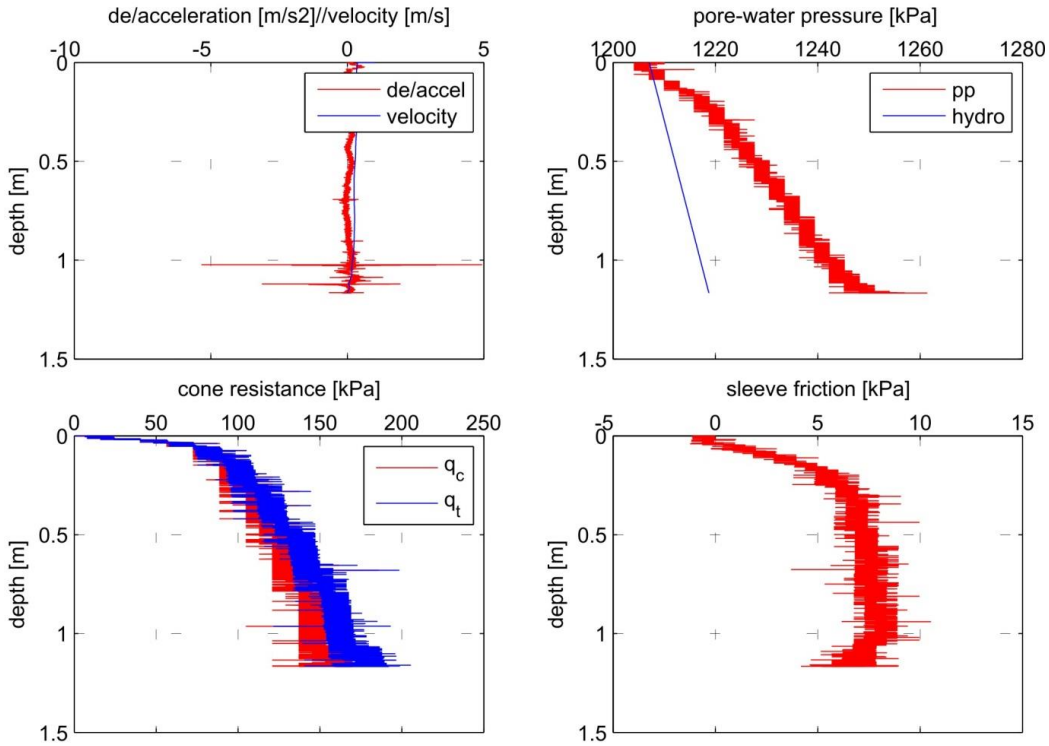


ARAO5C -26-CPT

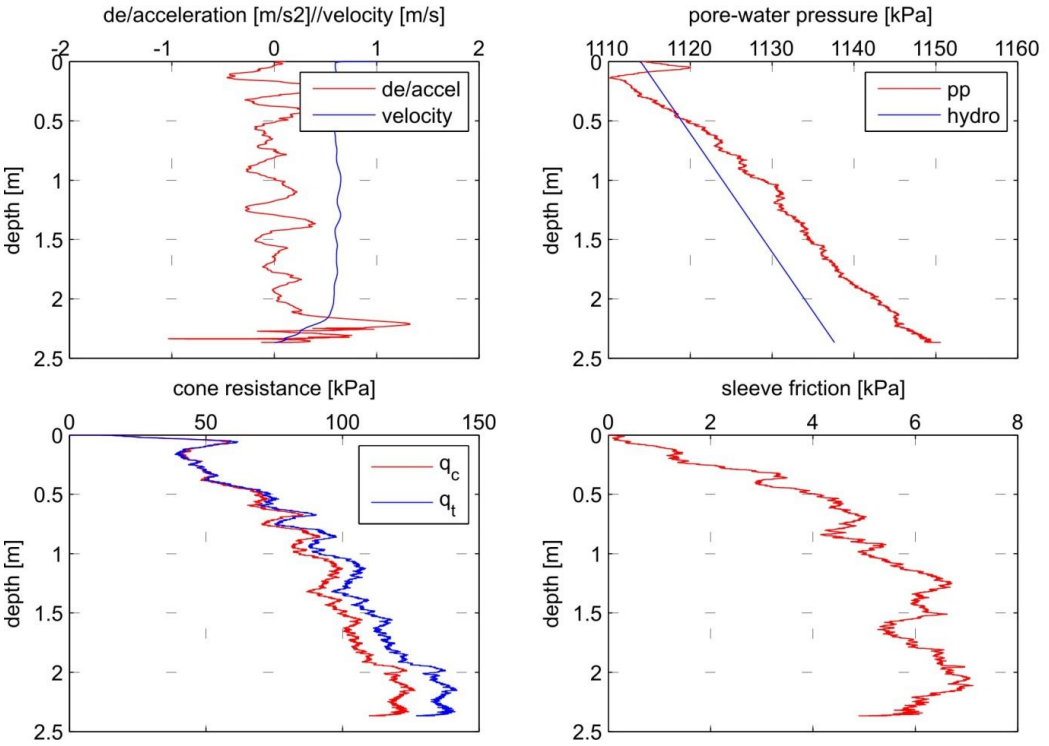

ARAO5C -27-CPT

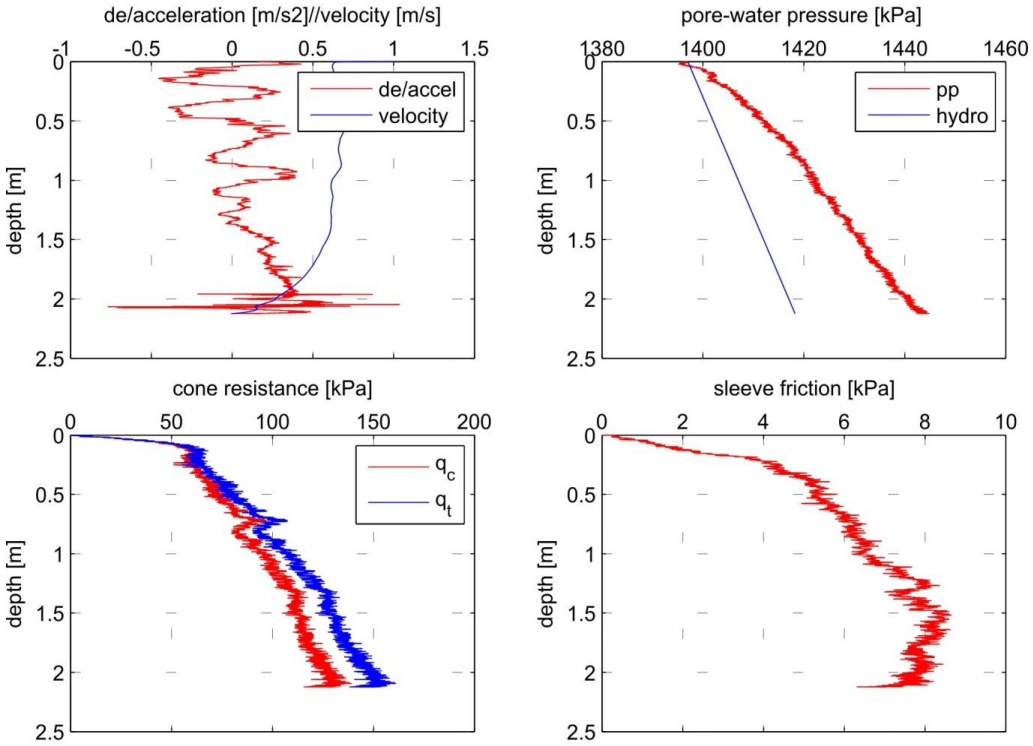


ARAO5C -28-CPT

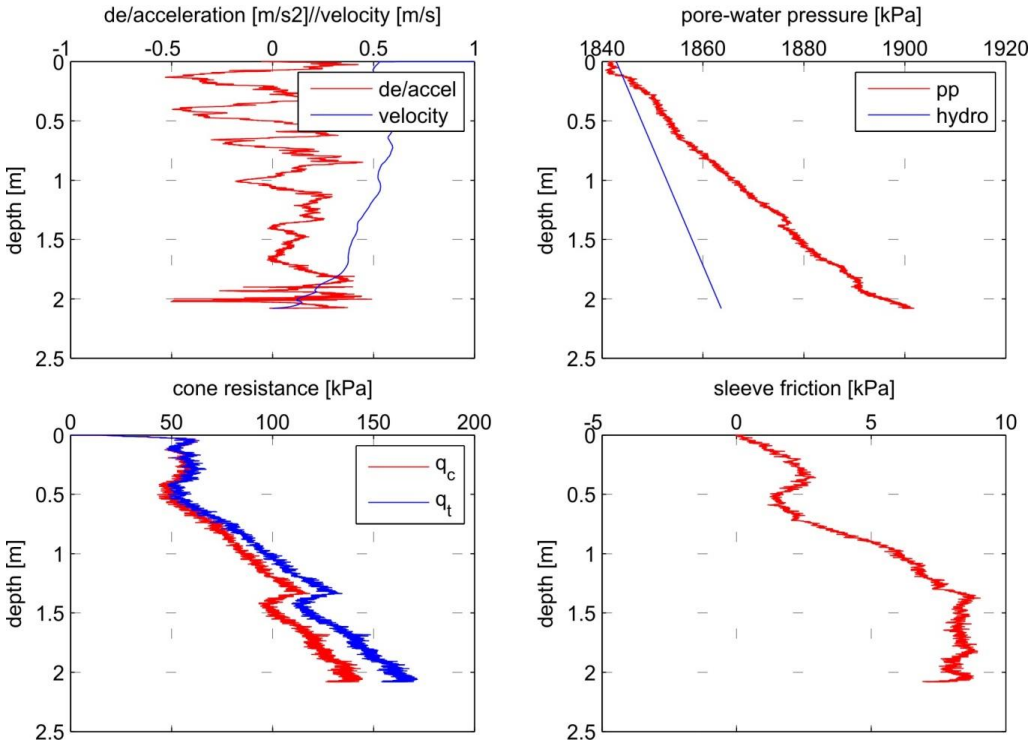

ARAO5C -29-CPT

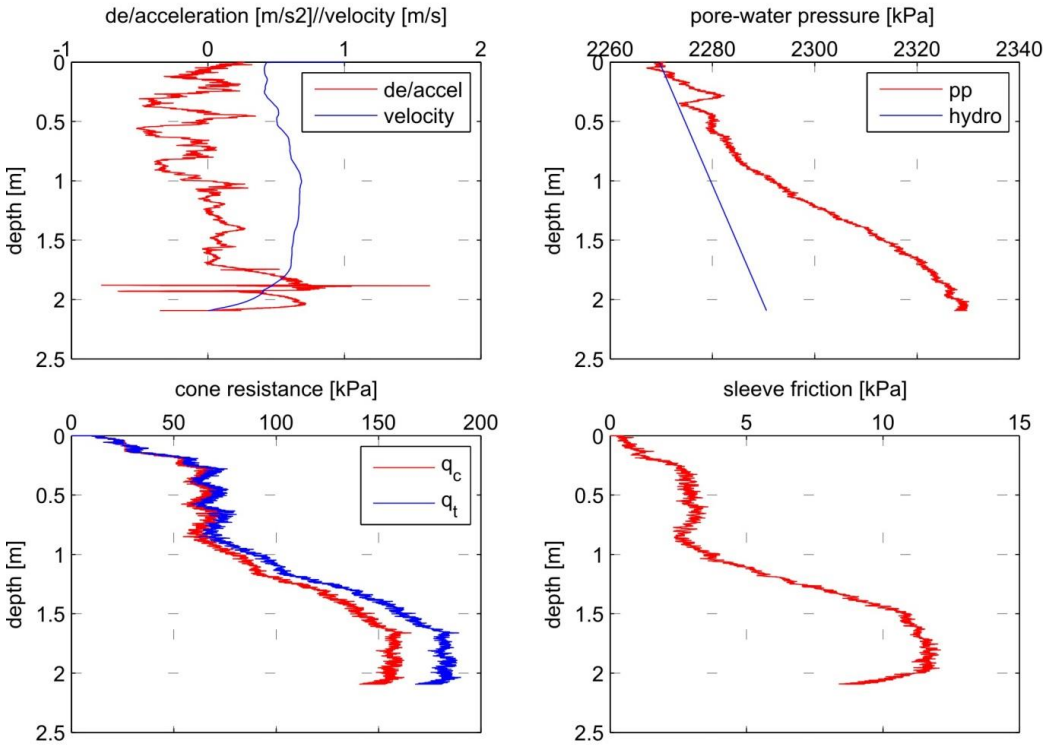


ARAO5C -30-CPT

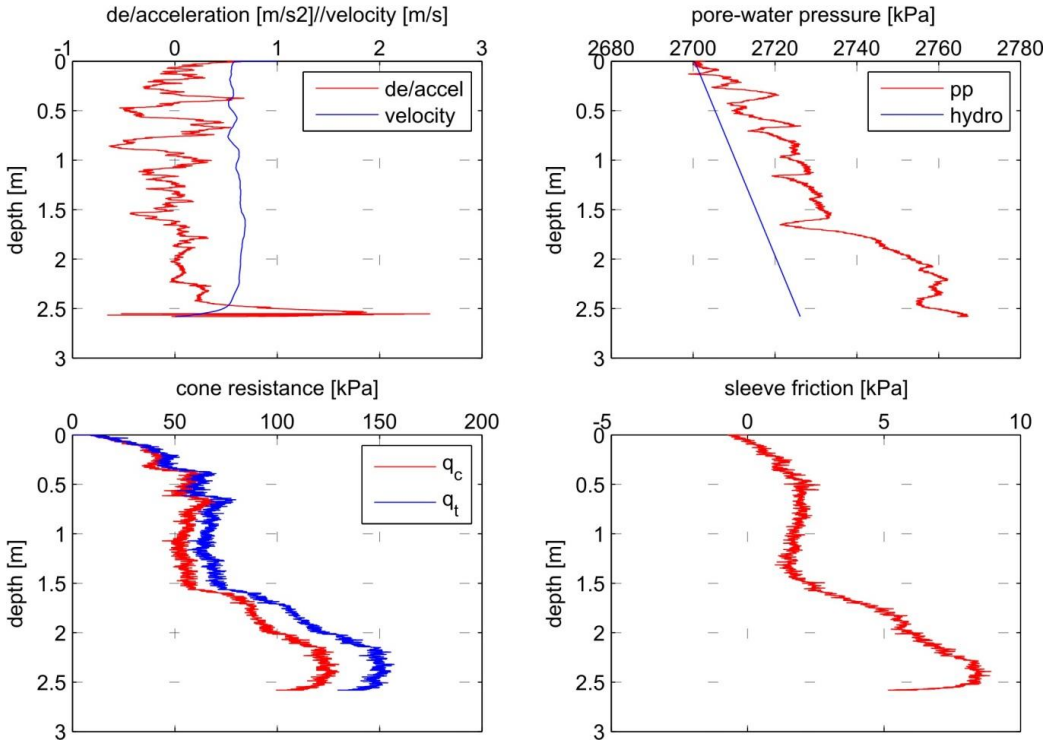

# CHAPTER 9 - Water column study

**C. Y. Gang, J. Y. Lee and T. W. Ko**

## *9.1. Introduction*

The Arctic Ocean has warmed over the past few decades (Polyakov et al., 2007, Solomon et al., 2007, Steele et al., 2008). This area is currently experiencing rapid environmental change due to natural and anthropogenic factors that include warming and other physical changes as well as biology and ecosystem structure changes (Bates and Mathis, 2009). In particular, change in extent and thickness of Arctic sea ice is recognized as a key indicator of Arctic climate change (Shimada et al., 2006). These changes and feedbacks could have profound impacts on the Arctic Ocean marine carbon cycle and the importance of the Arctic for the global carbon cycle, including the balance of carbon dioxide ($CO_2$) sinks and sources. $CO_2$ is one of the major components in understanding global warming and climate change research. Atmospheric $CO_2$ is absorbed by the ocean or emitted from the ocean to the atmosphere by physical and biological processes. The absorbed $CO_2$ exists as dissolved inorganic carbon (DIC) in the ocean and it is converted by phytoplankton into particulate organic carbon (POC) through photosynthesis. The POC is remineralized by bacteria into dissolved organic carbon (DOC) and/or $CO_2$. The Arctic Ocean has great potential for uptake of atmospheric $CO_2$ because of high biological production and low temperature. According to Bate and Mathis (2009), the Arctic Ocean accounts for 5 to 14% of the total ocean $CO_2$ uptake. However, knowledge about the distribution of $CO_2$, air-sea $CO_2$ fluxes and carbon cycle in the Arctic Ocean is uncertain due to relatively few observations and rapid climate changes. Although the Arctic Ocean takes up atmospheric $CO_2$, other greenhouse gases, such as nitrous oxide ($N_2O$) and methane ($CH_4$) can be released in the atmosphere through nitrification, denitrification, decay of detritus and thawing Arctic permafrost, which is a likely positive feedback to climate warming. It is unclear whether the decrease in radiative forcing from $CO_2$ uptake is offset by other greenhouse gases or not. In oceanographic point of view, it is important to identify what forcings drive sea ice reduction in the Arctic Ocean.

We, therefore, conducted a 16-day Arctic expedition in the period of August 31 to September 15, 2014 using the Korea ice breaker RV Araon to reveal the spatial distribution of water mass in the Beaufort Sea within Canada EEZ (Fig. 9.1). The specification of the observations at the stations is listed in Table 9.1.

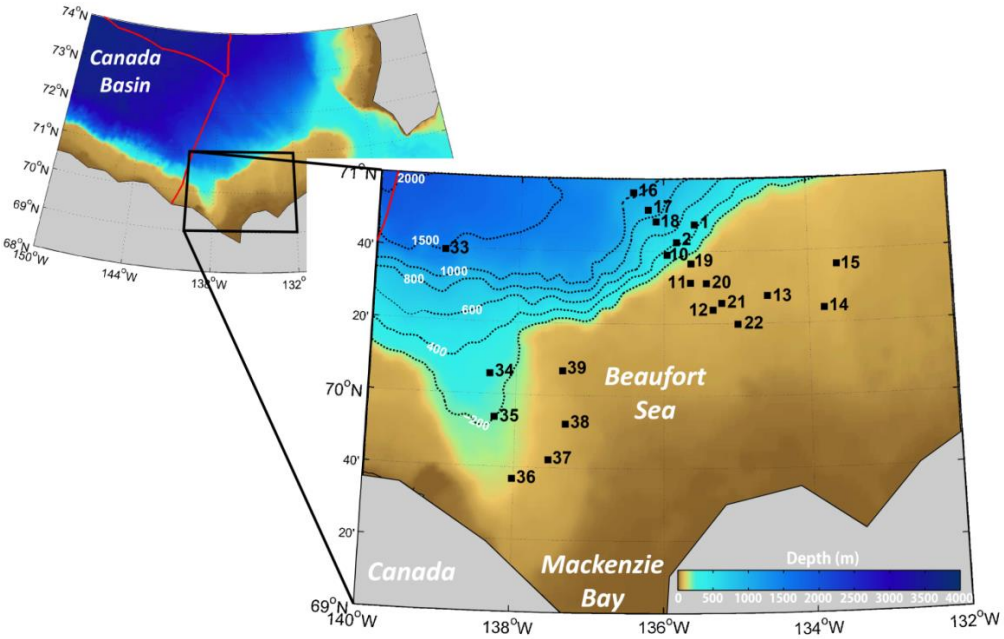


**Figure 9.1 - Map of the region with the position of the CTD stations indicated by filled a black square with color-mapped bathymetry. Black dashed contour lines are every 500 m for depths between 1000 m and 4000 m and every 200 m between 0 m and 1000 m depth. Red lines denote US EEZ and Canada EEZ lines.**

**Table 9.1 - Specifications of CTD observation stations.**

| Station | File name | Start Time (UTC) | | Latitude | | Longitude | | Depth (m) |
|---|---|---|---|---|---|---|---|---|
| | | YY-MM-DD | hh:mm:ss | Deg. | Min. | Deg. | Min. | |
| St. 01 | ARA05C01CTD1 | 2014-08-30 | 15:20:41 | 70N | 47.334 | 135W | 34.044 | 413 |
| St. 02 | ARA05C02CTD1 | 2014-08-31 | 00:53:31 | 70N | 42.378 | 135W | 49.050 | 408 |
| St. 10 | ARA05C03CTD1 | 2014-08-31 | 16:13:43 | 70N | 38.958 | 135W | 56.814 | 274 |
| St. 11 | ARA05C04CTD1 | 2014-09-01 | 03:42:29 | 70N | 31.212 | 135W | 37.542 | 59 |
| St. 12 | ARA05C05CTD1 | 2014-09-01 | 05:47:17 | 70N | 23.766 | 135W | 18.816 | 57 |
| St. 13 | ARA05C06CTD2 | 2014-09-01 | 08:30:13 | 70N | 23.766 | 134W | 33.666 | 52 |
| St. 14 | ARA05C07CTD1 | 2014-09-01 | 11:12:20 | 70N | 27.540 | 133W | 46.962 | 52 |
| St. 15 | ARA05C08CTD1 | 2014-09-01 | 13:36:54 | 70N | 24.072 | 133W | 35.526 | 63 |
| St. 16 | ARA05C09CTD1 | 2014-09-06 | 15:04:59 | 70N | 35.922 | 136W | 25.116 | 1009 |
| St. 17 | ARA05C10CTD1 | 2014-09-06 | 22:09:36 | 70N | 56.154 | 136W | 12.678 | 843 |
| St. 18 | ARA05C11CTD1 | 2014-09-07 | 06:30:09 | 70N | 51.402 | 136W | 05.958 | 739 |
| St. 19 | ARA05C12CTD1 | 2014-09-07 | 11:04:03 | 70N | 48.108 | 135W | 36.900 | 67 |
| St. 20 | ARA05C13CTD1 | 2014-09-07 | 13:08:53 | 70N | 36.516 | 135W | 24.132 | 56 |
| St. 21 | ARA05C14CTD1 | 2014-09-07 | 15:22:52 | 70N | 31.008 | 135W | 11.742 | 57 |
| St. 22 | ARA05C15CTD1 | 2014-09-07 | 17:00:07 | 70N | 25.584 | 134W | 58.386 | 48 |
| St. 33 | ARA05C16CTD1 | 2014-09-11 | 15:16:12 | 70N | 39.342 | 139W | 02.142 | 1529 |
| St. 34 | ARA05C17CTD1 | 2014-09-12 | 00:56:31 | 70N | 05.622 | 138W | 21.120 | 241 |
| St. 35 | ARA05C18CTD1 | 2014-09-12 | 06:24:19 | 69N | 53.640 | 138W | 16.458 | 197 |
| St. 36 | ARA05C19CTD1 | 2014-09-12 | 09:29:26 | 69N | 36.666 | 138W | 00.810 | 97 |
| St. 37 | ARA05C20CTD1 | 2014-09-12 | 11:49:29 | 69N | 42.066 | 137W | 32.316 | 56 |
| St. 38 | ARA05C21CTD1 | 2014-09-12 | 13:47:09 | 69N | 52.050 | 137W | 18.876 | 50 |
| St. 39 | ARA05C22CTD1 | 2014-09-12 | 16:00:14 | 70N | 06.726 | 137W | 21.924 | 50 |

## *9.2. Methods*

### 9.2.1. CTD Casting

The CTD installed on the RV Araon was used for profiling and identifying vertical variation of temperature and salinity. Along the transects of hydrographic stations, hydro-casts of CTD (SBE 911*plus* CTD)/Rosette system with additional sensors (e.g., in situ data on phytoplankton concentrations (fluorometer), optical clarity (transmissometer), dissolved oxygen, altimeter and methane gas) were conducted to measure the vertical profiles of conductivity, temperature, depth, and other biochemical parameters (Fig. 9.2a). During the CTD up-casting, a 24 position rosette with 10-L Niskin bottles was used to obtain water samples from discrete depths for biological and geochemical analysis.

### 9.2.2. Ocean Current Measurement

A 300 kHz RDI lowered Acoustic Doppler Current Profiler (LADCP) was mounted on the CTD/Rosette frame to measure a full-depth profile of current velocities (Fig. 9.2b). Using the conventional "shear method" for processing (e.g., Fischer and Visbeck, 1993), overlapping profiles of vertical shear of horizontal velocity were averaged and gridded to form a full-depth shear profile. The bin size was chosen as 5 m and the number of bins was 20.


**Figure 9.2 - Hydrographic observation equipment: (a) SBE911plus CTD profiler and rosette water sampler, (b) 300 kHz RDI lowered ADCP.**

### 9.2.3. Seawater sampling

Seawater sampling was carried out at 16 stations using a CTD/rosette sampler holding 24-10L Niskin bottles (OceanTest Equipment Inc., FL, USA) (Fig. 9.3).

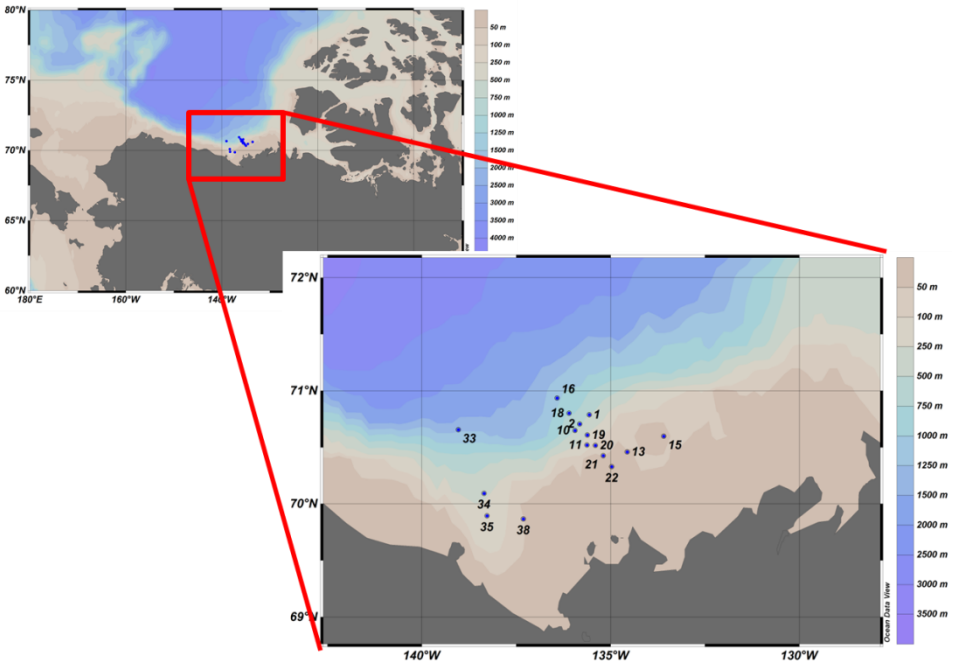


**Figure 9.3 - Seawater sampling stations and cruise track during ARA05C.**

### 9.2.4. Dissolved inorganic carbon and total alkalinity

Seawater samples for DIC and TA measurements were drawn from the Niskin bottles of CTD/rosette system into pre-cleaned 500 ml borosilicate bottles. DIC and TA samples were subsequently poisoned with 100 µl of 50% $HgCl_2$ to halt biological activity, sealed, and returned to Korea Polar Research Institute for analysis. DIC and TA samples will be analyzed using a VINDTA (Versatile Instrument for the Determination of Total Alkalinity) system at the Korea Polar Research Institute.

### 9.2.5. pH of seawater

Seawater samples for pH measurements were drawn from the Niskin bottles into pre-cleaned 150 ml polyethylene bottles. The samples were delivered to the Analytical Chemistry Lab in RV Araon and then measured pH of seawater on board using a pH measurement system (Fig. 9.4).

**Figure 9.4 - pH measurement system.**

### 9.2.6. Nutrients

Samples for nutrients ($NH_4^+$, $NO_2^-$, $NO_3^-$, $PO_4^{3-}$, $SiO_4^{2-}$) were collected from the Niskin rosette into 50 ml conical tubes and immediately stored in a freezer at −24°C prior to chemical analyses. The samples will be analyzed with standard colorimetric methods using a Quatro Auto Analyzer in Korea Polar Research Institute.

### 9.2.7. Underway pCO2 measurement

The flux of $CO_2$ across the sea surface is directly proportional to the difference in the fugacity of $CO_2$ between the atmosphere and the seawater. The fugacity is obtained by correcting the partial pressure of $CO_2$ ($pCO_2$) for non-ideality of the gas with respect to molecular interactions between $CO_2$ and other gases in air, thus making $pCO_2$ an important parameter to measure (Pierrot et al., 2009). To investigate air-sea exchange rate of $CO_2$, $pCO_2$ were monitored in real time using an automated flowing $pCO_2$ measuring system (Model 8050, General Oceanics Inc., USA) (Fig. 9.3). The system is compact and operates by directing seawater flow through a chamber (the equilibrator) where the $CO_2$ contained in the water equilibrates with the gas present in the chamber (the headspace gas). To determine the $CO_2$ in the headspace gas, it was pumped through a non-dispersive infrared analyzer (LICOR), which measured its $CO_2$ mole fraction instantaneously, and then returned to the equilibrator thus forming a closed loop. Periodically, atmospheric air was also pumped through the analyzer and its $CO_2$ mole fraction was measured. The analyzer was calibrated with four $CO_2$ standard gases at regular intervals.

**Figure 9.5 - Automated flowing $pCO_2$ measuring system.**

### 9.2.8. $CH_4$, $N_2O$ and $CO_2$ measurements

Seawater samples for $CH_4$, $N_2O$ and $CO_2$ measurements were drawn from the Niskin bottles of CTD/rosette system into glass jar bottles. A 50 ml of $N_2$ gas was subsequently injected into the glass jar bottles using a glass syringe to make a headspace. The glass jar bottles were then put into a water bath (20°C) for more than one hour. To minimize underway data loss, measurements of $CH_4$, $N_2O$ and $CO_2$ concentrations in water column were carried out when RV Araon stopped at stations for other works (e.g., core work). A 40 ml of the headspace gas was drawn from the glass jar bottles using the glass syringe, and then injected into a gas chromatography equipped with a flame ionization detector (FID) and an electron capture detector (ECD) to measure $CH_4$, $N_2O$ and $CO_2$ concentrations in water column. During the cruise, underway measurements of $CH_4$ and $N_2O$ were also carried out along the cruise track. Seawater was pumped into the equilibrator and the headspace gas in the equilibrator was drawn into the gas chromatography system (Fig. 9.4). For one cycle, it takes 40 minute to analyze $CH_4$ and $N_2O$ in ambient air and seawater, including calibration gases.

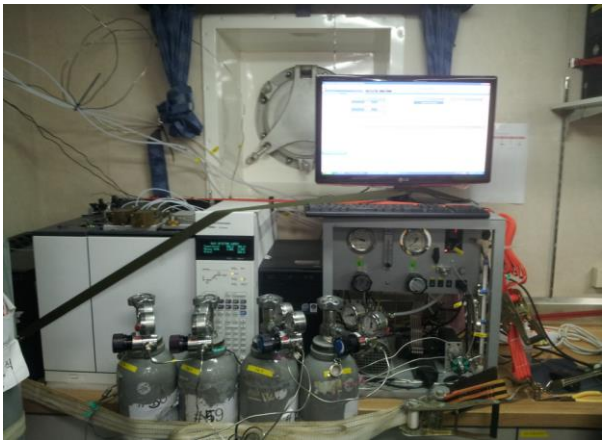

**Figure 9.6 - Gas chromatography system for measurements of $CH_4$, $CO_2$ and $N_2O$.**

### *9.3. Results*

The samples for DIC/TA, nutrients measurements should be analyzed after all samples are returned to Korea Polar Research Institute. For pH of seawater, underway data of $pCO_2$, $CH_4$, $CO_2$ and $N_2O$, the procedures for calculation (e.g., unit conversion, Fig. 9.7) are required to produce accurate data set. We therefore do not report any data for these chemical components here.

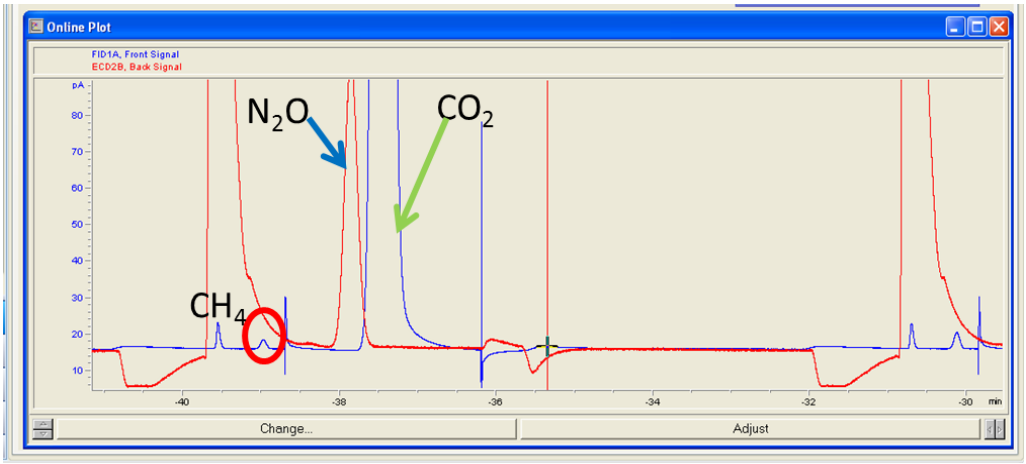


**Figure 9.7 - Raw data of $CH_4$, $CO_2$ and $N_2O$ in water column.**

### *References*


Bates NR, Mathis JT. 2009. The Arctic Ocean marine carbon cycle: evaluation of air-sea $CO_2$ exchanges, ocean acidification impacts and potential feedbacks. Biogeoscience, 6, 2433–2459.

Fischer J and Visbeck M. 1993. Deep velocity profiling with self-contained ADCPs. *Journal of Atmospheric and Oceanic Technology*, 10, 764-773.

Polyakov et al., 2007. Observational program tracks Arctic Ocean transition to a warmer state, *EOS Trans. AGU*, 88, 398-399, doi:10.1029/2007EO400002.

Shimada K, Kamoshida T, Itoh M, Nishino S, Carmack E, McLaughlin F, Zimmermann S, and Proshutinsky A. 2006. Pacific Ocean flow: Influence on catastrophic reduction of sea ice cover in the Arctic Ocean. *Geophysical Research Letters*, 33, doi:1029/2005GL025624.

Solomon S, Qin D, Manning M, Alley RB, Berntsen T, et al. 2007. Technical Summary. In: *Climate Change 2007: The Physical Science Basis. Contribution of Working Group I to the Fourth Assessment Report of the Intergovernmental Panel on Climate Change*. (Eds.) S. Solomon, D. Qin, M. Manning, Z. Chen, M. Marquis, et al., Cambridge, UK/New York, Cambridge University Press.

Steele M, Ermold W, and Zhang J. 2008. Arctic Ocean surface warming trends over the past 100 years. *Geophysical Research Letters*, 35, L02614, doi:10.1029/2007GL031651.

# CHAPTER 10 - Biodiversity Study

**I.C. Kim, T.K. Kim, J.E. Kim, C.B. Jeong and J.H. Yim**

## *10.1. Introduction*

The Beaufort Sea is a marginal sea of the Arctic Ocean, located north of the Northwest Territories, the Yukon, and Alaska. The Mackenzie River empties into the Canadian part of the sea, west of Tuktoyaktuk, which is one on the few permanent settlements on the sea shores. The sea, characterized by severe climate, is frozen over most of the year. Historically, only a narrow pass up to 100 km is opened in August-September near shores, but recently due to climate change in the Arctic the ice-free area in late summer has greatly increased (Beaufort Sea, Encyclopedia Britannica on-line).

Arctic seas hold a multitude of unique life forms highly adapted in their life cycle, ecology and physiology to the extreme and seasonal conditions of this environment. The Beaufort Sea hosts bout 80 species of zooplankton, more than 70 species of phytoplankton, and nearly 700 species of polychaetes, bryozoans, crustaceans and mollusks, but their total volume is relatively small owing to the cold climate. The knowledge of the marine bacterium of Beaufort Sea is still very low.

Therefore, the K-POD project has collected marine bacterium from Beaufort Sea for understanding of biodiversity and their metabolites related to extreme adaptation in cold environment of the Beaufort Sea.

## *10.2. Methods*

1) Marine bacteria sampling used by CTD/Rosette at each station. Niskin bottles can be tripped at different depths for seawater sampling at 22 stations.
2) Metagenome sampling by SV filters (0.25 um) from sea water at 22 stations.
3) Sediment core sampling by box-core sampler at 21 stations.

## *10.3. Expected results*

### 10.3.1. Marine Bacteria

Bacteria are common inhabitants of sea water, and may contribute up to about 50% of the total biomass within this habitat. The K-POD project has collected marine bacterial samples from sea water and box-cores. The K-POD project isolated marine bacteria from marine samples in MA, R2A, SZB (marine bacteria), YPG (marine fungi) and ISP4 (marine actinomyces) media. K-POD will try to study the biodiversity and metabolic flow for understanding extreme adaptation in the Beaufort Sea.

### 10.3.2. Metagenome study

Metagenomics is the study of metagenomes, genetic material recovered directly from environmental samples. Metagenomics has the potential to advance knowledge in a wide variety of fields. The K-POD project has collected the metagenome samples from sea water of Beaufort Sea. From samples, K-POD will try to study biodiversity and useful genes for understanding environments.

## *10.4. Summary and conclusions*

The K-POD project has collected various marine bacteria from 22 stations of Beaufort Sea (Table 10.1 & Fig. 10.1). We will try to understand the marine bacteria biodiversity and their metabolites related to adaptation in this extreme environment.

**Table 10.1 - K-POD stations and work in Beaufort Sea.**

| Station | Locations | Depth (m) | CTD / dep. No. / SV No. | Box-core (Core No.) |
|---|---|---|---|---|
| ST# 1 | 70-47-3328N, 135-34-0492W | 418.0 | 1 / 10 / 2 | 1 / 2 |
| ST# 2 | 70-42-3883N, 135-48-8724W | 420.0 | 1 / 9 / 2 | 1 / 2 |
| ST#10 | 70-38-9589N, 135-56-8033W | 280.0 | 1 / 7 / 2 | 1 / 2 |
| ST#11 | 70-31-2164N, 135-37-5478W | 63.0 | 1 / 7 / 2 | 1 / 2 |
| ST#12 | 70-23-7278N, 135-18-7483W | 60.0 | 1 / 7 / 2 | 1 / 2 |
| ST#13 | 70-27-5440N, 134-33-6664W | 54.0 | 1 / 7 / 2 | 1 / 2 |
| ST#14 | 70-24-0772N, 133-46-9675W | 56.0 | 1 / 6 / 2 | 1 / 2 |
| ST#15 | 70-35-9242N, 133-35-4931W | 63.0 | 1 / 7 / 2 | 1 / 2 |
| ST#16 | 70-56-1581N, 136-25-1178W | 1,014.0 | 1 / 9 / 2 | - |
| ST#17 | 70-51-3927N, 136-12-6358W | 848.0 | 1 / 9 / 2 | 1 / 3 |
| ST#18 | 70-80-1367N, 135-48-0820W | 740.0 | 1 / 9 / 2 | 1 / 2 |
| ST#19 | 70-36-5167N, 135-36-9046W | 64.0 | 1 / 7 / 2 | 1 / 2 |
| ST#20 | 70-31-0116N, 135-24-1372W | 62.0 | 1 / 6 / 2 | 1 / 2 |
| ST#21 | 70-25-5848N, 135-11-7426W | 56.0 | 1 / 6 / 2 | 1 / 2 |
| ST#22 | 70-19-7558N, 134-58-3849W | 50.0 | 1 / 6 / 2 | 1 / 2 |
| ST#33 | 70-39-3456N, 138-02-1452W | 1,535.0 | 1 / 10 / 2 | 1 / 2 |
| ST#34 | 70-39-3456N, 138-21-1199W | 240.0 | 1 / 8 / 2 | 1 / 2 |
| ST#35 | 69-53-6405N, 138-16-4598W | 198.0 | 1 / 6 / 2 | 1 / 2 |
| ST#36 | 69-36-6719N, 138-00-8821W | 100.0 | 1 / 7 / 2 | 1 / 2 |
| ST#37 | 69-42-0681N, 137-32-3191W | 61.0 | 1 / 6 / 2 | 1 / 2 |
| ST#38 | 69-52-0499N, 137-18-8777W | 57.0 | 1 / 6 / 2 | 1 / 2 |
| ST#38 | 70-06-7309N, 137-21-9256W | 54.0 | 1 / 6 / 2 | 1 / 2 |
| Total | | | 22 / 163 / 44 | 21 / 43 |

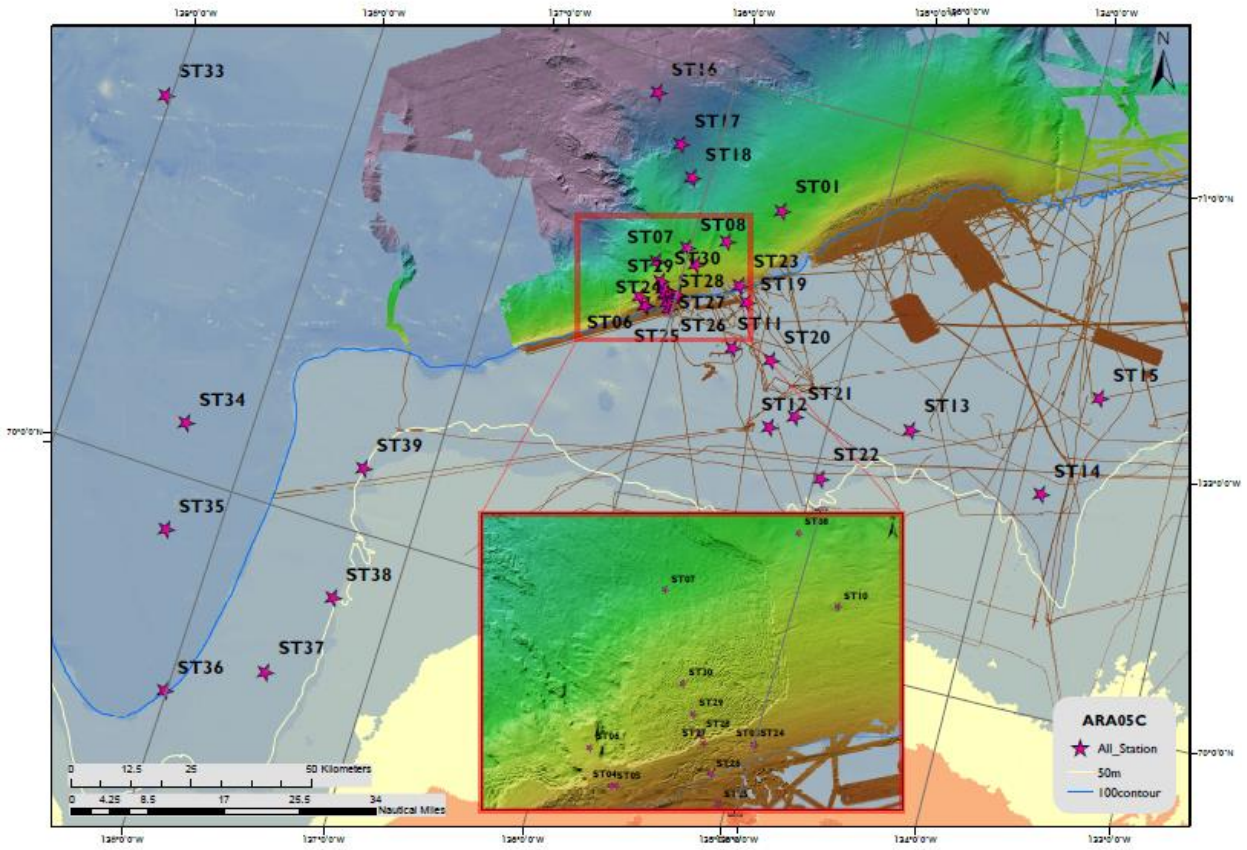


**Fig 10.1 - Stations of ARA05C cruise.**

# CHAPTER 11 - Atmospheric observations

**K.-H. Jin**

## *11.1. Introduction*

Ever decreasing sea ice in the Arctic Ocean casts important questions regarding possible changes to energy, water, carbon dioxide, and methane circulation in the Arctic region, as well as probable consequences of those changes. To answer those questions, we need to make in-situ observations of air-sea interactions in Arctic Ocean. In 2014 summer, the Korean ice-breaking research vessel RV Araon voyaged the Beaufort/Chukchi Seas from August 27 through September 16. Atmospheric observations encompassed not only monitoring basic meteorological parameters such as wind, air temperature, and pressure, but also observations on greenhouse gases (like carbon dioxide, water vapor, and methane), aerosols, and flux measurement system. The overview of atmospheric observations is summarized in Figure 11.1.

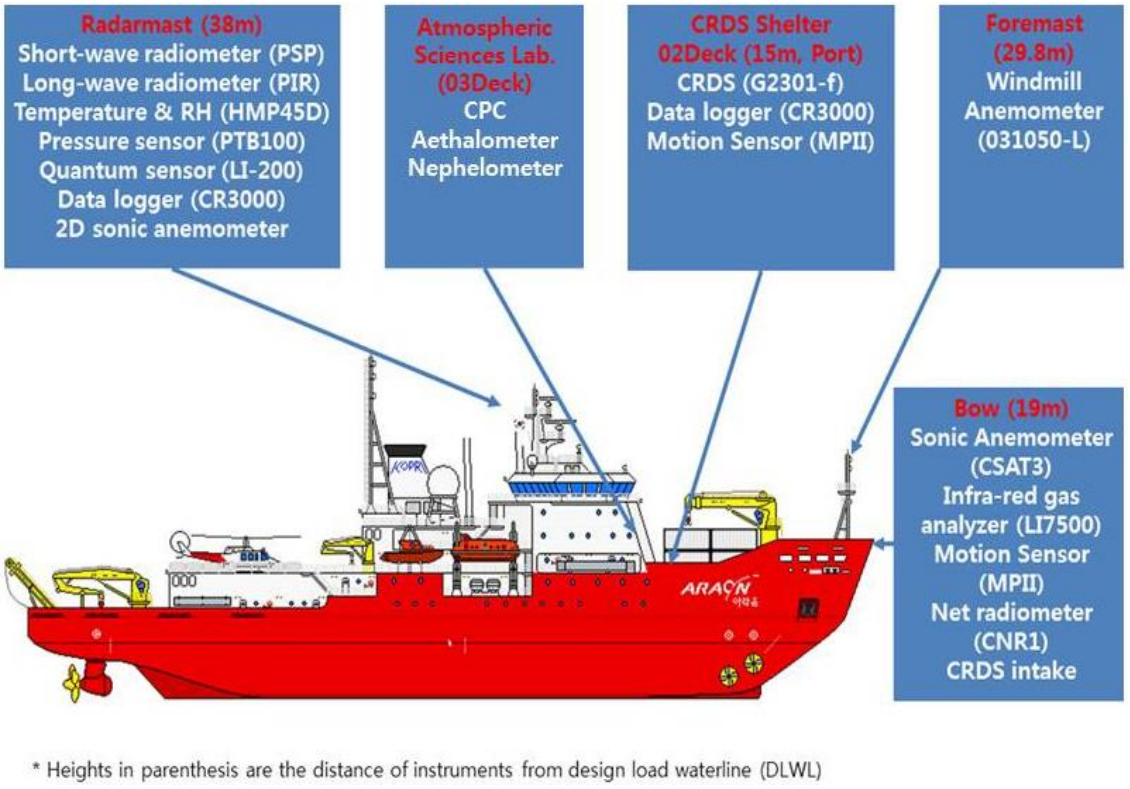


**Figure 11.1 - Overview of atmospheric observations on RV Araon.**

## *11.2. Instrumentation*

### 11.2.1. Air-sea interaction

Air-sea interactions have been measured in terms of exchanges of momentum, heat, water, and $CO_2$ during the ARA05C cruise. An eddy-covariance system was installed on the foredeck consisting of a 3-D sonic anemometer (CSAT3), an open-path gas analyzer (LI-7500),

a motion sensor (Motion PAK II) (Fig. 11.2), and a closed-path gas analyzer (CRDS g2301-f, Fig.11.3). In order to study chaotic eddy motions, these instruments sample at high rate, i.e., 10Hz. The open-path gas analyzer measures carbon dioxide and water vapor concentration at the sensor path-length, whereas the closed-path gas analyzer draws air from the foredeck to CRDS container located about 34 m away. Momentum flux and sensible heat flux are estimated from the sonic anemometer data and latent heat flux and carbon dioxide flux are computed from the sonic anemometer data and gas analyzer data. The data logger in the CRDS container collects the data, and the desktop computer in the Atmospheric Sciences Laboratory receives and monitors the data in real-time. Note that the raw dataset goes through several steps of correction (i.e., post-process) in terms of density, frequency-response, and motion after the cruise. In ARA05B cruise, ice-freezing on the sensors severely deteriorated data quality, but this cruise severe icing was not an issue.

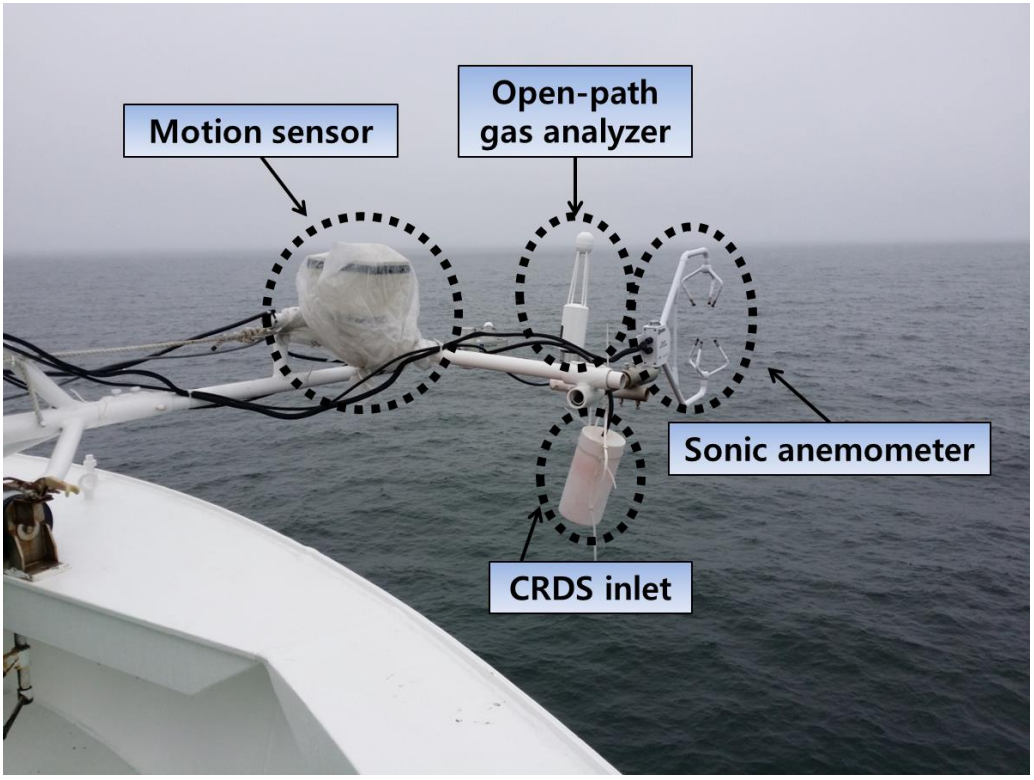


**Figure 11.2 - Instruments at the bow.**

**Figure 11.3 - Close path gas analyzer (CRDS) in the CRDS container.**

### 11.2.2. Meteorological condition

Essential meteorological variables such as air temperature, humidity, wind, precipitation, solar radiation (shortwave radiation), and longwave radiation are obtained from sensors on the radar-mast at 10-min interval (Fig. 11.4).

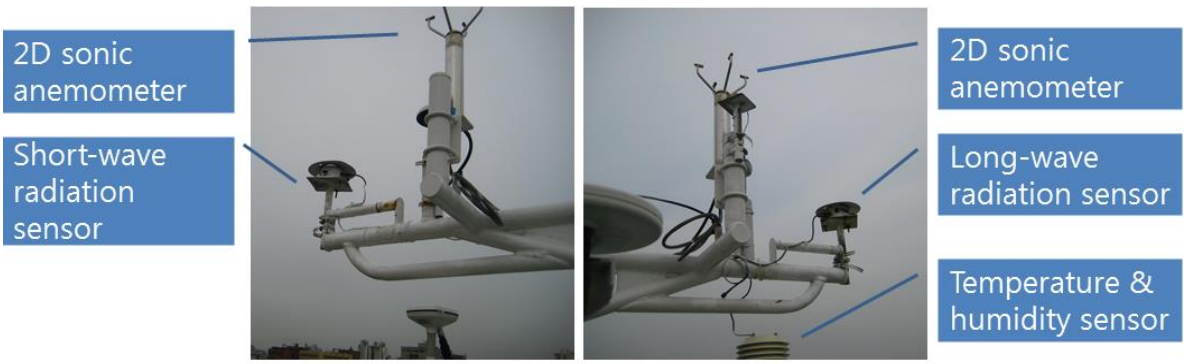


**Figure 11.4 - Instruments at the radar-mast (from 2013 Arctic cruise report).**

### 11.2.3. Aerosol Observations

The aethalometer (AE, Magee Scientific, USA) collects the sample (with a flow rate of 5 LPM) on a quartz fiber filter tape, performs a continuous optical analysis for the quantification of black carbon emitted from the combustion, and yields the mass concentration ($ng/m^3$) of black

carbon (up-left panel in Fig. 11.5). The number concentrations (#/cm$^3$) of aerosols are determined in real-time by using two condensation particle counters (CPC, CPC 3772 and CPC 3776, TSI, USA, bottom-left panel in Fig. 11.5). The nephelometer (3563, TSI, USA) measures the angular integral of light scattering that yields the quantity called the "scattering coefficient", used in the Beer-Lambert Law to calculate total light extinction (right panel in Fig. 11.5).

**Figure 11.5 - Aerosol measuring instruments: (Up-left) Aethalometer, (Bottom-left) Condensation Particle Counters (CPC3772 and CPC3776), and (Right) Nephelometer.**

## *11.3. Preliminary Results*

### 11.3.1. Air-sea interaction

Some preliminary fluxes of sensible heat (Fig. 11.6) and latent heat (Fig. 11.7) are shown below. Based on a simple quality control (QC), apparent missing and erroneous data were omitted in the figure. Sensible and latent heat flux shows a generally upward flux. The motion sensor, measuring three-directional accelerations and angular rates, is needed for the calibration of biases of eddy covariance flux measurements due to the ship motion. One motion sensor is installed near CSAT3 to capture its motion. After the cruise, the motion correction will be applied every 30 minutes (Miller *et al*., 2008), and the corrected data will be saved for a further analysis.

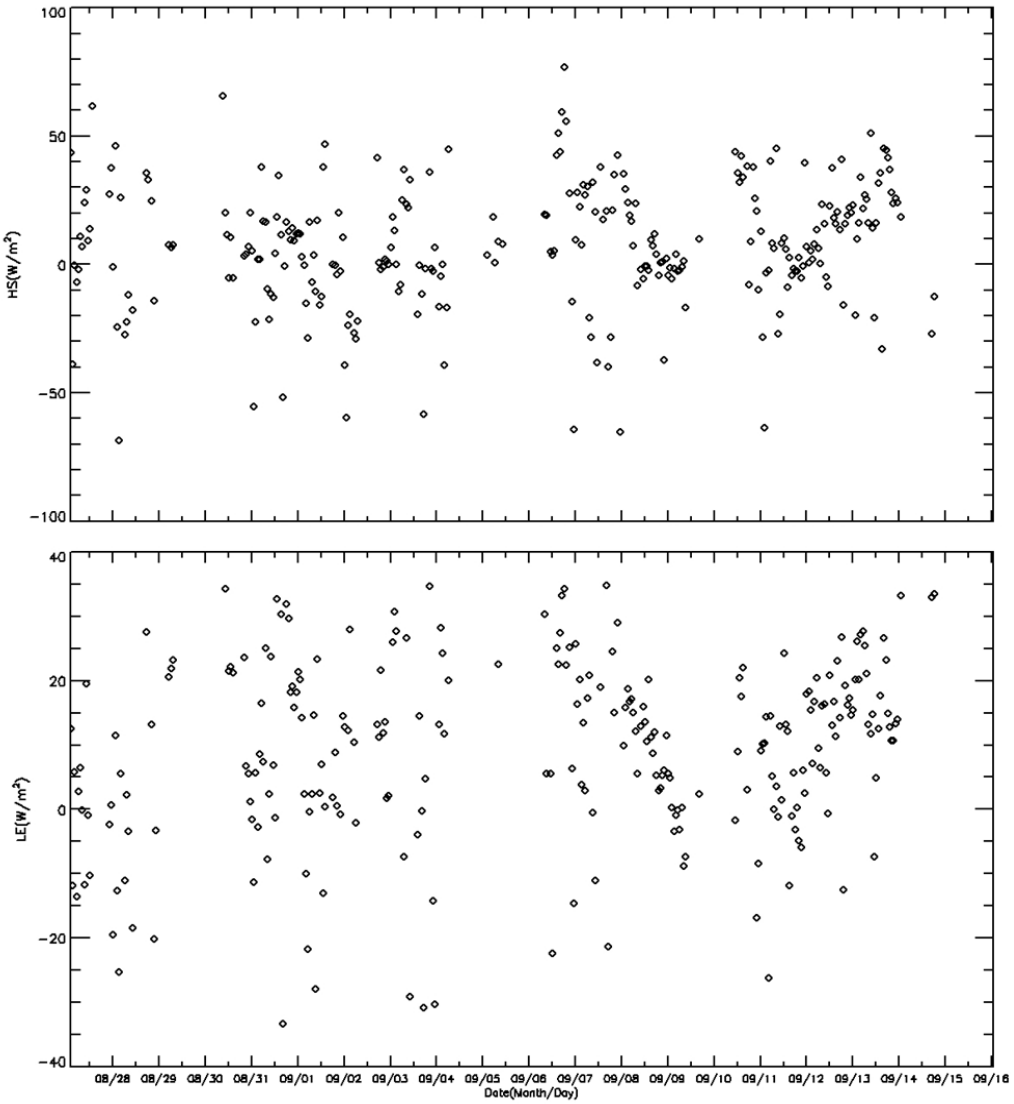


**Figure 11.6 - Time series of sensible heat flux (top) and latent heat flux (bottom).**

### 11.3.2. Meteorological conditions

Figure 11.7 shows meteorological conditions during the cruise (from the top panel, air temperature, relative humidity, air pressure, wind speed and wind direction). Air temperature during the cruise ranged from -4.0℃ to 11.9℃ with average of 2.0℃. Relative humidity (RH) ranged from 61.9% to 100% with average of 86.2%. Compared with RH records in the 2013 Arctic cruise (ARA04C), the environment was generally more dry during the 2014 cruise. Atmospheric pressure showed variation between 99.1 kPa to 102.4 kPa. Note that wind speed and direction shown here are apparent, not true; true wind direction and speed will be calculated considering the ship's course and speed after the cruise.

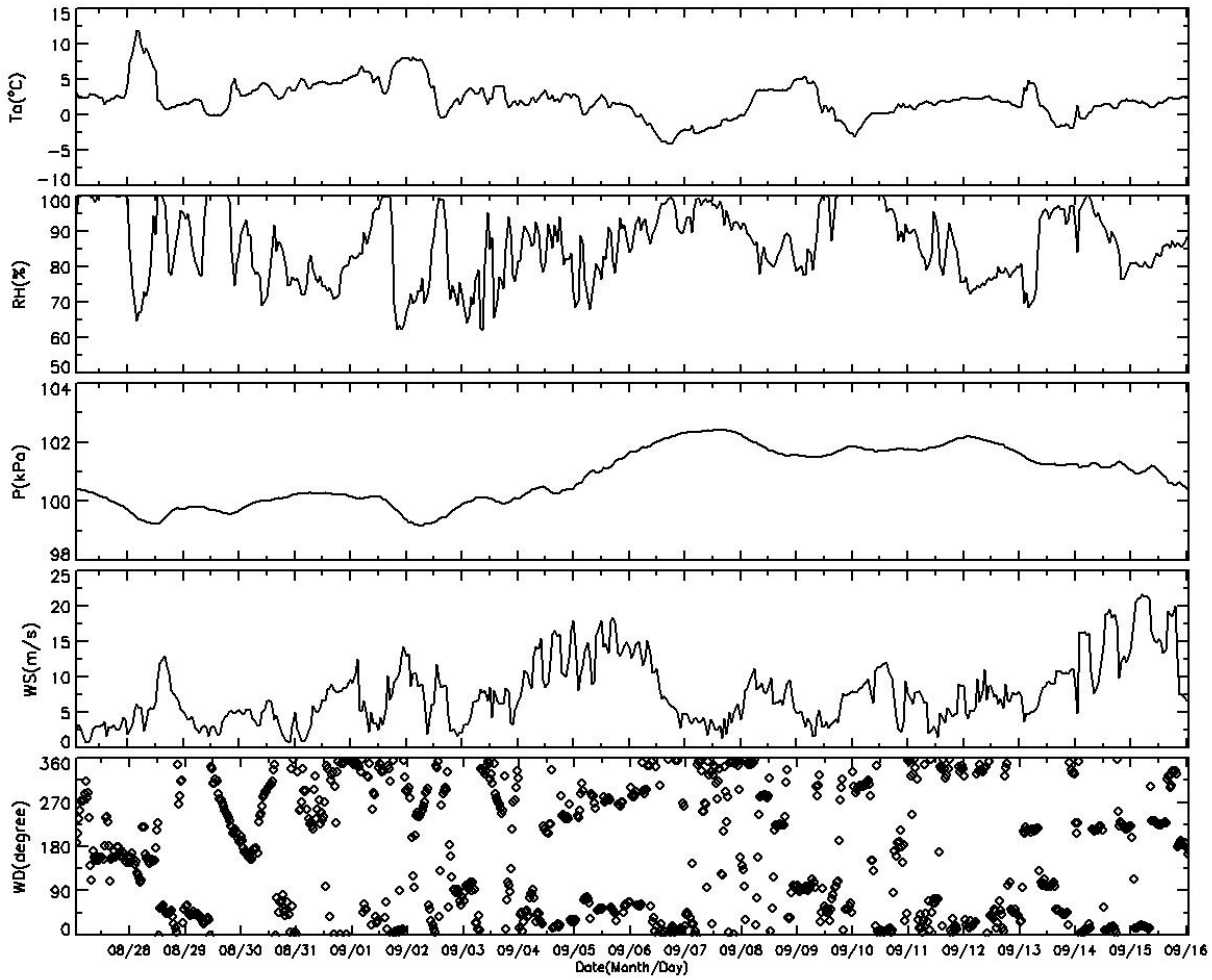


**Figure 11.7 - Meteorological variables during the cruise.**

### 11.3.3. Methane, water vapor and aerosols measurements

During the ARA05C cruise, the CRDS was operated in $CH_4$-$H_2O$ mode in the CRDS shelter as a part of eddy covariance system (Crosson, 2008; Fig 11.8). Methane measured by the CRDS showed range of 1.88 to 1.98 ppm with average of 1.90 ppm (Fig. 11.9). Water vapor concentration measured by the CRDS ranged from 3.7 mmol/mol to 10.0 mmol/mol and with an average of 5.8 mmol/mol. Water vapor concentrations measured by the LI7500 ranged from 2.3 mmol/mol to 10.1 mmol/mol with an average of 5.9 mmol/mol. The two instruments showed similar results. The aethalometer, CPC, and nephelometer continuously measured various aerosol properties. In this report, the mass density (ng/m$^3$) of black carbon (BC) measured by the aethalometer is presented (Fig. 11.10). However, other data will be processed after the cruise.

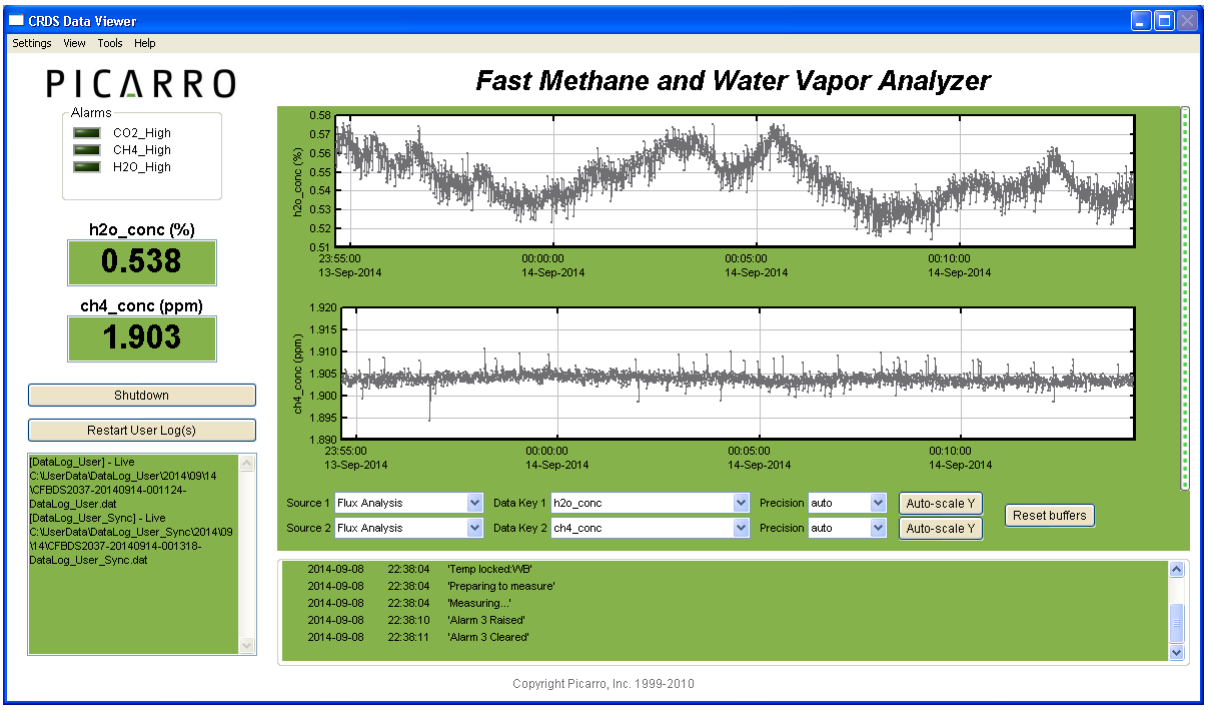


**Figure 11.8 - Real-time monitoring of $CH_4$ and $H_2O$ in flux mode.**

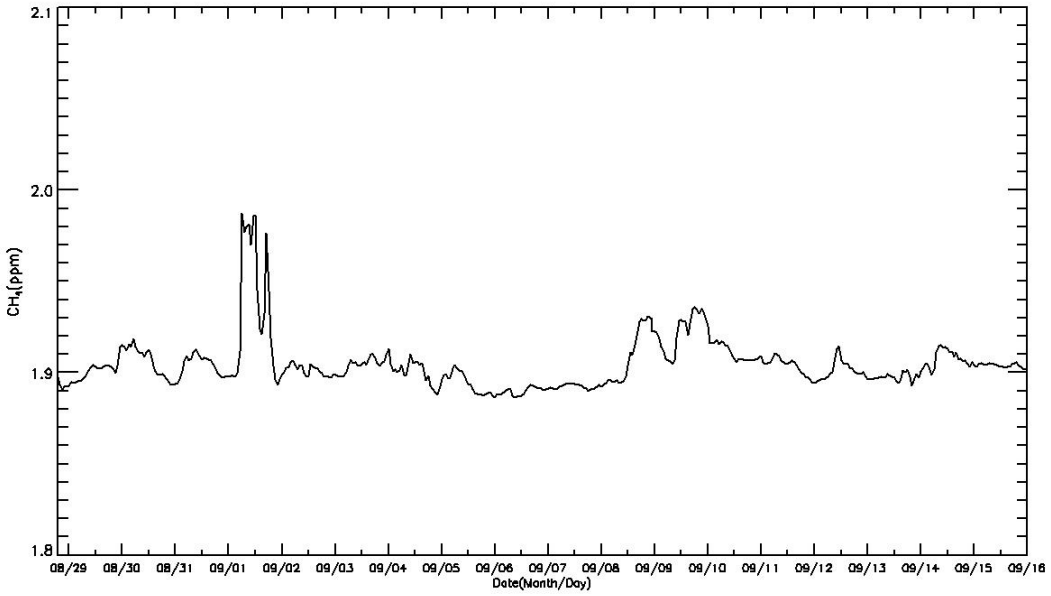


**Figure 11.9 - Methane concentration variation during the cruise.**

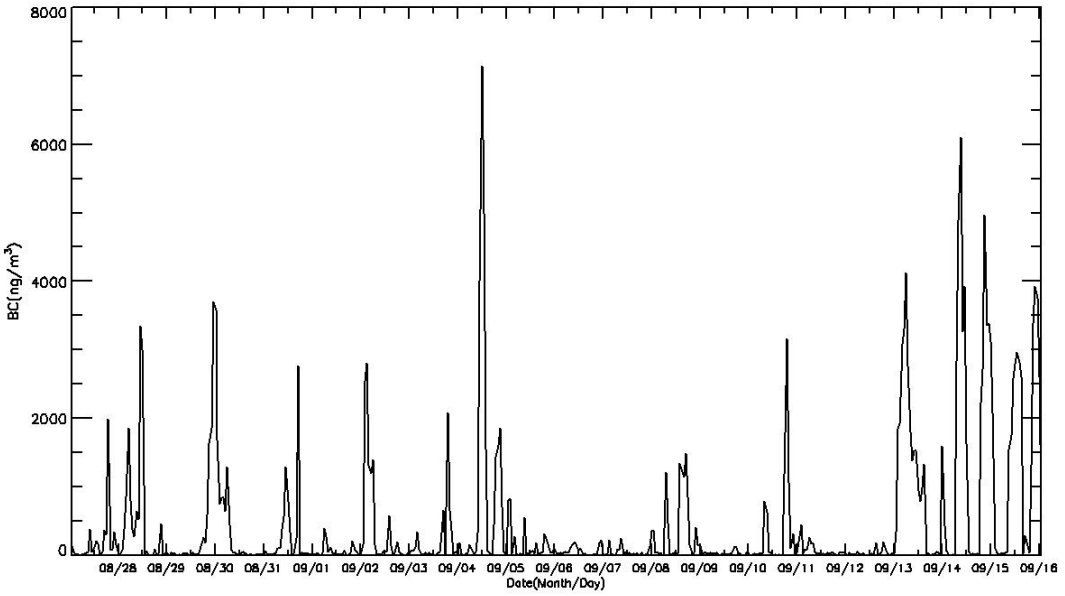


**Figure 11.10 - Mass density of black carbon measured during the cruise.**

## *11.4. Summary*

During the ARA05C cruise, all the atmospheric equipment operated quite well. Icing problems on the eddy-covariance system were much less severe compared to last cruise (ARA05B). Other meteorological sensors and aerosol instruments also produced good quality data. However, despite the importance of direct observation at sea, there still exist lots of challenges including ship motion, nasty weather and sea condition. Post-processing is needed for data that include any wind information. The navigation data are needed to get true compass wind

direction and speed. The motion sensor and navigation data together can correct the biases of eddy covariance fluxes. The motion correction for the fluxes will be done after the cruise.

### *References*


British-Standard-Institute. 1977. Methods of testing soil for civil engineering purposes, BS 1377. BSI, London, BSI, London.

Hansbo S. 1957. A new approach to the determination of the shear strength of clay by the fall-cone test. Rep., Stockholm.

Curry JA, Rossow WB, Randall D, and Schramm JL. 1996. Overview of Arctic cloud and radiation characteristics. *J. Climate*, 9: 1731–1764.

Dallimore SR, Paull CK, Collett TS, Jin YK, Mienert J, Mangelsdorf K, Riedel M. 2012. Drilling to investigate methane release and geologic processes associated with warming permafrost and gas hydrate deposits beneath the Beaufort Sea Shelf. IODP Pre-Proposal 806, available online at http://iodp.org/

Hong J, Kim J, Choi, T, Yun J, and Tanner B. 2000. On the effect of tube attenuation on measuring water vapor flux using a closed-path hygrometer. *Korean J. Agricultural and Forest Meteorology*, 2: 80–86.

Jacobson M Z. 2002. Control of fossil-fuel particulate black carbon and organic matter, possibly the most effective method of slowing global warming. *J. Geophys. Res.* **107**.

Kinnard C, Zdanowicz CM, Fisher DA, Isaksson E, de Vernal A, and Thompson LG. 2011. Reconstructed changes in Arctic sea ice over the past 1,450 years. *Nature*. 479: 509–512.

LI-COR Environmental Division. 2004. *LI-7500 $CO_2$/$H_2O$ Analyzer: Instruction Manual*. LI-COR, Inc., 155pp.

Lunne T, Robertson PK, Powell JJM. 1997. Cone penetration testing in geotechnical practice. Spon Press, London

Miller SD, Hristov TS, Edson JB, and Friehe CA. 2008. Platform motion effects on measurements of turbulence and air-sea exchange over the open ocean. *J. Atmos. & Ocean. Tech.* 25: 1683–1694.

O'Regan M, de Vernal A, Hill P, Hillaire-Marcel C, Jakobsson M, Moran K, Rochon A, St-Onge G. 2010. Late quaternary paleoceanography and glacial dynamics in the Beaufort Sea, IODP pre-proposal #753, available online at http://iodp.org/.

Paull, CK, Ussler W, Dallimore SR, Blasco SM, Lorenson TD, Melling H, Medioli BE, Nixon FM, McLaughlin F. 2006. Origin of pingo-like features on the Beaufort Sea Shelf and their possible relationship to decomposing methane gas hydrates. *Geophysical Research Letters.* 34: 1031-5.

Semiletov IP, Pipko II, Repina I, Shakhova NE. 2007. Carbonate chemistry dynamics and carbon dioxide fluxes across the atmosphere–ice–water interfaces in the Arctic Ocean: Pacific sector of the Arctic. *J. Marine Systems*. 66: 204–226.

Serreze MC, Barrett AP, and Cassano JJ. 2011. Circulation and surface controls on the lower tropospheric air temperature field of the Arctic. *Journal of Geophysical Research*. 116: D07104, doi:10.1029/2010JD015127.

Stegmann S, Moerz T, and Kopf A. 2006. Initial Results of a new Free Fall-Cone Penetrometer (FF-CPT) for geotechnical *in situ* characterisation of soft marine sediments. *Norwegian Journal of Geology*. 86: 199-208.

Stegmann S, Strasser M, Anselmetti FS, Kopf A. 2007. Geotechnical *in situ* characterisation of subaquatic slopes: The role of pore pressure transients versus frictional strength in landslide initiation. *Geophysical Research Letters.* 34, doi:10.1029/2006GL029122.

Steiner A. 2013. Sub-Sea floor Characterization and Stability of Submarine Slope Sediments using Dynamic and Static Piezocone Penetrometers. University of Bremen, Bremen.

Taylor AE, Dallimore SR, Hill PR, Issler DR, Blasco S, and Wright F. 2013. Numerical model of the geothermal regime on the Beaufort Shelf, arctic Canada since the Last Interglacial. *Journal of Geophysical Research: Earth Surface*, 118: 2365–2379.

Wood DM. 1985. Some fall-cone tests. *Geotechnique*, 38: 64-68.